FAILURE MECHANISMS IN UNIDIRECTIONAL COMPOSITES UNDER TRANSVERSE AND LONGITUDINAL TENSION

A Dissertation

by

LINQI ZHUANG

Submitted to the Office of Graduate and Professional Studies of
Texas A&M University
in partial fulfillment of the requirements for the degree of

DOCTOR OF PHILOSOPHY

Chair of Committee,	Ramesh Talreja
Committee Members,	Vikram Kinra
	J.N. Reddy
	Anastasia Muliana
Head of Department,	Rodney Bowersox

May 2018

Major Subject: Aerospace Engineering

ABSTRACT

This dissertation deals with analysis of failure mechanisms in unidirectional reinforced fiber composites under axial and transverse tensile loads. These two failure modes are fundamental in governing the performance of composite materials in most applications. In spite of many years of research in the mechanisms underlying these failure modes, gaps in their understanding have remained. This dissertation attempts to fill those gaps.

Two particular issues are addressed in the studies conducted here: 1) under transverse tension, what is the process by which fiber/matrix debond cracks link up to form transverse cracks, and 2) under longitudinal tension, how does a fracture plane form? In the study, related to transverse tension, plausible mechanisms for transverse crack formation are considered in two scenarios: Scenario 1 where a pre-existing single fiber/matrix debond crack kinks out into the matrix and induces fiber/matrix debonding at neighboring fibers, and Scenario 2 where multiple pre-existing debond cracks link up by the debond growth and crack kink-out process. A 2-D finite element model consisting of a circular region of matrix with a central fiber surrounded by six fibers in a hexagonal pattern is used for the local stress analysis. The region is embedded in a homogenized unidirectional composite of rectangular outer boundary. Energy release rates (ERRs) of interface cracks and kinked-out cracks are calculated under applied tension normal to fibers. Results show that Scenario 2 is more likely to lead to formation of a transverse crack than Scenario 1. The study related to longitudinal tension considers a broken fiber

as the nucleation site for formation of a plane whose unstable growth leads to failure. To analyze the conditions for formation of this "critical fracture plane", an axisymmetrical finite element model is constructed with the broken fiber at the center surrounded by intact fibers. Here, too, two scenarios are considered: one, where the broken fiber results from the manufacturing process, and two, where a fiber fails at a weak point under loading. In the first case, a matrix crack is found to initiate from the broken fiber end and grow normal to the fiber axis, while in the second case, a matrix crack kinks out of an assumed short fiber/matrix debond crack and grows out toward the neighboring fibers.

The studies conducted here provide valuable input into multiscale approaches that link the local failure to global response of composite structures.

ACKNOWLEDGEMENTS

It's sad that my journey at Texas A&M University is coming to an end. There are too many people I would like to thank. First of all, I would like to thank my Ph.D. advisor Dr. Talreja for bringing me to the world of composites research and guiding me step by step. It's a truly life changing eight years. I would also like to thank Dr. Varna, my Ph.D. advisor in Sweden for his detailed discussions, advice and even critics. I am very fortunate to have not one but two of the best advisors in the world. Their dedications to research and the standard they've set motivate me to become a better version of myself every single day.

Thanks also go to Dr. Kinra for being my mentor at teaching fellow program and sharing valuable teaching tricks and experience to me, and to Dr. Reddy, Dr. Muliana for being my committee members and for their guidance and support throughout the course of this research.

I would also like to thank the department faculty and staff, particularly Ms. Gail Rowe and Ms. Karen Knabe, for helping me with many official formalities. I also want to extend my thanks to all the friends I met here at Texas A&M University for making my time at Texas A&M University a great experience

Finally, thanks to my mother, for bringing life to me and giving me the opportunity to see this wonderful world, and to my father and my wife, for always standing by me, throughout ups and downs. I would not be here without them. This dissertation is for all my loved ones!

CONTRIBUTORS AND FUNDING SOURCES

This work was supervised by a dissertation committee consisting of Professor Ramesh Talreja, Professors Vikram Kinra and J.N. Reddy of the Department of Aerospace Engineering and Professor Anastasia Muliana of the Department of Mechanical Engineering. All work for the dissertation was completed independently by the student.

Graduate study was supported by graduate research assistantship from Department of Aerospace Engineering and a teaching fellowship from Texas A&M University.

NOMENCLATURE

ERR	Energy Release Rate
FE	Finite Element
FFM	Finite Fracture Mechanics
IFF	Inter Fiber Failure
PEEK	Polyether Ether Ketone
UD Composites	Unidirectional Composites
VCCT	Virtual Crack Closure Technique
XFEM	Extended Finite Element Method

TABLE OF CONTENTS

Page

LIST OF FIGURES

Page

LIST OF TABLES

Page

1. INTRODUCTION

1.1 Background

1.1.1 Characteristics of continuous fiber reinforced polymer based composites

Composite materials are building blocks for a very broad range of industrial applications. The word “composite” literally describes the characteristics of materials, which are made up of at least two different constituents. In a composite material, more stiffer constituents which are called *reinforcements* are often embedded in a more compliant constituent called *matrix*. For reinforcements, they could be made of various materials and in the form of continuous fibers, short fibers and particles. For matrices, they are mostly made of polymers and metals. Because of numerous possible arrangements of constituents, the failure of composites can be vastly complicated compared to monolithic materials such as metals. To analyze the failure of composites, we need to first have an understanding of their constituents. It should be noted that in the following, unless mentioned otherwise, composite materials (or composites) refer to continuous fiber reinforced polymer based composites.

1.1.1.1 Fiber reinforcements

Depending on the applications, many fiber reinforcements are available. Among these, carbon fibers and glass fibers are extensively used in polymer-based composites for a wide range of industrial applications such as in aerospace, wind energy and automotive industries.

Carbon fiber usually consists of small crystallites of “turbostratic” graphite. The representative structure of a carbon fiber is presented in Figure 1.1. For years, the use of carbon fiber reinforced composites has been driven by the applications in aerospace, automotive and sports goods industries. Recently, carbon fiber reinforced composites have also seen their applications increasing in Wind energy industry as turbine blade size continues to increase.

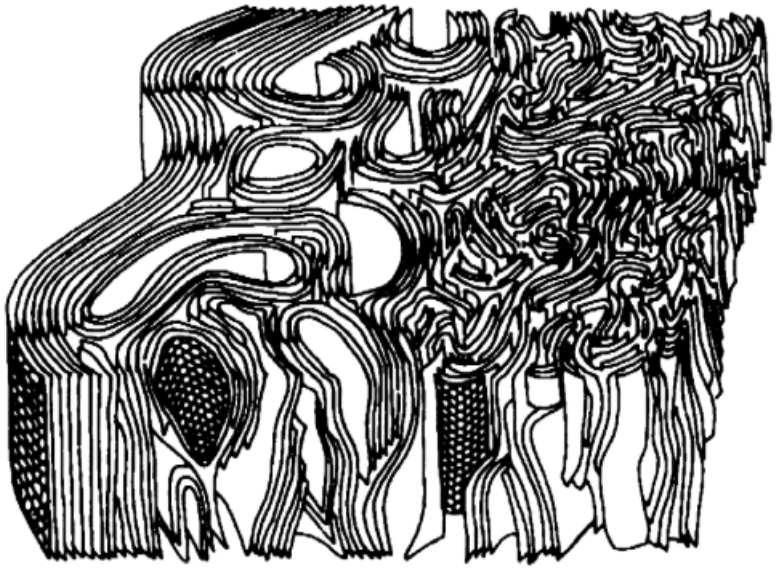

Figure 1.1 Schematic representation of carbon fiber structure (Figure reprinted from [1])

Depending on the manufacturing process, there are two major types of carbon fibers used. One is polyacrylonitrile (PAN) based fibers and the other is mesophase pitch-based fibers. Both fibers were introduced back in the 1960s. Carbon fibers are usually 4~8μm in diameters, and have much higher strength and modulus compared to

other typical fiber reinforcements such as glass fibers. Figure 1.2 shows the table reprinted from [2] containing typical mechanical properties of carbon fibers.

Mfr.	*Fiber type*	*Filament count*	*Filament diameter* (μm)	*Surface area* ($m^2 g^{-1}$)	*Tensile strength* (MPa)	*Tensile modulus* (GPa)	*Tensile strain* (%)	*Density* ($g\ cm^{-3}$)
Amoco	T-300	1k, 12k	7.0	0.45	3650	231	1.4	1.76
[Thornel]	T-40	12k	5.1	0.5	5650	290	1.8	1.81
	T650/42	6k, 12k	5.1	0.5	4620	290	1.6	1.78
	T-50	3k, 6k	6.5	0.45	2900	390	0.7	1.81
Hexcel	AS4	3k, 12k			3930	221	1.7	1.79
	IM4	12k			4138	276	1.5	1.73
	IM7	6k, 12k			5379	276	1.8	1.77
	UHM	3k, 12k			3447	441	0.8	1.87
Mitsubishi	TR30	3k			3530	235	1.5	1.79
rayon	TR50	12k			4900	235	2.1	1.80
[Pyrofil]	MR50k	12k			5490	294	1.8	1.80
	SR50	12k			4220	490	0.9	1.88
Sigrafil	C30		6.8		3000	230	1.4	1.78
	C35		7.0		3200	210	1.4	1.8
Tenax	HTA	1k, 24k	7.0		3950	238	1.5	1.77
	UTS	12k	7.0		4800	240	2.0	1.8
	IMS	6k, 24k	5.0		5500	290	1.9	1.8
	UMS	12k	4.7		4500	435	1.1	1.81
Toho	HTA	3k, 12k	7.0		3920	235	1.7	1.77
rayon	ST4	12K	7.0		4810	240	2.0	1.78
[Besfight]	IM600	12k, 24k	5.0		5790	285	2.0	1.80
	HM35	12k	6.7		3240	345	0.9	1.79
	TM40	12k	6.2		3430	390	0.9	1.85
	UM68	12k	4.1		3330	650	0.5	1.97
Toray	T300*	1 – 12k	7.0		3530	230	1.5	1.76
[Torayca]	T300J*	3k, 12k	7.0		4210	230	1.8	1.78
* available	T700S	12k	7.0		4900	230	2.1	1.80
from	T800H*	6k	5.0		5490	294	1.9	1.81
Soficar	T1000G	12k	5.0		6370	294	2.2	1.80
	M40J*	6k	5.0		4410	377	1.2	1.77
	M50J	6k	5.0		4120	475	0.8	1.88
	M60J	3k, 6k	5.0		3820	588	0.7	1.94
	X665	6k	5.0		3430	637	0.5	1.98
	M40*	6k, 12k	7.0		2740	392	0.7	1.81
Zoltek	Panex33	48k, 320k	7.4		3600	228		1.78
[Panex]	Panex30				1552	221		1.75

Figure 1.2 Table showing typical carbon fibers mechanical properties (Figure data reprinted from [2])

It should be noted that data presented in Figure 1.2 are mainly the mechanical properties along fiber axis and carbon fibers are generally considered as transversely

isotropic. Compared to their longitudinal properties, it is more difficulty to test carbon fiber transverse properties and obtained results vary significantly among different studies [3-5]. Based on the available literature, the transverse modulus of carbon fibers is in the range of 6GPa ~30GPa.

Most glass fibers are based on silica (SiO_2) with additions of oxides of calcium, boron, sodium, iron and aluminum [6]. Compared to carbon fibers, the diameters of glass fibers are large, in a range of 10μm ~ 17μm for most of commercial ones [7]. In contrast to carbon fibers, glass fibers are considered as isotropic and properties for most commonly used glass fibers are presented in Figure 1.3.

	Physical properties								
	A-Glass	*C-Glass*	*D-Glass*	*E-Glass*	*ECR-Glass*	*AR-Glass*	*R-Glass*	*S-2-Glass*	*No boron E-Glass*
Tensile strength, MPa									
−196 °C		5380		5310	5310			8275	
23 °C	3310	3310	2415	3445	3445	3241	4135	4890	3450
371 °C				2620	2165		2930	4445	
538 °C				1725	1725		2140	2415	
Young's modulus, GPa									
23 °C	68.9	68.9	51.7	72.3	72.3	73.1	85.5	86.9	80.5
538 °C				81.3	81.3			88.9	
Elongation at break, %	4.8	4.8	4.6	4.8	4.8	4.4	4.8	5.7	4.6

Figure 1.3 Table showing typical glass fibers mechanical properties (Figure data reprinted from [7])

Both carbon and glass fibers are essentially brittle. As a result, they do not have a well-defined tensile strength as it depends on the presence of flaws (at surface or internal) along fiber axis, as demonstrated in Figure 1.4 for carbon fibers. To account for the flaws, the fiber strength is usually treated on a statistical basis. The statistical nature

of fiber strength is vital when it comes to analyzing the longitudinal failure of composites, as will be discussed in Section 3.

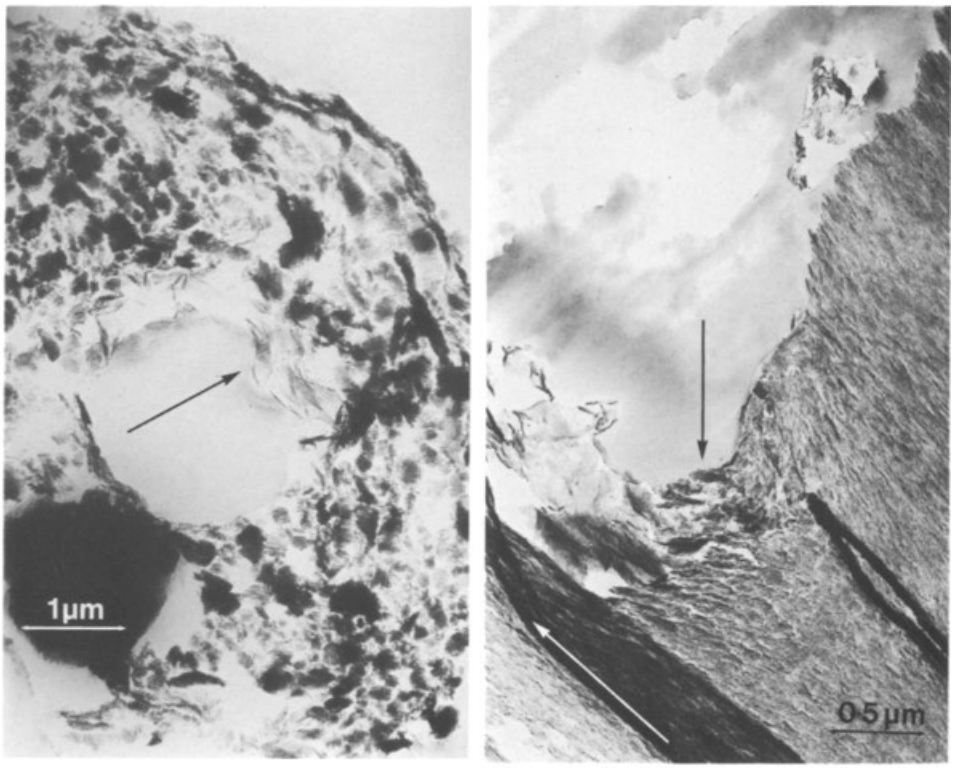

a) b)

Figure 1.4 Illustration of flaws a) inside a carbon fiber and b) at the carbon fiber surface (Figure reprinted from [1])

1.1.1.2 Polymer matrices

Two types of polymer matrices are widely adopted in applications. One is thermosetting resins and the other is thermoplastics. The most common thermosetting resins are epoxy, unsaturated polyester and vinyl ester. For thermosetting polymers, cross-linking process transforms liquid resin into a hard solid and this is usually

achieved by curing. Depending on the manufacturing process, curing could be achieved at room temperature but most often it is performed under a cure schedule which involves heating to one or more temperature levels to achieve optimum cross-linking [6]. As a result of relatively high temperature of curing, chemical shrinkage during curing and thermal stress due to cooldown can lead to the development of residual stress in composites.

Thermoplastics, unlike thermosetting resins, are not cross-linked. As a result, solid thermoplastics could be reheated to a viscous state and be reused. However, the manufacturing processes for thermoplastics are also more difficult than that for thermosets, as it often involves high temperature. Some of the most common thermoplastics are polypropylene and Polyether ether ketone (PEEK).

As a result of cross-linking process, thermosetting resins are generally considered brittle while thermoplastics could undergo substantial inelastic deformation, which results in relatively high failure strain. Meanwhile, thermoplastics tend to exhibit good resistance to chemical attacks and good thermal stability [6], which make them good candidates for high-temperature applications.

1.1.1.3 Fiber/matrix interface

The unique properties of composites could not be achieved by either fiber reinforcements or polymer matrices acting alone. Fiber/matrix interface plays a vital part in it. Since the introduction of composites, fiber/matrix interface has been one of the

most investigated topics and yet it is still one of the most debatable areas in composites research, from its exact definition to properties characterizations.

An interface is mostly understood as the common boundary between fibers and matrix, bonding the constituents together for transfers of loads, and often considered to have zero thickness or (volume) [8]. Such definition has been debated for years as to whether interface is indeed zero thickness, or a three-dimensional region close to fiber/ matrix boundary with unique properties different from either fiber or matrix. According to [8], a more proper term for such three-dimensional region should be "interphase" and an interphase contains " the surface of classical fiber-matrix contact as well as the region of finite thickness therefrom of which chemical, physical and morphological features are different from the bulk material. Imposed on this region are the processing conditions which allow chemical reactions, residual stresses and volumetric changes to take place." An example of the interphase could be seen in Figure 1.5 where partial crystallization of matrix occurs near the fibers.

Due to the existence of the interphase region, depending on the fiber/matrix bonding qualities, composites can have fiber/matrix interface debonding, or interphase failure. As a result, when it comes to the "interface strength", it is still debatable whether it should be counted as the amount of work to separate the fiber/matrix common surface (bond) or to fail the interphase. Regarding the former, various experimental techniques such as "fiber pull-out" test have been developed to calculated the interfacial bonding strength. For more detailed reviews of corresponding techniques, readers are encouraged

to read [8, 9]. It is much more challenging to characterize the properties of interphase; one of the few examples is in [10].

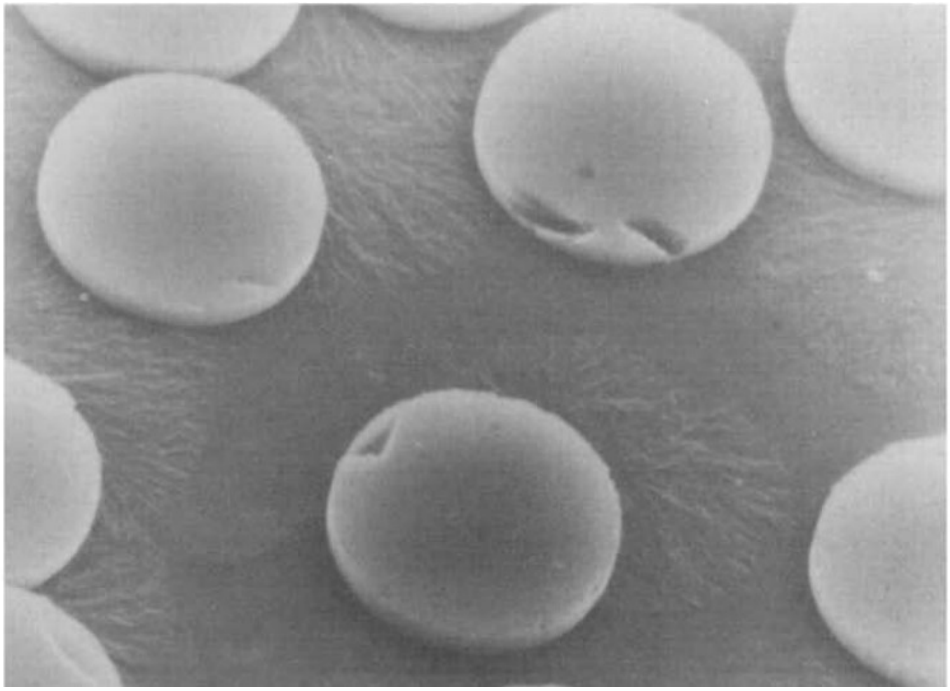

Figure 1.5 Illustration of interphase region in Carbon/PEEK composites (Figure reprinted from [11])

1.1.2 Failure modes of composites

Based on the discussion above, it is clear that the structure of a fiber reinforced composite has hierarchy: from macro-scale composite laminates to a much smaller scale of interphase. As a result of such unique characteristics of composite materials, when subjected to loading, multiple failure modes could occur simultaneously or sequentially at different scales, which make it extremely challenging to analyze the failure of

composite materials. In the following sections, we will narrow our discussions on two most commonly found failure modes within composites.

1.1.2.1 Literature review: Failure of unidirectional composites under transverse tension

When subjected to transverse tension, i.e., normal to the fiber axis, cracking within the plies of a composite laminate, often referred to as matrix cracking or transverse cracking, is inevitably the first failure event to occur. Although by itself transverse cracking may not affect the performance of the laminate significantly, but as shown in Figure 1.6, it could lead to the initiation of other failure modes, e.g. delamination and fiber breakage, which can have detrimental effects on the load bearing capability of the laminate. Therefore, understanding what governs the initiation and evolution of cracking within the plies is of great interest. The early studies of this failure mode, (e.g. [12-16]),were focused on explaining the observed multiplication of the matrix cracks by simple one-dimensional models. More rigorous mechanics treatments of the evolution of the crack number density and its effects on laminate stiffness reduction were developed later [17-20]. For a more comprehensive review on transverse crack multiplication and stiffness degradation prediction, readers are encouraged to see [21]. Common to all such analyses is the assumption of homogenized plies in which cracks appear according to a strength or a fracture toughness based criterion, and then multiplication of cracks occurs under increased loading when the local stresses between the cracks satisfy a failure criterion.

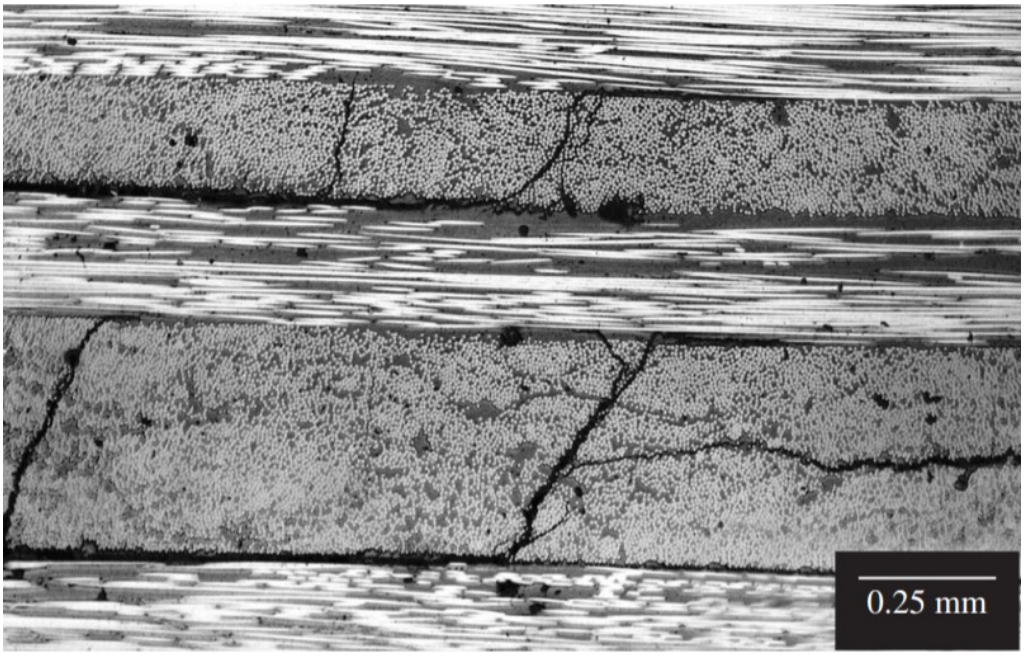

Figure 1.6 Delamination induced by transverse cracking (Figure reprinted from [22])

In recent years, the detailed process of matrix crack formation within the plies has been examined by considering the local stress fields in the matrix between the fibers. Among the earliest works in this direction were studies of the effect of tri-axiality in the local stress field on cavitation in the matrix polymer [23]. Further studies of this phenomenon led to the development of a dilatation energy density criterion for brittle cracking in the matrix [24] and its predictions agreed well with experimental data [25]. Since the favorable locations for satisfaction of the criterion are points in the matrix close to the fiber surfaces, it is reasonably assumed that the matrix failure leads to debond cracks at the fiber/matrix interfaces. Other assumed criteria for the debond crack initiation resort to fiber/matrix interface properties such as strength or fracture toughness based on finite fracture mechanics [26], or a combination of these via a cohesive zone

model for single-fiber debonding [27] or multiple-fiber debonding [28]. The interface properties in a cohesive zone model cannot be found independently and must be inferred or calibrated. It is worth noting that the inferred interface properties depend on the stress state on the fiber/matrix interface at incipient failure. A comprehensive review of various methods to infer the interfacial strength has been given in [29].

Experimental observations [30, 31], such as the one shown in Figure 1.7, suggest that the individual fiber/matrix debond cracks connect through the matrix to form transverse cracks. The results obtained in these studies do not provide sufficient details of the mechanisms by which the debond cracks connect. Since in situ observations are difficult to make other than perhaps for model composites, numerous studies have attempted to understand the governing conditions underlying the mechanisms involved by analysis. For this, single fiber composite is widely adopted due to its relative simplicity. Figure 1.8 shows the general set-up of a single fiber composite subjected to transverse tension where a single fiber is placed at the center of a matrix material, and the whole specimen is subjected to transverse tension. For fiber/matrix interfacial debond growth, a single-fiber composite has been considered in an analytical study [32] and in numerous numerical studies (e.g. [33-38]). The kinking out of a debond crack has also been studied in a single-fiber model [39]. Recognizing the importance of the presence of neighboring fibers on the debonding and crack kinking process, later studies considered a two-fiber model [40] and found that the presence of a nearby fiber accelerates the initiation of debond crack growth in the central fiber only when it is aligned with the external loading direction, and for the rest of positions, it inhibits the

debond crack growth in the central fiber. An experimental and numerical study [41] of a model composite indicated that the presence of multiple fibers and their distribution affect the transverse crack formation process. Various numerical studies have been reported [42-44] to simulate the transverse crack formation with the consideration of the effect of non-uniform fiber distribution.

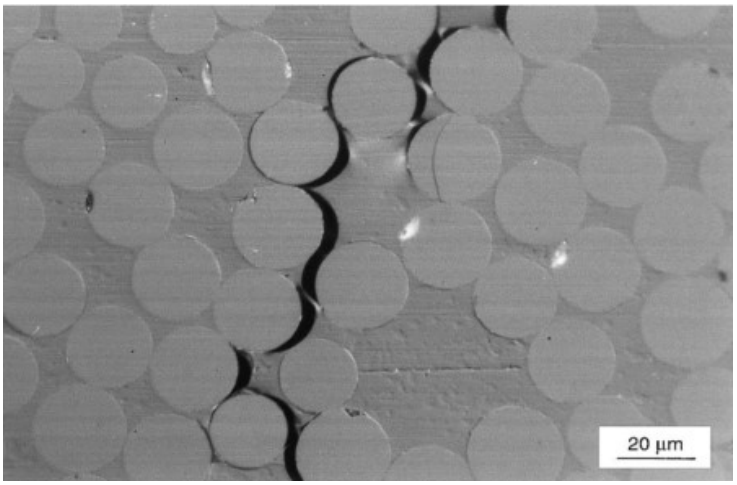

Figure 1.7 Microscopic feature of transverse crack (Figure reprinted from [30])

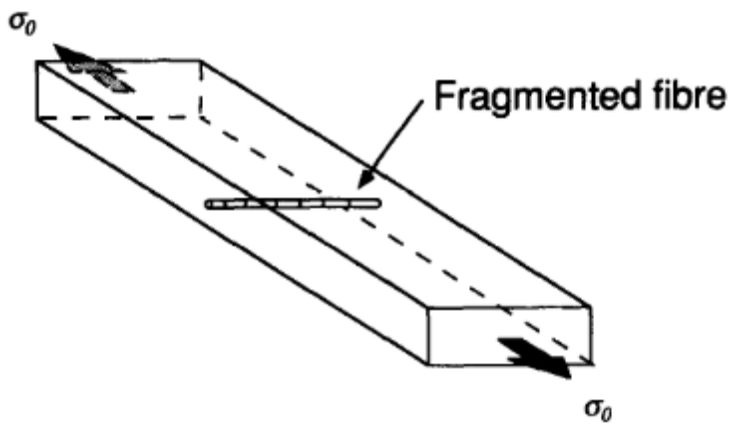

Figure 1.8 Illustration of single fiber composite subjected to transverse tension (Figure reprinted from [45])

Despite the fact that transverse cracking has been investigated by numerous researchers, it needs to be noted that none of these studies, however, explicitly analysed the debond crack linking mechanism in the transverse crack formation process. Clearly, the linking of the fiber/matrix debond cracks must play a key role in the transverse crack formation process. Without understanding this role, the effects of fiber volume fraction and fiber clustering in non-uniform fiber distribution on the composite transverse strength cannot be explained. To understand the debond crack linking process, the conditions governing the kinking out of a debond crack must be clarified.

1.1.2.2 Literature review: Failure of unidirectional composites under longitudinal tension

When a composite is subjected to longitudinal tension, final failure is governed by the failure of unidirectional (UD) plies aligned along the loading direction. Such failure usually starts with an individual fiber breaking at its weakest location, leading to the stress redistribution along fiber axis as well as stress enhancement in nearby intact fibers. With the further increase of applied load or load cycles, more fibers break, along with other forms of damage such as fiber/matrix debonding and matrix cracking. Final failure of such plies occurs when the so-called "critical fracture plane" is formed and its unstable growth leads to the separation of the entire composite.

Due to the statistical nature of the fiber breakage process, numerous statistical models have been proposed in order to predict the final failure of composites. Among all the models, the majority of them assume only fibers carry the axial loads and a UD composite fails when certain number of fibers are broken.

The first comprehensive analytical model to predict the tensile failure of a UD composite was developed by Rosen [46]. In his model, the axial loads are assumed to be carried by fibers only, and the extra load caused by the fiber breakage is shared by rest of the fibers in a cross-section. The strength of the fibers is assumed to follow Weibull distribution. Based on the "weakest link" theory that assumes a fiber fails when the local stress exceeds its lowest strength value, the composite failure occurs when a cross-section fails. Zweben [47], Zweben and Rosen [48] later proposed a statistical model based on the accumulative weakening of fibers that included the stress concentration.

The basis of their model lies on the argument that the breakage of a single fiber will cause stress concentration in the nearest fibers in a 2-D fiber array, which will then increase the probability of failure of the nearest two fibers, and the breakage of these fibers will subsequently cause a higher stress concentration in the surrounding fibers which will further increase the probability of failure of those fibers. The final failure of a composite is assumed to occur when a first multi-fractured group of fibers is formed. A few years later, Harlow and Phoenix [49, 50] also developed their own statistical model to predict the failure of UD composites. It should be noted that, until now, the analytical models we have discussed are all considered as the "chain of bundles" models, that is each fiber is considered as one chain within a bundle, and the weakest fiber fails first, the composite then fails when the fiber bundle fails. The "chain of bundles" model constitutes majority of the early years' models to predict the final failure of a UD composite until Batdorf [51] proposed his model concentrating on the formation and growth of multiple fiber fractures. In his work, Batdorf also adopted weakest link theory to predict the isolated single fiber breakage (singlet), double fractures (doublet) and multiple fractures (multiplets) with respect to increasing applied load. A UD composite is considered to fail when a Griffith-type instability occurs that corresponds to a certain number of broken fibers at the same location. This approach significantly simplifies the procedures in previous "chain of bundles" models and he and his co-worker [52] as well as others [53] found that the number of broken fibers at the same location causing instability most often varies from 6-14 fibers. This prediction was supported by the fractography investigation by Purslow [54], who found that the number of broken fibers

within a bundle in the fracture surface of a UD composite fell within that range of numbers, as shown in Figure 1.9. Besides the analytical models discussed, numerous numerical models were also developed to predict the failure of UD composite with focus on fiber fractures, for example, in [55-61]. These models, although agreeing relatively well with the experimentally obtained failure strain of a UD composite, are all focused only on the fiber breakages, which do not capture the exact failure mechanism of the UD composite.

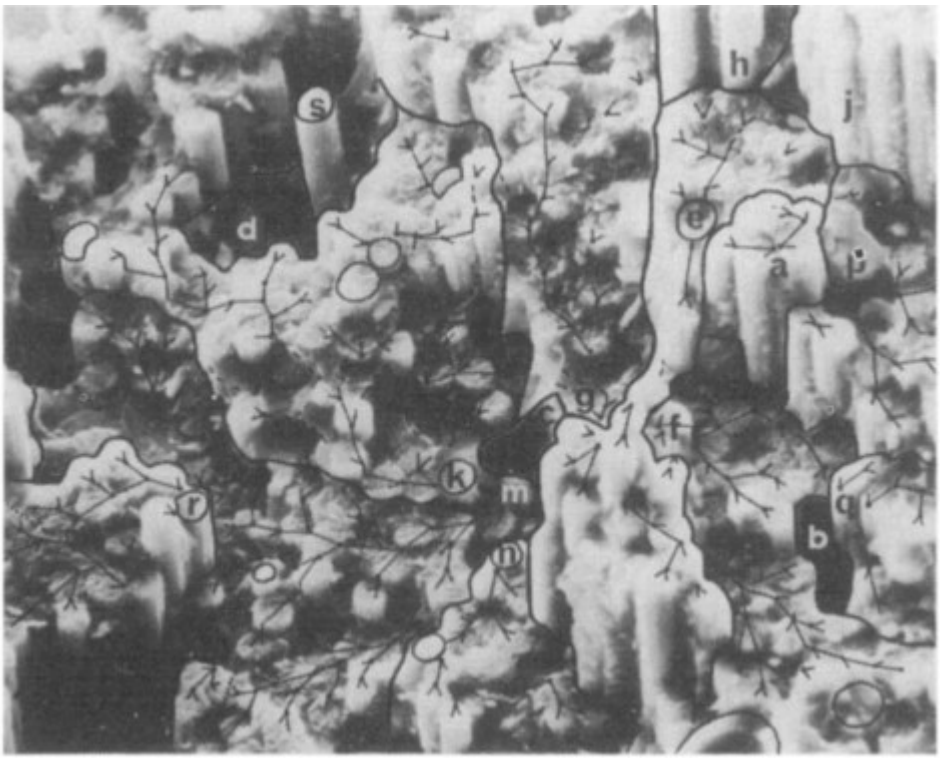

Figure 1.9 Fracture surface of a UD composite. (Figure reprinted from [54])

Recently, with the help of X-ray tomography technique [62-68], we have gotten more insights on the longitudinal failure of UD composites, especially the characteristics of the "critical fracture plane". Take the experimental work conducted by Garcea et al [67] for example. As shown in Figure 1.10, the fracture plane contains clusters of broken fibers and a closer look at these two figures reveals that the fracture plane is not strictly planar and broken fibers are in fact connected by the means of fiber/matrix interface debonding and matrix cracking. This important feature could not be captured by the models discussed above as interface debonding and matrix cracking are both ignored in the development of the models. Despite the direct experimental findings concerning the role of fiber/matrix debonding and matrix cracking in the formation of "critical fracture plane" and how do these affect the failure process of composites under longitudinal tension remains unclear.

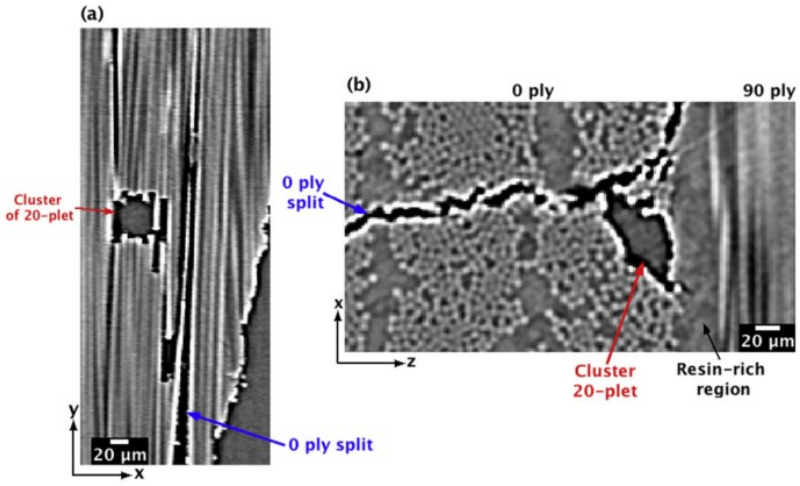

Figure 1.10 Illustration of "critical fracture plane" observed by X-ray tomography (Figure reprinted from [67])

1.1.2.3 Urgent need to fully understand failure mechanisms in composites

Numerous studies cited above have contributed to our understanding of the failure in composites. However, despite the progress made, it is noteworthy that too often the failure models have focused on "matching" the predicted failure strain or stress with experimental data without addressing the underlining failure mechanisms. This approach has limited use and can lead to unreliable predictions.

To begin with, it is much easier to adjust the input parameters in failure modeling to match the selected experimental results than to have fixed material values that are obtained from independent tests. The risk in adjustable parameters is that the model predictions can become significantly off outside the range in which the parameters were fixed. Interestingly, this issue was also discussed in a recent blog published on the website of European FibreMOD program [69] where the author called to "stop the hypocrisy of nicely matching experimental validations". Based on his previous work [66], Swolfs concluded that although the model predicted the failure load reasonable well, the internal damage development was severely off, which hampers the predictive capability of the model. Therefore, the input parameters entering a model should be those that govern the failure process and they should be identified at the outset of the modeling effort. Clearly, this cannot be done without the proper understanding on the failure mechanisms.

Knowing the failure mechanisms also has positive impact on designing structures for industrial applications. Currently, most composite component designs are overly conservative. Take wind turbine blades as an example. Here, inter-fiber failure (IFF) is

usually considered as the first failure event within composites. The presence of IFF would lead to stiffness degradation as well as subsequent failures such as delamination. From a structural point of view, delamination is more severe than IFF for the integrity of the composite structure. As a result, it is important to evaluate the tendency for delamination after IFF occurs, which requires understanding of IFF related failure mechanisms for the particular blade composite layups. Once these failure mechanisms are known, the designer needs only to apply needed reinforcement to the IFF hotspot region where IFF causes high tendency for delamination rather than reinforce the entire structure. This procedure is a major improvement towards optimizing the composite material usages in blade design and thus makes wind turbine blade design more cost-effective.

1.2 Problem statement and objectives

Based on the discussions in the previous sections, there should be no doubt that proper understanding of composite failure mechanisms is vital for failure model development as well as for improved industrial applications.

In this dissertation, plausible failure mechanisms in UD composites under transverse and longitudinal tension are investigated. Realizing the gap in current understanding of the mechanisms related to the transverse tension case, we will specifically study the link-up process of individual fiber/matrix debonds. Similarly, for the longitudinal tension case, we will investigate the mechanisms for the “critical

fracture plane" formation with focus on the role of fiber/matrix debonding and matrix cracking.

The specific objectives of present dissertation research are:

1. To analyze the individual debond crack link-up process under transverse tension and to identify the most important material parameters governing the transverse failure process;
2. To clarify the roles of fiber/matrix interface debonding and matrix cracking in the failure process under longitudinal tension in order to help explain the observed discrepancy between the predictions of existing failure models and experimental observations.

1.3 Approaches

In the present dissertation research, the failure mechanisms of UD composites under transverse tension are investigated by Finite Element (FE) analysis. In the FE model, Energy Release Rate (ERR) is considered as the driving force for fiber/matrix interface debonding as well as debond crack kinking and is calculated through Virtual Crack Closure Technique (VCCT). The VCCT was first proposed by Rybicki in [70] and was then adopted in various FE codes to enable the mode separation calculation. Readers can refer to [71, 72] for complete reviews of VCCT and its implementation in commercial software.

The failure mechanisms under longitudinal tension are also studied by FE analysis. In the FE model, the competition between matrix cracking and fiber/matrix

debonding from fiber break is evaluated. To account for the potential debond crack kinking, ERR of kinked crack is calculated based on VCCT and kinked crack propagation is simulated through Extended Finite Element Model (XFEM), which is FE method to model crack propagation without remeshing as originally proposed in [73]. Finally, the effect of the neighboring fiber breakages on the longitudinal failure is discussed based on a statistical model accounting for the statistical distribution of fiber strength.

1.4 Layout of the dissertation

In this section (Section 1), the characteristics of fiber reinforced polymer based composites have been discussed for a general reader not familiar with this material system. The literature related to the two specific failure modes was reviewed to give the current state of understanding of this field and to point out the important issues remaining to be addressed. Following that, we presented the problems to be investigated in the current dissertation and outlined the approaches to address the problems.

In Section 2, the obtained results concerning failure mechanisms under transverse tension are presented. Most of the discussion is based on the published work by the author in 2018 [74]. In this section, two plausible debond crack link-up scenarios are investigated. For each scenario, inter-fiber distance is varied in order to assess the effects of neighboring fibers on investigated debond link-up scenarios. Experimental results from existing literature are also considered to evaluate the obtained results.

Section 3 discusses the failure mechanisms of UD composites under longitudinal tension. Most of the discussion is based on the published work by the author in 2016 [75]. Results presented in this section clarify the roles of fiber/matrix interface debonding and matrix cracking on the failure process, the two important aspects that are often ignored in the literature.

In the final section (Section 4), major conclusions from the dissertation research are presented and recommendations for future research are made.

2. FAILURE MECHANISMS OF UD COMPOSITES UNDER TRANSVERSE TENSION*

2.1 Introduction

As discussed in Section 1, the microscopic observations reveal that the macro-sized transverse crack is indeed formed by the link-up of individual fiber/matrix interfacial debonds, which is not well understood and often overlooked. As a result, in this section, we will try to clarify the failure mechanisms of UD composites under transverse tension with focus on investigating the link-up process of individual debonds. Two most likely link-up scenarios are discussed: 1. where one fiber is debonded and subsequent debond growth and kink-out induces debonding of a nearby fiber, and 2. where multiple debonds are present in close vicinity and the linking between each other. To achieve completeness, a brief discussion on the initiation of fiber/matrix interfacial debonding is also presented based on the reported literature results.

2.2 Initiation of fiber/matrix interface debonding under transverse tension

For composites, it is well recognized that fiber/matrix interface plays an important role in the overall transverse failure process. Numerous research efforts have been devoted in order to clarify the exact mechanism for the initiation of fiber/matrix

*Part of this section is reprinted with permission from Zhuang, L., R. Talreja, and J. Varna, "*Transverse crack formation in unidirectional composites by linking of fibre/matrix debond cracks"*. Composites Part A: Applied Science and Manufacturing, 2018. **107**: p. 294-303. Copyright 2018 by Elsevier.

debonding, apart from the obvious poorly bonded fiber/matrix interface during manufacturing process. As one of the most logical starting points, the fiber/matrix interface strength has always been a focus by various studies. The approach assumes that fiber/matrix interface debonding initiates when the local stress at a point of fiber/matrix interface exceeds its strength. HobbieBrunken et al. [76] conducted both experimental and numerical analysis and concluded that fiber/matrix interfacial normal strength governs failure under transverse tension and provide its measurement based on in-situ observation of damage initiation in 90° plies of a cross-ply laminate. Besides strength-based approach, another typical way to study this issue is by using Finite Fracture Mechanics (FFM) where the initiation of fiber/matrix interfacial debonding is governed by a stress and energy criterion. Some of the FFM examples could be found in [26, 77]. With the development of computational techniques, Cohesive Zone Modelling (e.g [78, 79]) becomes a popular FE tool to investigate the onset of interfacial debonding where the debonding process is modelled as the separation of elements when the stress and energy criterions are both met.

Based on the discussion above, one would expect the improvement on fiber/matrix interfacial properties should be the key to increase transverse strain to failure of a UD composite, as the strength and fracture toughness of fiber/matrix interface both improve. However, it is proven that the transverse failure strain of a UD composite remains low and often in a range of 0.4% ~ 0.6% regardless of the improvement of fiber/matrix interfacial properties. Such results indicate that approaches

discussed above might not properly capture the actual mechanism of fiber/matrix interface debonding in a composite material.

In 1995, Asp et al.[23] conducted an poker-chip test on typical epoxy matrix materials and found that the strain to failure of epoxy under poker-chip test (equi-triaxial tension) was much lower (0.5% ~0.8%) than that under uniaxial tension (1.8% ~7%). They suggested that micro-cavitation is the main mechanism for epoxy failure at lower strain level under equi-triaxial loading. For fiber reinforced composites, because of the constraint of stiffer fibers, the stress state near fiber/matrix interface is always triaxial regardless of the loading. As a result, Asp et al. [24] further postulated that under equi-triaxial or nearly equi-triaxial stress state, cavitation occurs when the critical value of dilatational energy density exceeds and results in the initiation of matrix crack, as shown in Figure 2.1. The same authors further applied this critical dilatational energy density criterion for prediction of transverse failure in a glass-fiber UD composite [25] and achieved good agreement with experimental results. In this scenario, fiber/matrix interface debonds as a result of unstable growth of nearby cavitation induced matrix cracks into interface.

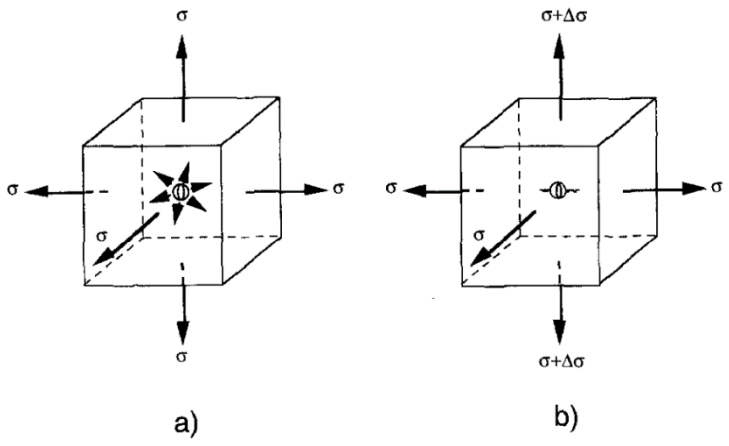

Figure 2.1 Illustration of cavitation and matrix cracking under a) equi-triaxial stress state where star like matrix crack forms as a result of cavitation and b) matrix crack resulting from cavitation grows perpendicular to dominant principal stress direction. (Figure reprinted from [24])

The idea of cavitation induced matrix cracking has gain more and more recognitions within composites research community in recent years and is further supported by a most recent work in [80] where the authors found tri-axial stress state governs epoxy cavitation using Molecular Dynamic (MD) simulation. However, it should be noted that cavitation induced matrix cracking still represents a particular scenario in composites and no experiment has confirmed this postulation due to obvious difficulty to conduct experiment under such small scale. As a result, it's fair to conclude that the exact mechanism for fiber/matrix interface debonding onset is still up to debate and we will leave it here and proceed to discuss the link-up of individual debonds in the following section.

2.3 Transverse crack formation by linking of individual fiber/matrix debonds

2.3.1 Scenario I: One pre-existing fiber/matrix debond

2.3.1.1 FE model description and validation

The finite element (FE) model adopted in this study is shown in Figure 2.2a. Due to the symmetry, only half of the region is shown. As seen in the figure, the central fiber is debonded on one side with the center of the arc-shaped debond crack lying on the horizontal tensile load axis. The debonded fiber is surrounded by six fibers placed in a hexagonal pattern. The circular region of seven-fiber assembly is embedded in a homogenized composite of rectangular outer boundary. The homogenized composite in a FE model is of importance as Pupurs and Varna [81] found that the ignorance of it would lead to significant errors in ERR calculation of debond under longitudinal tension. The distance between the surfaces of the central fiber and the neighbouring fibers, denoted *ID,* is varied in order to study the effects of inter-fiber spacing. The fiber radius r_f = 4μm and the radius RMO of circular matrix region (Figure 2.2a) are chosen such that the fiber volume fraction V_f within this region equals to the global fiber volume fraction of the composite. The half-height and the width of the model are chosen as H=20×RMO and W=40×RMO, respectively, beyond which the calculated ERR of the debond crack is taken not to be affected by the size of the model.

As shown in Figure 2.2a, the x-displacement is applied uniformly to the right edge (x = W) of the model, while it is constrained on the left edge, to induce the strain ε_x = 0.5%. 2-D quadratic plane strain elements (PLANE 183) were adopted in the FE model and in addition to that, contact elements were generated on the debond surface in

ANSYS. For the FE models adopted in the present study, each one has around 200,000 ~ 260,000 elements generated. The ERR is calculated by the virtual crack closure technique (VCCT) using the ANSYS FE software [82]. It has been well documented that for an interface crack between two dissimilar materials (here: debond), Mode I and Mode II components of the ERR are not well defined [71, 83-85]. As a result, the calculated ERR modes here depend on the size of the near tip element. Figure 2.2b shows the typical mesh near debond tip adopted in the current study where uniform quadrilateral element were generated ahead and behind the debond tip. The size of the near tip element is $r_f \cdot d\theta$. In the present study, the dependence of obtained ERR on element near tip element size was investigated and obtained normalized ERR (ERR / G_0) results for debond angle θ=10° are shown in Figure 2.3. For full expression of G_0, readers can refer to [40]. From Figure 2.3 it is shown that G_I and G_{II} tend to converge as element size decreases, similar finding has also been reported in [83]. As element size increases, the obtained ERRs becomes more constant. As a result, in the present study, the element size of $d\theta$ = 0.5° was selected. To validate the present FE model, the obtained ERR results based on this element size is compared with ERR results calculated by Boundary Element Method (BEM) in [40] for a single glass-fiber composite case. To simulate the single fiber case, the four fibers surrounding central fiber, as well as the effective composite were replaced with matrix properties. The comparison results are shown in Figure 2.4, the obtained ERR was normalized with G_0 (3.38J/m^2) to be consistent with results shown in [40]. As displayed in Figure 2.4, the

ERR obtained by current model agrees well with the one obtained by BEM, which validates the accuracy of present FE model.

The material system used in the present study is carbon fibers in an epoxy matrix with volume fraction V_f =0.6. The elastic material properties for each constituent are displayed in Table 2.1. The transverse properties of carbon fiber were estimated based on the discussions in [3-5]. In order to generate a preferred failure initiation site in the composite, two different values of the inter-fiber spacing were chosen as: *IDn* (*ID/rf*) =0.15 and *IDn*=0.35 (as a reference, the inter-fiber spacing in a uniform hexagonally packed UD composite of V_f =0.6 is IDn≈0.48), which could be consider as a local cluster of fibers where the interactions between fibers are significant. For Scenario I, we first investigated the pure mechanical loading case for generality followed by a discussion on thermal stresses effect.

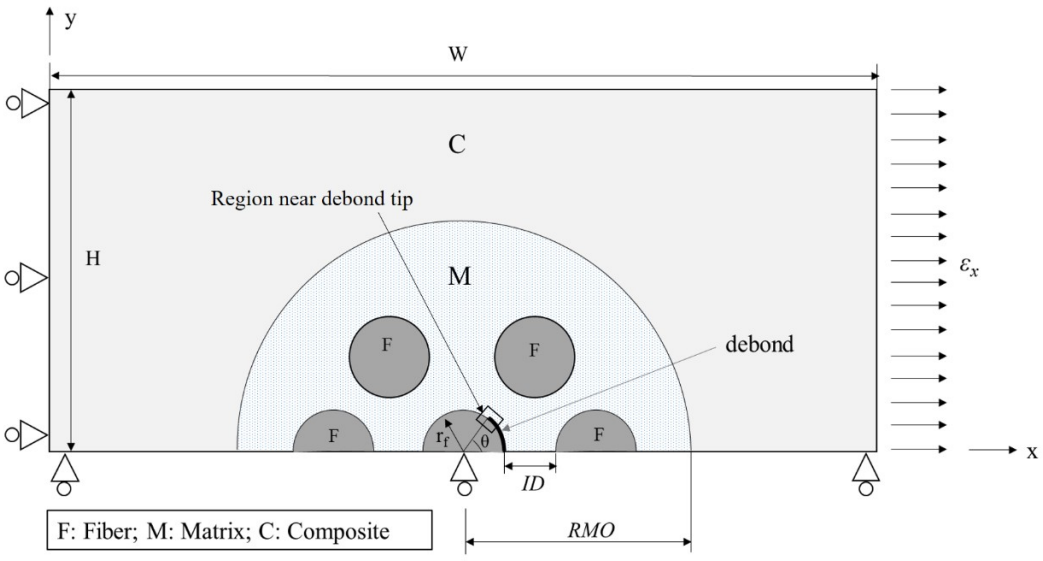

a)

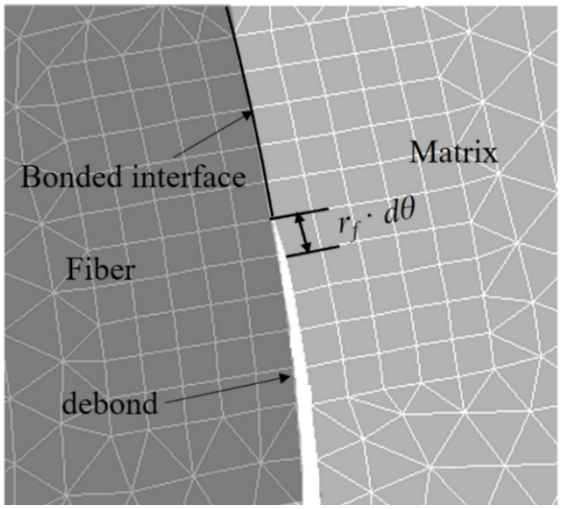

b)

Figure 2.2 a) The fiber/matrix interfacial debonding model b) Illustration of FE mesh near debond tip

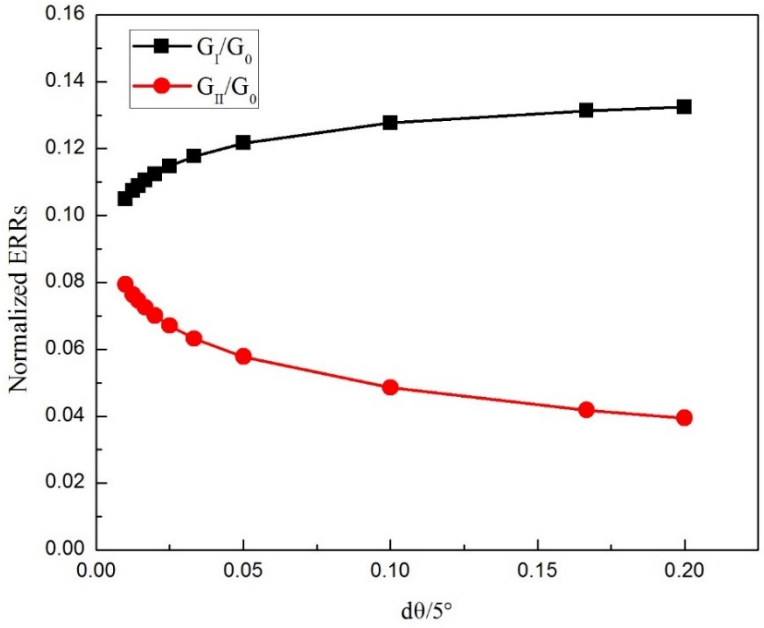

Figure 2.3 Influence of near tip element size on ERRs

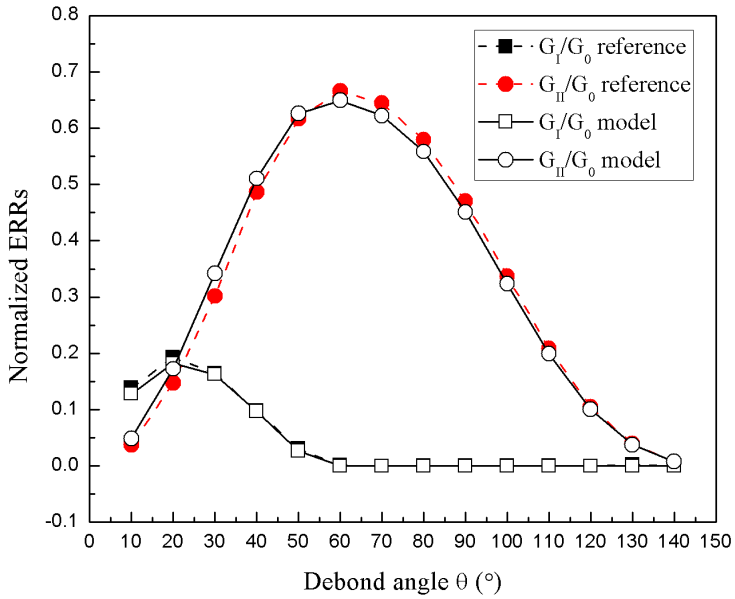

Figure 2.4 Comparison of obtained ERR results for a single fiber composite with numerical model in reference [40]

Table 2.1 Thermo-elastic properties of constituents

Material	E_1 (GPa)	E_2 (GPa)	υ_{12}	G_{12} (GPa)	υ_{23}	α_1 (1/°c)	α_2 (1/°c)
CF	500	30	0.2	20	0.45	$-1\cdot10^{-6}$	$7.8\cdot10^{-6}$
Epoxy	3.5	3.5	0.4	1.25	0.4	$60\cdot10^{-6}$	$60\cdot10^{-6}$
CF/EP (V_f=0.6)	301.4	11.04	0.27	4.06	0.54	$0.66\cdot10^{-6}$	$35.85\cdot10^{-6}$

2.3.1.2 Debond growth along fiber/matrix interface

Once debond initiates, the debond growth along fiber/matrix interface was studied in the present section. Results for the two cases of *IDn* = 0.15 and 0.35 under pure mechanical loading ε_x = 0.5% are shown in Figure 2.5. As displayed in Figure 2.5,

all ERR of the debond crack are lower at closer inter-fiber spacing as a result of constraint effect of neighbouring fibers (see details in author's previous work in [86]). For both cases, the debond growth is in mixed-mode. Both Mode I ERR component (G_I) and Mode II ERR component (G_{II}) increase first and then decrease with increasing debond angle θ, and the same trend results for total ERR G_T ($G_T = G_I + G_{II}$). When debond crack grows to an angle $\theta \approx 70^o$, a finite contact zone is detected between two debond surfaces and G_I diminishes while G_{II} remains high. This angle is of interest with regard to the kinking of the debond crack, as suggested by the experimental observations [87] of debonding on the free surface and numerical computations[39] for a single-fiber composite. Based on these studies, it is reasonable to assume that even though the Mode II ERR is high beyond $\theta \approx 70^o$, the debond growth on the fiber surface is governed by the Mode I ERR and would therefore cease at this angle.

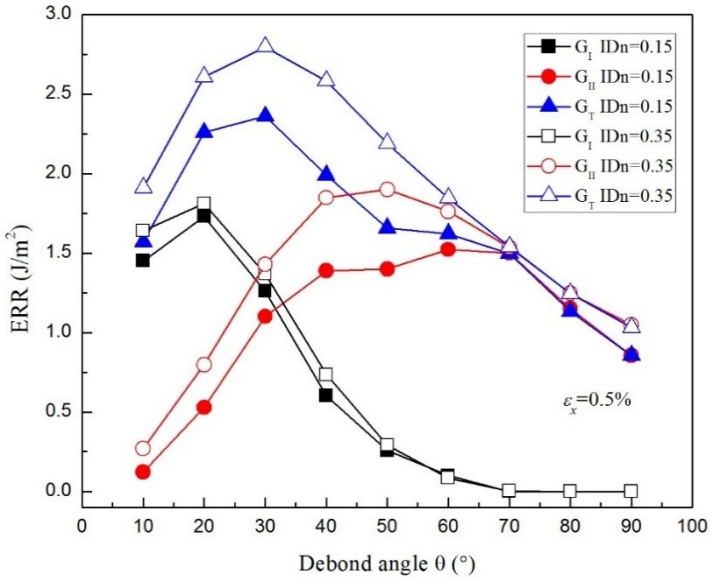

Figure 2.5 ERR of debond crack subjected to pure mechanical loading

To further explain the observed ERR behaviors, the relative radial displacement, i.e., radial separation, of the two debond surfaces, is shown in Figure 2.6 for different debond arc angles θ at *IDn*=0.15. As seen in the figure, for larger angles (θ>30°), the radial surface separation towards the debond crack tip decreases, indicating a closing action. At θ=70°, the debond surfaces come clearly into contact and beyond this angle the contact zone increases with increasing debond angle. These results further support the ERR based inference, stated above, that beyond $\theta \approx 70^{o}$ the debond crack is not likely to grow.

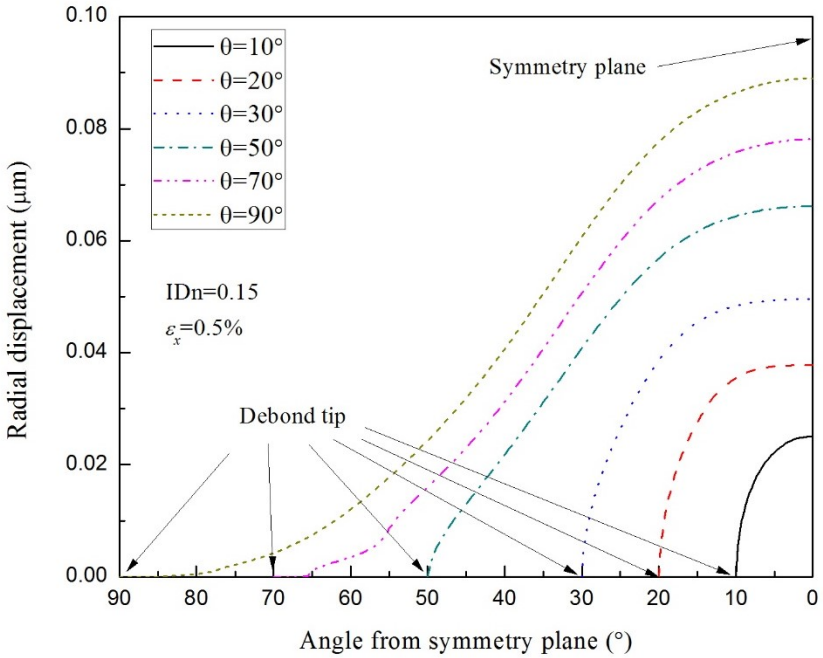

Figure 2.6 Radial separation of the debond crack surfaces at different θ

2.3.1.3 Crack kinking from fiber/matrix interface

In the previous section we have discussed the debond growth along fiber/matrix interface. However, debonds by itself would not form a macro-sized transverse crack. As found by numerous experimental studies such as [30, 31], the macro-sized transverse crack is formed by the coalesce of individual debonds through matrix cracking. As a result, in this section, we will discuss the potential debond crack kinking towards matrix from fiber/matrix interface.

Figure 2.7 illustrates the FE model used to investigate the potential debond crack kinking. For interface crack between two dissimilar material, He and Hutchinson [88] suggested that the interface crack tends to kink towards more compliant material, which is the matrix in the present study. The condition for kinking, however, depends on the resistance for either debond growth or debond kinking or the available driving force for either case. As a result, in this section, ERR for both kinked crack and debond will be discussed as the driving force for debond kinking and growth, respectively. The geometry indicated in Figure 2.7 is the same as in Figure 2.2a. For each debond angle θ, a kinked crack of length L=0.04r_f is assumed to emanate from debond tip and grow towards matrix in an angle θ_k with respect to the horizontal axis of the model. The kinking angle θ_k is determined based on the maximum energy release rate criteria: i.e. crack is assumed to kink out of interface in a direction that maximizes the ERR of kinked crack. As discussed by He and Hutchinson [88], the selection of initial kinked crack length is of great importance: too small of a selection would result in strong oscillation on obtained ERR. As a result, a case study on the influence of chosen kinked

crack length on obtained ERR in present model was conduct for *IDn* =0.35 and results are shown in Table 2.2. For the crack lengths considered in Table 2.2, there is only a small variation on the obtained ERR, more importantly, the trend for predicting ERR remains the same, as well as the predicting kinking angle. As a result, given the need for easier FE model meshing, larger kinked crack length L=0.04r_f is adopted in the present study to investigate the crack kinking. In the present study, no contact element was applied to the kinked crack surfaces as: 1. earlier study by Whitcomb [89] found that total energy release rate obtained from non-contact analysis agrees well with that of contact analysis when the crack tip surfaces are in contact and 2. it was found that there is no contact between kinked crack surfaces in all cases investigated. A convergence study was performed before obtaining any ERR results.

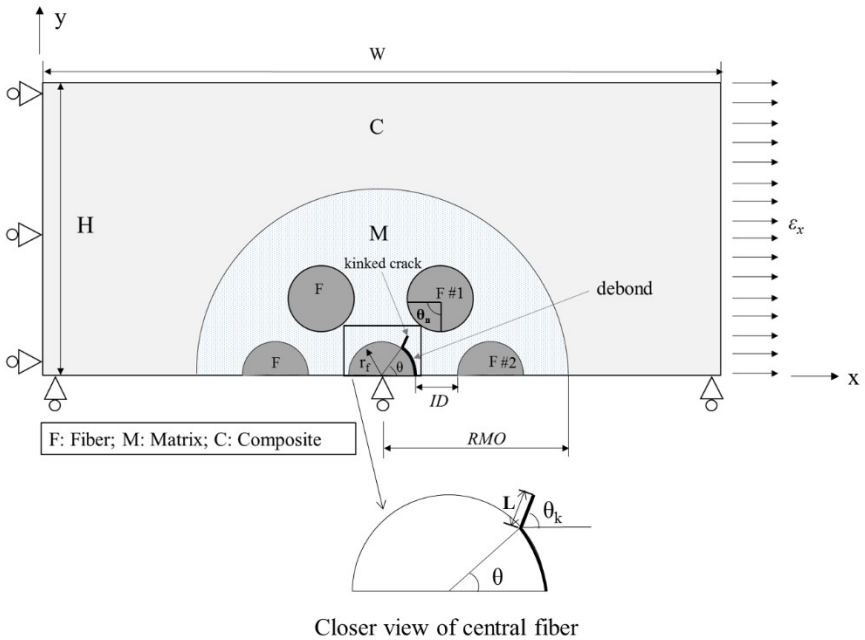

Figure 2.7 Illustration of crack kinking model

Table 2.2 Effect of assumed kinked crack length L (ε_x = 0.5%, *IDn*=0.35)

θ (°)	G_T (J/m^2)			
	L=0.005r_f	L=0.01r_f	L=0.02r_f	L=0.04r_f
20	3.9585	3.8434	3.7376	3.6644
30	4.9977	4.8055	4.5855	4.3292
40	5.2257	5.0566	4.8227	4.4803
50	4.7229	4.6329	4.4868	4.1983
60	4.0498	4.0028	3.9335	3.7628

Figures 2.8 and 2.9 display the obtained ERR for the kinked crack and the debond for two different inter-fiber spacing cases. For both cases, the potential kinking angle θ' is found to be between 75º ~ 95º for all the debond angles studied and increases with increasing debond angle. Once again although we only consider pure mechanical loading in the present studies.

As shown in Figure 2.8, although we predict the crack kinking based on the maximum energy release rate criterion, the obtained ERR of kinked crack indicates that debond crack tends to kink out of interface in pure Mode I. This is a well-known result which has also been found by other studies [75, 90]. From Figures 2.8 and 2.9 it is found that the ERR of kinked crack reaches its maximum value at $\theta \approx 30^o$ for *IDn*=0.15 and $\theta \approx 40^o$ for *IDn*=0.35. It should be note that Paris et al [39] found the debond angle for maximum ERR of kinked crack is between $\theta = 60^o$ and 70º for a single fiber composite. Such difference between present study and a single fiber composite case clearly demonstrate the influence of neighboring fibers. However, if one considers single fiber composite as large inter-fiber spacing to approach this case, a closer look at the results

would suggest that the debond grows further before kinking out of the interface as the inter-fiber spacing is increased.

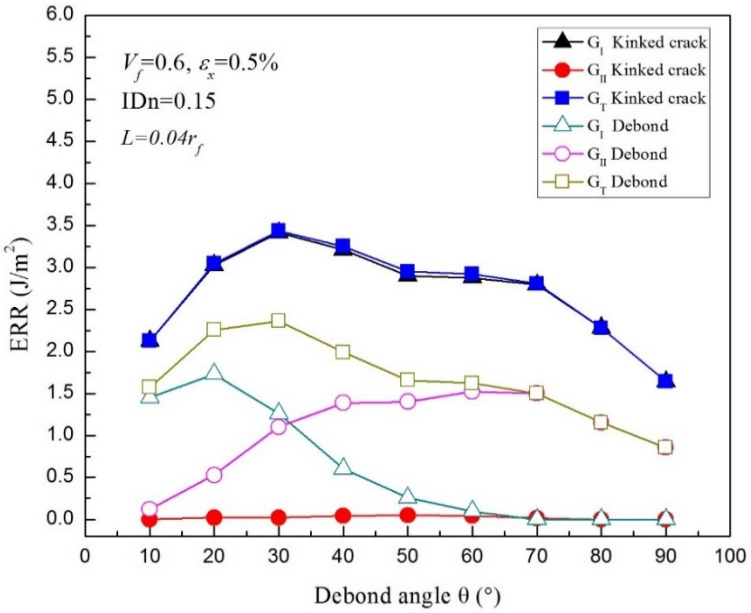

Figure 2.8 Comparison of ERR between kinked crack and debond for IDn=0.15

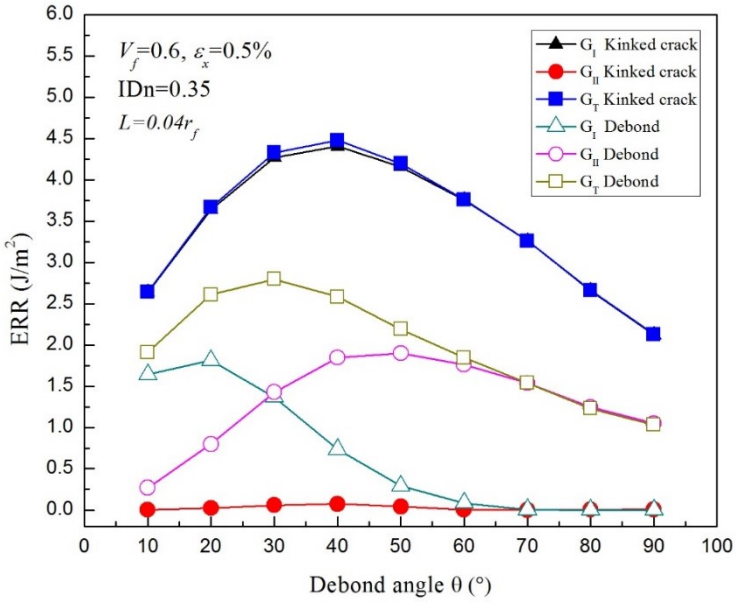

Figure 2.9 Comparison of ERR between kinked crack and debond for IDn=0.35

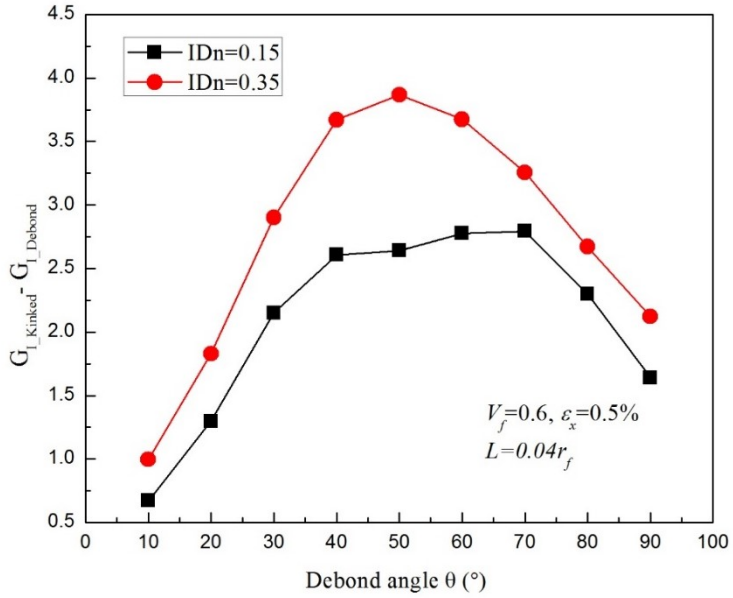

Figure 2.10 Difference in Mode I ERR between kinked crack and debond

A closer look at Figures 2.8 and 2.9 shows that the maximum ERR of kinked crack occurs when the Mode I component of debond is decreasing. The difference of Mode I ERR between kinked crack and debond increasing as debond angle increases until debond closes. This could be demonstrated better in Figure 2.10. As displayed in Figure 2.10, the difference of Mode I ERR between kinked crack and debond increases significantly when the ERR of kinked crack reaches the maximum value, indicating the highest tendency for kinking. As a result, it is reasonable to suggest that debond crack would most likely to kink out at a smaller debond angle compared to that in a single fiber composite. This conclusion is supported by a most recent microscopical observations [91] where the authors found the debond angle when kinking occurs are generally smaller in 90° layers of a cross-ply laminate than that in a single fiber composite. Their results are shown in Figure 2.11 for better demonstrate where θ_d is the debond angle when kinking occurs.

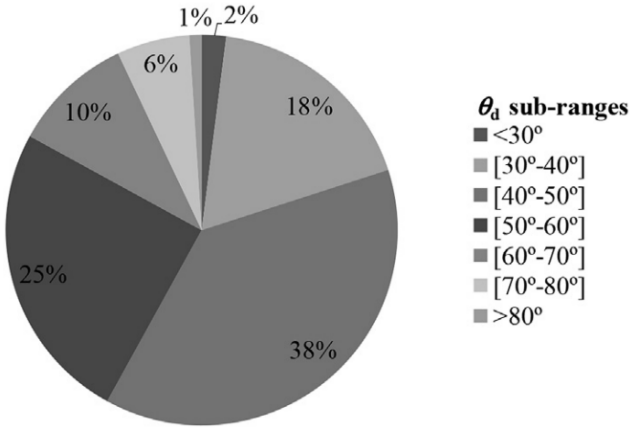

Figure 2.11 θ_d distributions based on experimental observation. (Figure reprinted from [91])

2.3.1.4 Matrix crack propagation and induces debonding in a nearby fiber

After the debond crack kinking, the propagation of the kinked crack towards neighboring fibers is simulated based on a procedure similar to the previous determination of the kinked crack: once the original kinked crack (denoted as "first kink") is determined, the direction of the following kinked crack propagation is based on the maximum energy release rate criterion, the same procedure continues until kinked crack propagates near neighboring fibers. In the present study, we assume debond to kink out of interface when the ERR of the kinked crack is the maximum and study three different step of propagation of matrix crack including first kink. Two different inter-fiber spacing cases are considered. The predicted kinked crack path towards neighboring Fiber #1for IDn=0.35 is shown in Figure. 2.12. Similar to the discussion in Section 2.3.1.2, kinked crack tends to propagate towards neighboring fiber in pure Mode I. It is found that the crack tends to propagate along the similar direction as kinking up to a certain length when the influence of nearby fiber is not too significant. The crack propagation process is stable as the ERR of kinked crack decreases as crack propagates which due to the constraint of neighboring fiber. This is a different result compared to the ones obtained using single fiber composite model [39] and it once again highlights the importance of neighboring fibers' influence. As shown in Figure. 2.12, when the kinked crack approaches the neighboring fiber, instead of propagating directly towards it, it diverts and tends to reach the neighboring fiber at a certain angle as a reflection of the complex stress field near neighboring fiber.

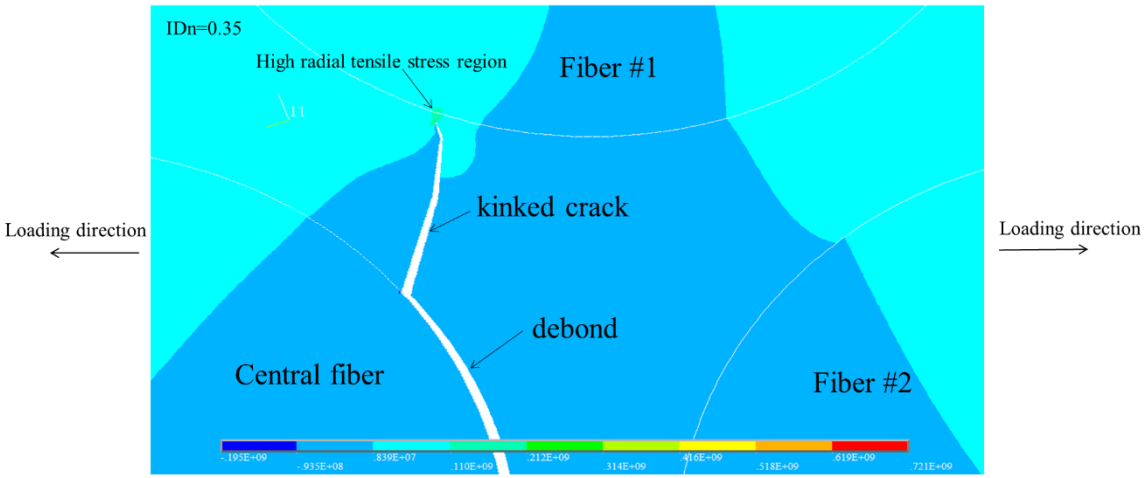

Figure 2.12 Predicted matrix crack and radial stress along Fiber#1 interface. (IDn=0.35, θ=40º)

Figure 2.13 display the normalized radial stress distribution (local radial stress / far field transverse normal stress) along the interface of Fiber #1 during kinked crack propagation (θ_n is indicated in Figure 2.7 and is positive clock-wise along Fiber #1). As shown in Figure 2.13, when the kinked crack gets closer to Fiber #1 (third kink) as indicated in Figure 2.12, a small region close to kinked crack tip with very high radial tensile stress developed in Fiber #1 and is increasing as kinked crack approaches, this localized high radial tensile stress, if reaching the critical value to break the bonds of fiber/matrix interface, will initiate fiber/matrix debonding process in Fiber#1. Investigation from [92] indicates that, once a new debond initiates in Fiber #1, it will immediately propagate along fiber/matrix interface close-wise and debond kinking process would also occur in Fiber#1 if the correct conditions are met. The repeat of the whole process will eventually become unstable which leads to the formation of macro-sized transverse crack. The similar failure process could be drawn for the case *IDn*=0.15

and is shown in Figure 2.14 and the experimental observations that match the whole debond linking process discussed above could be found in [93] (shown in Figure 2.15).

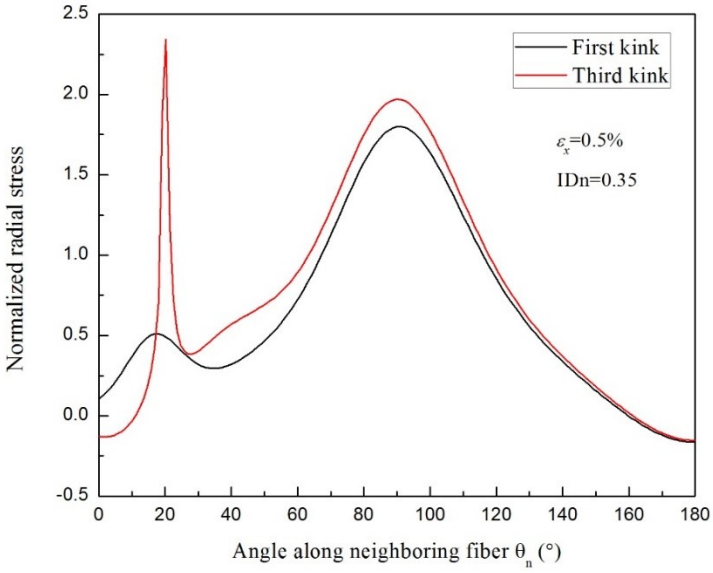

Figure 2.13 Radial stress distribution along interface for Fiber#1

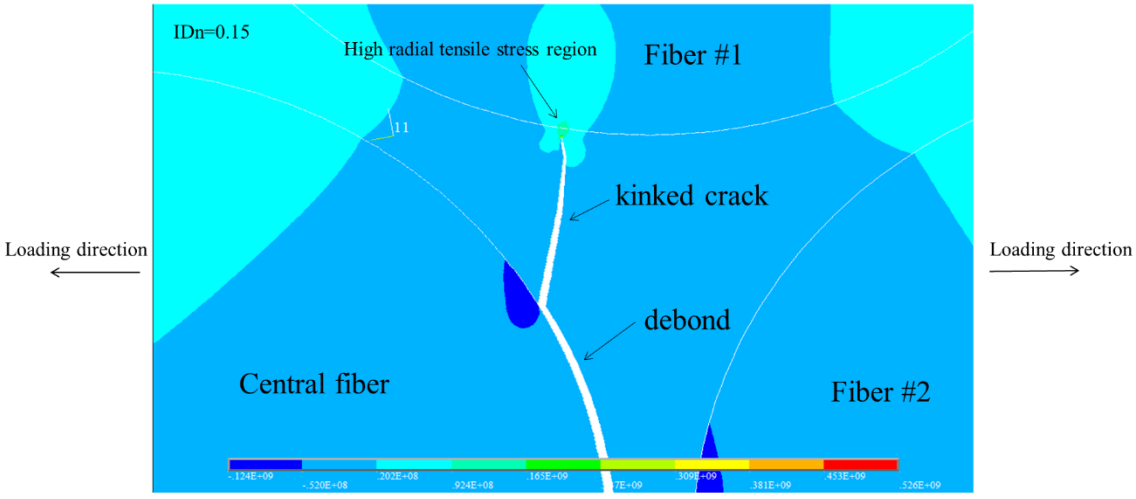

Figure 2.14 Predicted matrix crack and radial stress along Fiber#1 interface. (IDn=0.15, θ=35º)

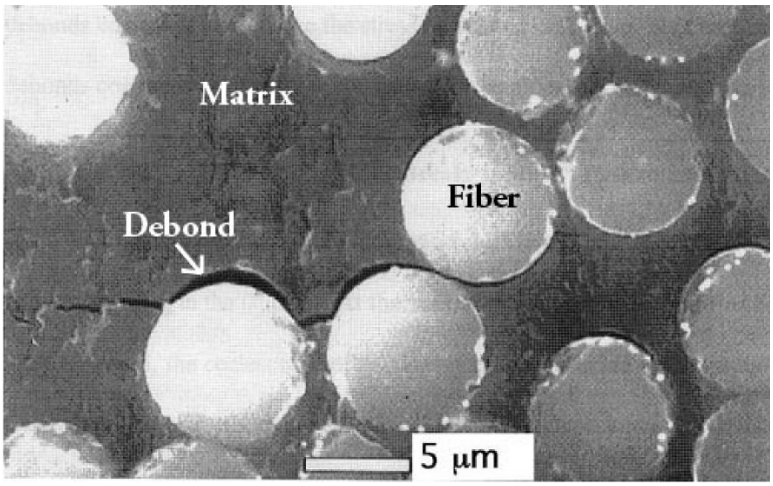

Figure 2.15 Scenario I typed debond link-up process (Figure reprinted from [93])

Finally, as indicated by the analysis above, for *IDn* = 0.15, the ERR values of debond and kinked cracks are lower for this spacing compared to those for *IDn* = 0.35 (see Figures. 2.8, 2.9 and 2.10), which suggests that the transverse crack formation in this scenario is more difficult as the inter-fiber spacing decreases.

2.3.1.5 Effects of thermal stresses

So far, we have investigated Scenario I based on pure mechanical loading in order to keep generality of the case. However, as discussed in the introduction section, processing of carbon/epoxy composites often involves cooldown from the curing temperature, it would be interesting to see the effects of local thermal stresses generated by cooldown process on the failure process discussed above. The effect of thermal stresses on single debond growth along interface has been studied by the same authors in

[86] and it is found that the presence of thermal stresses has a protective effect (reduce ERR of debond) on debond growth in a UD composite due to the overall compressive stress developed due to thermal cooldown. In this section, we continue to investigate the effect of the local thermal stresses on crack kinking.

To account for thermal stresses, A temperature change of ΔT = -100°C was applied uniformly to the model (Figure 2.7) and was followed by a uniform displacement at $x = W$ to result in the mechanical strain $\varepsilon_x = 0.5\%$. The residual stress field induced by chemical shrinkage due to curing was, however, not included directly. As shown in [94], the thermal cooldown is the main contributor to the development of residual stresses and in a linear thermo-elastic analysis the effect of chemical shrinkage can be formally included as a part of thermal stresses by taking a higher stress free temperature [95]. We selected the case of inter-fiber spacing *IDn* = 0.35 to demonstrate the thermal stresses effect.

Figure 2.16 shows the variation of ERR of kinked crack for pure mechanical loading and thermo-mechanical loading cases. The debond angle varies from $\theta = 10°$ to $\theta = 70°$ when crack kinking is not likely to occur as debond tip closes (see Figures 2.5 and 2.6). The definition of the kinked crack is the same as discussed in Section 2.3.1.2. from Figure 2.16 it's found that at small debond angle (up to θ=35°), the presence of thermal stresses reduces Mode I ERR of kinked crack. For larger debond angle (θ =35°-70°), it increases the Mode I ERR of kinked crack. It should be noted that despite the switch of trend with the increase of debond angle, the predicted potential kinking angle θ_k is found to be similar with or without the thermal stresses. Meanwhile, the observed

trend in Figure.2.16 could be explained by looking at the σ_{xx} distribution in matrix material surrounding the central fiber (Figure 2.17) after cooldown (before mechanical loading is applied) when no damage is assumed to exist. As shown in Figure 2.17, σ_{xx} in the matrix around central fiber is negative (compression) at a small angle and then becomes positive (tension). Since crack kinking direction is almost perpendicular to the loading direction (see discussion in Section 2.3.1.2), negative thermal stress component σ_{xx} is expected to inhibit the opening of kinked crack, which reduces the Mode I ERR of kinked crack, and vice versa.

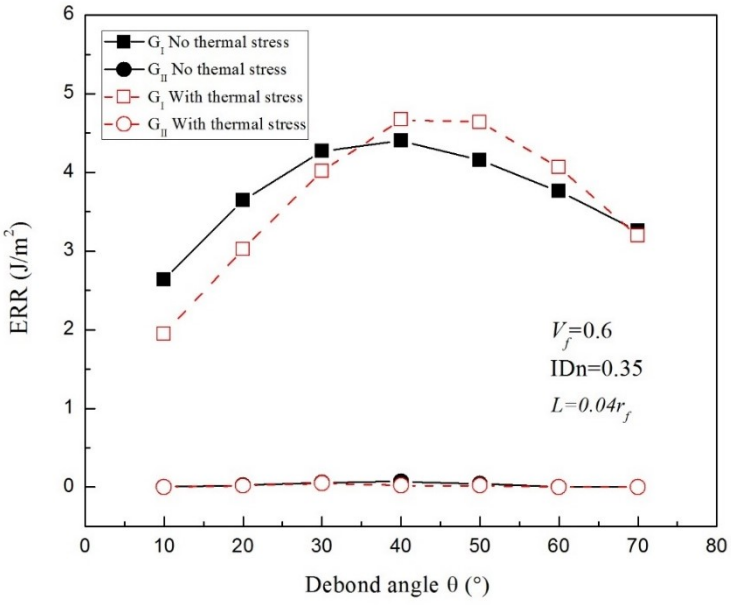

Figure 2.16 Variation of ERRs of kinked crack for pure mechanical and thermo-mechanical cases

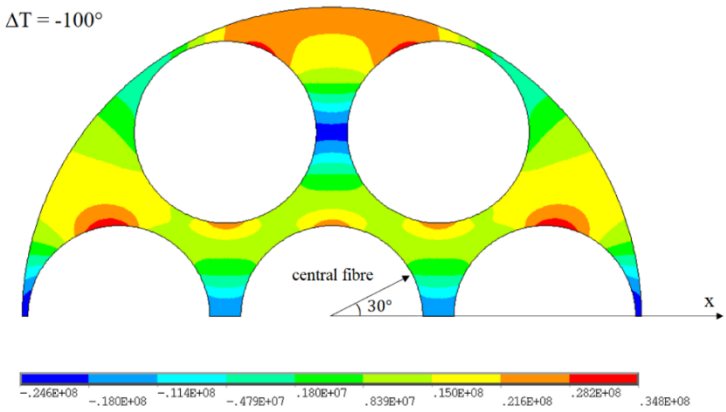

Figure 2.17 Thermal stress σxx distribution in matrix material surrounding central fiber after cooldown

2.3.2 Scenario II: Transverse crack formed by the link-up of nearby debonds

In Section 2.3.1, we have discussed the formation of macro-size transverse crack initiates from single fiber/matrix interfacial debond. It's also possible that multiple debond initiates before kinking of debond takes places. Several reasons could contribute to the initiation of multiple debonds in a short period of time. For example, it could be a result of poor fiber/matrix interfacial bonding, which allows thermal stresses to cause substantial amount of fiber/matrix interfacial debond even before the external load is applied [96] (Figure 2.18), or as a result of stress concentration within clusters of fibers when subjected to loading. As a result, it is of great importance to clarify the linkup process of individual pre-existing debonds. In order to simplify the problem, we only investigated the scenario of two debonds in the present study.

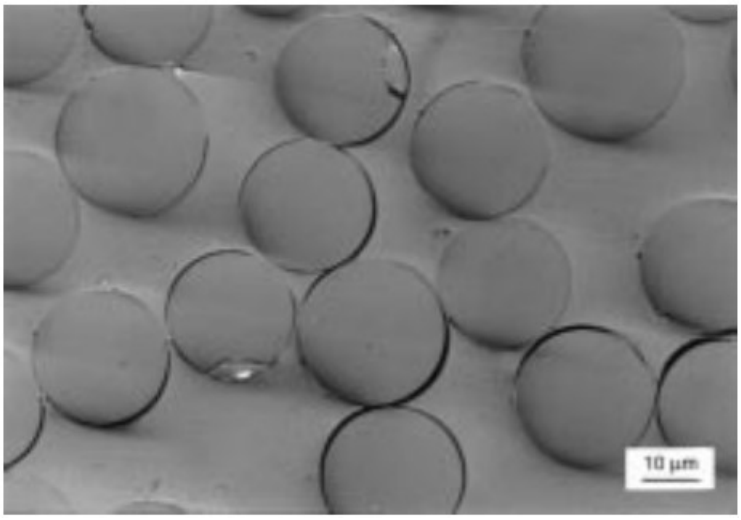

Figure 2.18 Cooldown induced debonds in a close vicinity (Figure reprinted from [96])

2.3.2.1 Fiber/matrix interfacial debond growth with presence of a nearby debond

Before we proceed to discuss the influence of a nearby debond, we first define two cases we will be investigating in the present study as indicated in Figure 2.19:

Case I: A nearby fiber/matrix debond at left side of Fiber #1 together with the central debond;

Case II: A nearby fiber/matrix debond at the right side of Fiber #3 together with the central debond.

For each case, the nearby debond size is characterized by its half angle θ' which equals to 60° to represent a nearly fully propagated debond. And we'll investigate the effects of nearby debond on central debond propagation as well as kinking process.

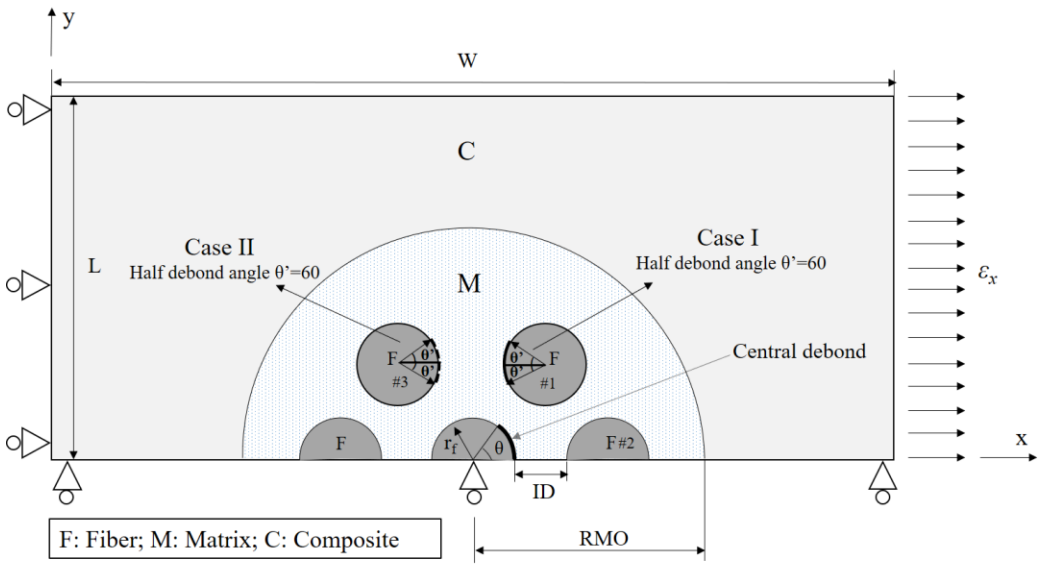

Figure 2.19 Illustration of the two debonds model

In Case I, the two debond cracks are closer than in Case II, and that would suggest that Case I is more favourable to transverse crack formation. However, since in mutual interaction of cracks, both crack tip stress field enhancement and shielding are involved, we consider both cases to gain a fuller understanding of the transverse crack formation process. The parameters of the FE models adopted for this section are the same as those shown in Figure. 2.2a except for the addition of the nearby debond. We once again focus on the mechanical loading first and consider two different inter-fiber spacings*: IDn*=0.15 and *IDn*=0.35.

Figures 2.20 and 2.21 show the obtained G_I and G_{II} of central debond in two-debond scenario and single-debond scenario discussed in the previous section. From Figures 2.20 and 2.21 it's shown the presence of a nearby debond increases the ERR of central debond significantly, and that enhancement intensifies with the decrease of inter-

fiber spacing. This is due to the interactions between two debond tips and the relaxation of the nearby fiber constraint with the presence of debond. In the present study, we also found that for the case of a smaller nearby debond angle θ'=5°, the ERR of the central fiber also increases, however, that increase is less significant and thus we chose not to include this case in the present dissertation. The peak for G_I of *IDn*=0.15 in Case I is mainly due the strong interaction between two debond tips, as displayed in Figure 2.22. That strong interaction also delays the closing of central debond tip as indicated by Figure 2.20. Meanwhile, although we did not present in the current, it does worth mentioning that the ERR of the two nearby debond crack tips especially for the one closer to central debond also increases with the increasing of central debond size.

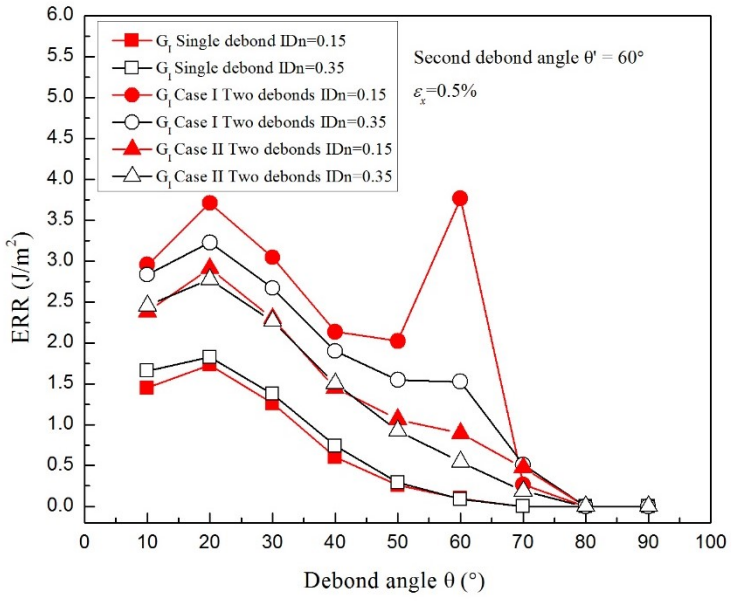

Figure 2.20 Comparison of GI of central debond between single debond and two-debond case

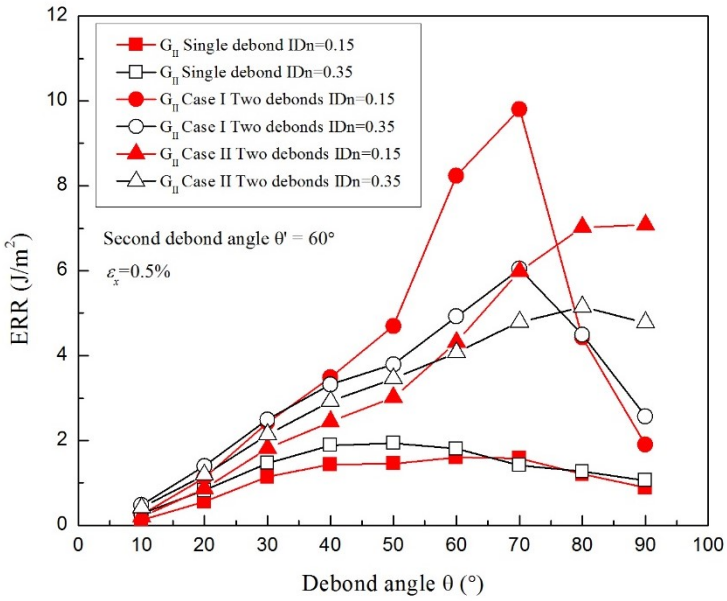

Figure 2.21 Comparison of GI of central debond between single debond and two-debond case

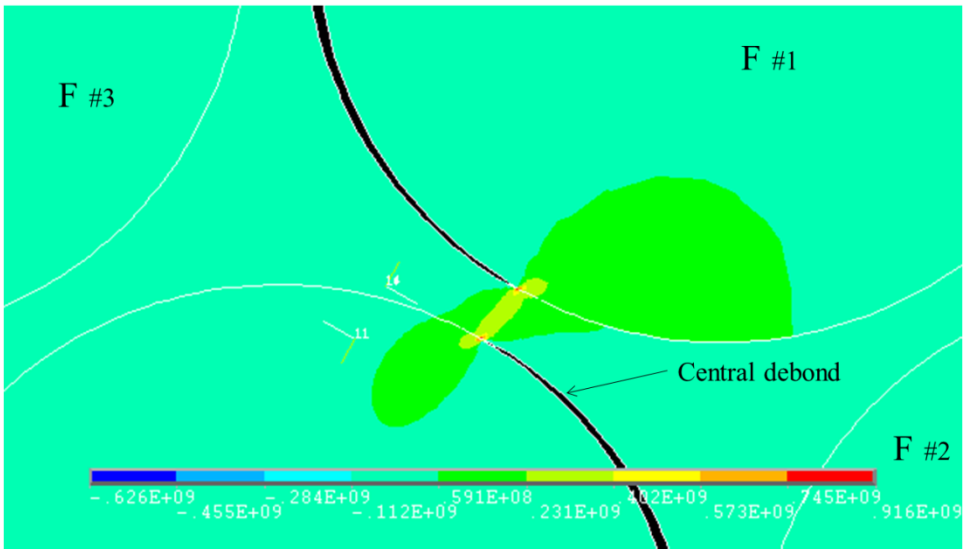

Figure 2.22 Illustration of θ=60° situation. IDn=0.15 (radial stress in central fiber is shown in this figure)

Based on the above findings, it is suggested that for two debonds that grows simultaneously, if inter-fiber distance are small enough, instead of kinking of link-up together, these two debonds might stay within corresponding interfaces. This situation has been captured by Romanov et al. [31] experimentally and is displayed in Figure 2.23 for illustration.

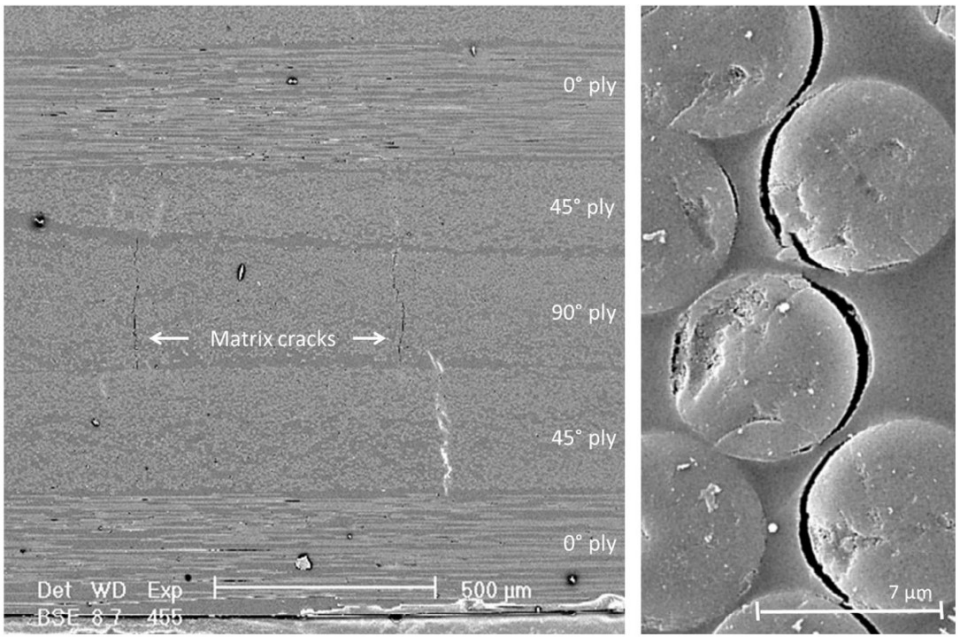

Figure 2.23 Debonds stay within interface (Figure reprinted from [31])

2.3.2.2 Crack kinking with the presence of a nearby debond

We have now known that presence of a nearby debond would enhance central debond growth based on the discussion above. It's interesting to see how it would affect the kinking process of central debond. Similar procedure as discussed in section 2.3.1.2 has been adopted with kinked crack length L chosen as $0.04r_f$.

Figures 2.24 and 2.25 display the obtained ERR results for kinked crack and compared them with those of corresponding debond. From Figures 2.24 and 2.25 it's shown that the ERR of kinked crack increase with decreasing inter-fiber spacing and the ERR of kinked crack in Case I is higher than the one in Case II of the same inter-fiber spacing as central fiber is closer to the nearby fiber in Case I. If we compare results shown in Figures 2.24 and 2.25 with results displayed in Figures 2.8 and 2.9, it is found that the presence of a nearby debond increases the ERR of kinked crack significantly, indication the positive effect on debond kinking process. Meanwhile, the debond angle where the ERR of kinked crack is maximum is also larger which due to the fact the larger the debond angle its, the closer kinked crack is to the nearby debond in Fiber#1.

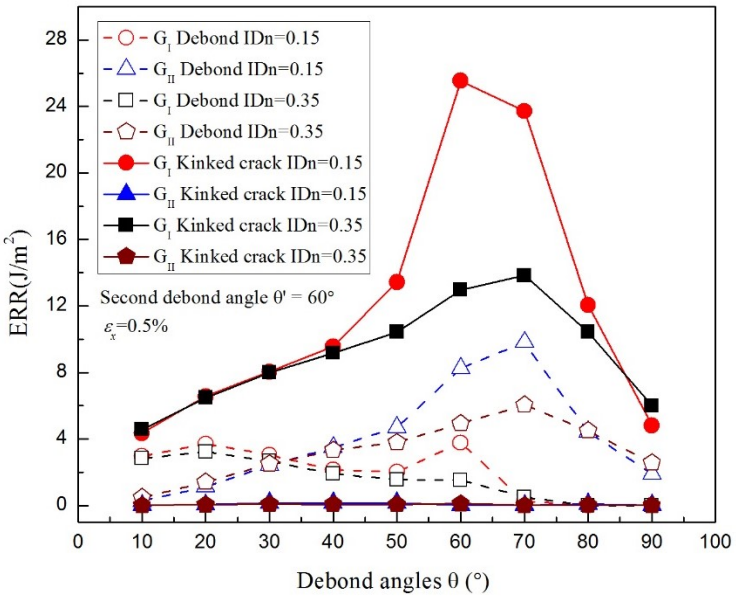

Figure 2.24 Comparison of kinked crack and debond ERR for Case I (L=0.04r_f)

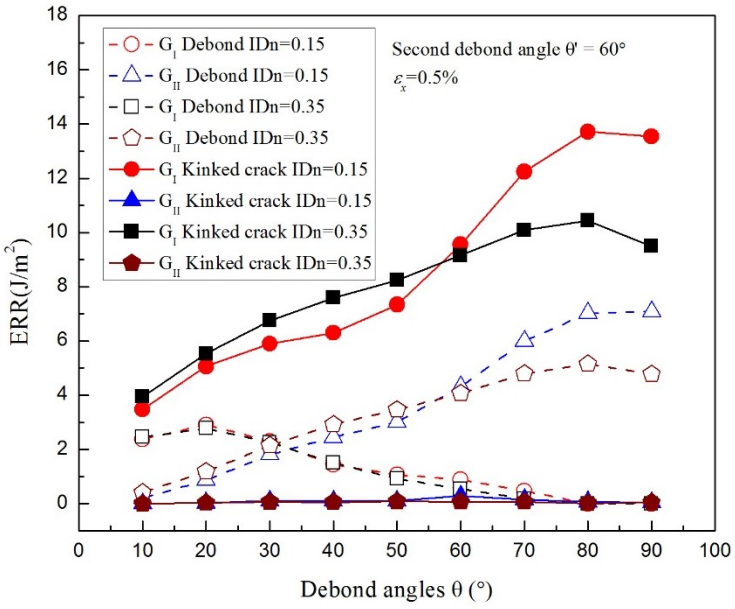

Figure 2.25 Comparison of kinked crack and debond ERR for Case II (L=0.04r_f)

As discussed in section 2.3.1.3, once debond kinked out of interface, the kinked crack propagates towards the neighboring fiber stably, which it's also valid for Case II in the two-debond scenario. However, it does not always hold for Case I as two debonds are closer. As shown in Table 2.3, for *IDn*=0.15, if we assume kinking occurs at θ=60° and compare the Mode I ERR of different kinked crack length L for single debond and two-debond case with nearby debond angle θ' =60° discussed in the present study as well as a case with intermediate nearby debond angle θ' =30°, it is very clear that kinked crack propagation is unstable when θ' =60°. Meanwhile, the results listed in Table 2.3 also suggest that when the second debond crack tip is closer to the kinked crack, it tends to intensify the growth rate of the kinked crack. On the other hand, when the

neighbouring fiber is fully bonded or insufficiently debonded, it dampens the growth of the kinked crack.

Based on the discussion in the present section, it's expected that if multiple debonds exist in the close vicinity of each other, the debond growth, kinking and final link-up process should be much faster compared to scenario I as the presence of nearby debonds increases the driving force for both debond growth and kinking and more importantly, that enhancement becomes more significant as the increase of debond size. This conclusion is also supported by the experimental work conducted by Sjögren and Berglund [96] as they found for the link-up of pre-existing debonds was very rapid and continued over only a limited strain range for glass fiber reinforced cross-ply laminates.

Table 2.3 Mode I ERR for different kinked crack length (*IDn*=0.15)

	Two-debond θ'=60°	Two-debond θ'=30°	Single debond
L	G_I (J/m^2)	G_I (J/m^2)	G_I (J/m^2)
0.04r_f	25.1437	6.1269	2.8772
0.08r_f	31.6954	5.6734	2.4617
0.12r_f	44.2344	5.1556	2.0195

2.3.2.3 Effects of thermal stresses

We are now investigating the effect of thermal stress on debond growth along central fiber/matrix interface and debond crack kinking. Following the same approach discussed in Section 2.5, a temperature change ΔT = -100°C was applied uniformly to the corresponding model and was followed by a uniform displacement at $x = W$ to

result in the mechanical strain $\varepsilon_x = 0.5\%$. In this section, we selected to investigate the case of inter-fiber spacing *IDn* =0.15 and results are presented in Figures 2.26 and 2.27.

As shown in Figure 2.26, the presence of thermal stresses show the same effect on debond growth as discussed in [86] : it reduces the ERR of debond in central fiber for both cases discussed in Scenario II but does not change the debonding behavior as the overall trend of ERRs remains the same. Regarding the thermal stresses effect on debond crack kinking, for Case I, the presence of thermal stresses reduces the Mode I ERR of kinked crack for all the debond angles studied. This result somehow contradicts to the result obtained for Scenario I (Figure 2.16), which could be contributed to the influence of the neighboring debond. The result for Case II displayed in Figure 2.27 could further support above assertion: for small debond angle, the influence of the neighboring debond is negligible and thus the influence of thermal stresses on kinked crack follows the same trend as the case in Scenario I (it reduces Mode I ERR of kinked crack first and then increases). As debond continue growing, the presence of neighboring debond is starting to be felt and now the presence of thermal stresses reduces Mode I ERR of kinked crack again, which is similar to Case I.

Based on the discussion in this section, it is clearly that the presence of thermal stresses would inhibit the debond growth in a UD composite, while its effect on debond kinking is more complicated, which depends on many factors such as the location of neighboring debond. However, despite the its influence on ERR, the presence of thermal stresses does not change the overall conclusions we drawn on debond growth and debond crack kinking based on pure mechanical loading.

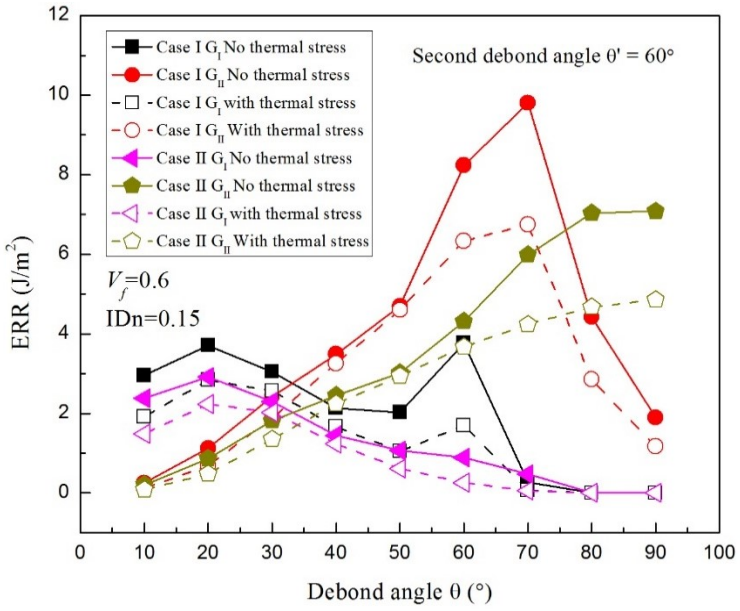

Figure 2.26 Effects of thermal stress on ERRs of the debond crack for Case I and Case II

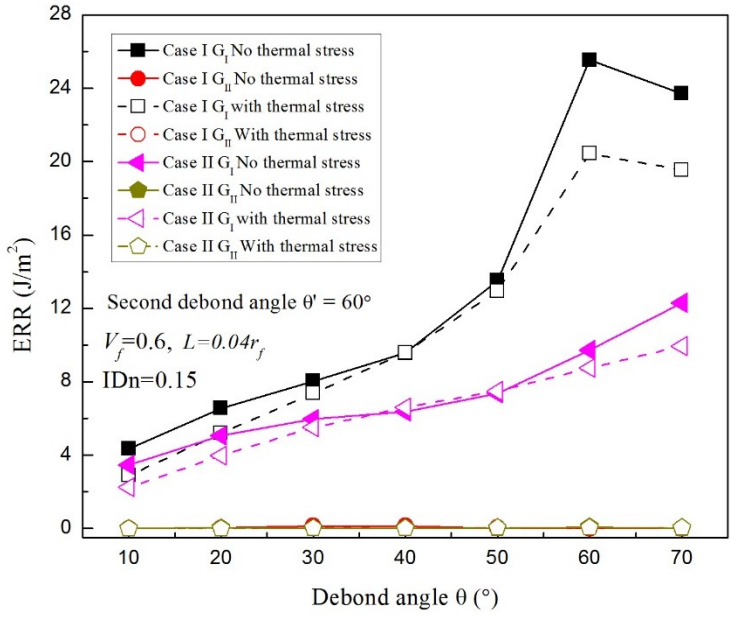

Figure 2.27 Effects of thermal stress on ERRs of the kinked crack for Case I and Case II

2.4 Summary

In the present study, two plausible transverse crack formation mechanisms have been investigated. One is when transverse crack initiates from a single fiber/matrix interfacial debond, in which case, the link-up mechanism will consist of debond crack growth, its kinking out in the matrix, and the propagation of the kinked crack towards a neighboring fiber, leading to the initiation of the fiber/matrix interfacial debonding in the neighboring fiber. The whole process repeats until the linked-up crack grows unstably. It has also been found that scenario I is a preferred mechanism for composite with relatively low fiber volume fraction as the driving forces of debond growth, kinking and propagation of the kinked crack increase with increasing inter-fiber spacing. The second mechanism is multiple debonds inter-connecting one another, which is more likely to occur in composites with high fiber volume fraction and the whole process requires less work than the first mechanism.

The obtained results in the present study have clarified the various debond link-up processes and highlighted their importance in the transverse failure process. The numerical analyses match the documented experimental trends very well. Finally, it need to be noted that although the FE model described in the present paper is well-suited to investigate the failure mechanism, it is not able to predict the accurate failure strain for composites under transverse tension. As discussed above, the inter-fiber spacing has direct consequence on the transverse failure mechanism, and on the driving force for debond growth, kinking as well as kinked crack propagation. In real composites, fibers are non-uniformly distributed and their distribution also depends on the given

manufacturing process. As a result, a model that accounts for the non-uniform fiber distribution due to a given manufacturing process is highly desired for accurate prediction of the transverse failure strain.

3. FAILURE MECHANISMS OF UD COMPOSITES UNDER LONGITUDINAL TENSION*

3.1 Introduction

Due to the architecture of fiber reinforced composite itself, multiple failure events could occur simultaneously or sequentially when subjected to applied load, which make it challenging to investigate the failure of composites. In a composite laminate, transverse cracking discussed in Section 2 is often considered as the initiation of the failure or one of the earliest failure events. Meanwhile, it's proven that final failure of a composite laminate is controlled by the 0° layers along One of the examples is shown in Figure 3.1, as both static and fatigue strength of boron/epoxy laminates with different layers all collapse into the diagonal line of UD plies strength [97].

Compared to the study on transverse failure, one of the major difficulties to investigate failure of a UD composite under longitudinal tension is the lack of direct experimental observations. This is due to the characteristic of such failure, as it involves individual fiber breakage occurring inside the composite, which makes direct observations extremely difficult especially for carbon fiber reinforced composites. For years, observations could only be made based on final fracture surface or through single fiber composite test. Recently, with the development of experimental technique such as

*Part of this section is reprinted with permission from Zhuang, L., R. Talreja, and J. Varna, "*Tensile failure of unidirectional composites from a local fracture plane"*. Composites Science and Technology, 2016. **133**: p. 119-127. Copyright 2016 by Elsevier.

the use of X-ray tomography, a direct observation of fiber breakage and accumulation of broken fibers is made possible.

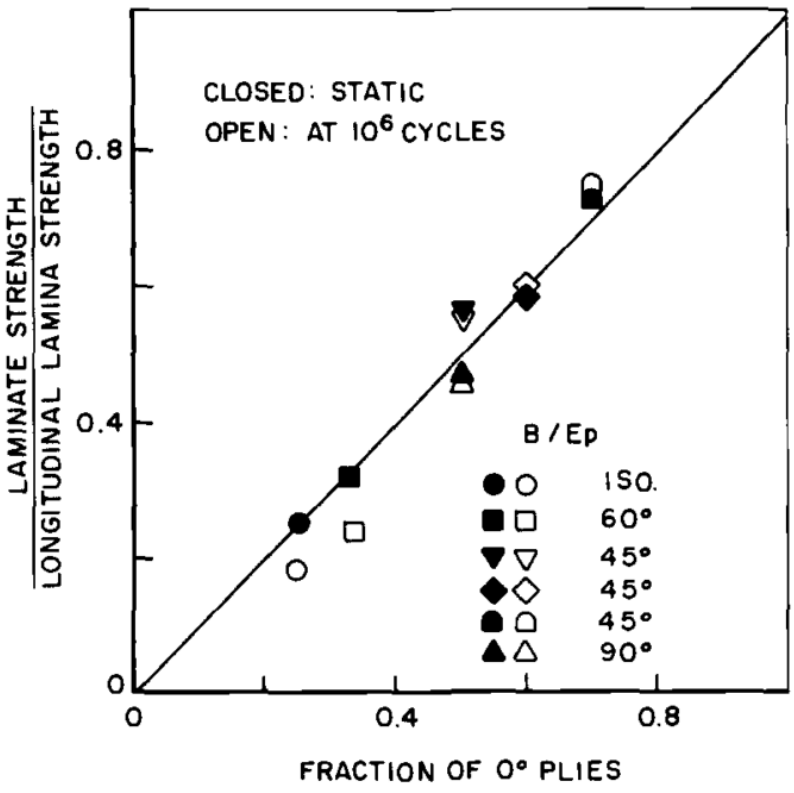

Figure 3.1 Illustration of relationship between laminate strength and UD plies strength (Figure reprinted from [97])

Figure 3.2 displays the typical characteristic of UD composite failure process under longitudinal tension based on X-ray microtomography [62]. As shown in Figure 3.2, upon loading, individual fiber breaks at discrete locations, with further increase of applied load, more fiber breaks closer to the original broken fibers and catastrophic failure occurs when a so-called “critical fracture plane” is formed and the whole plane propagate unstably, causing the separation of the UD composite. Such “critical fracture

plane" contains only several broken fibers. The exact mechanism for the formation of such plane, or in other word, how does individual broken fibers connect with each other is still unknown and often ignored in failure model developments. As a result, one should expect the results obtained from any models that overlooking the mechanism of "critical fracture plane" formation to be questionable despite the claim of good agreement with experimental results.

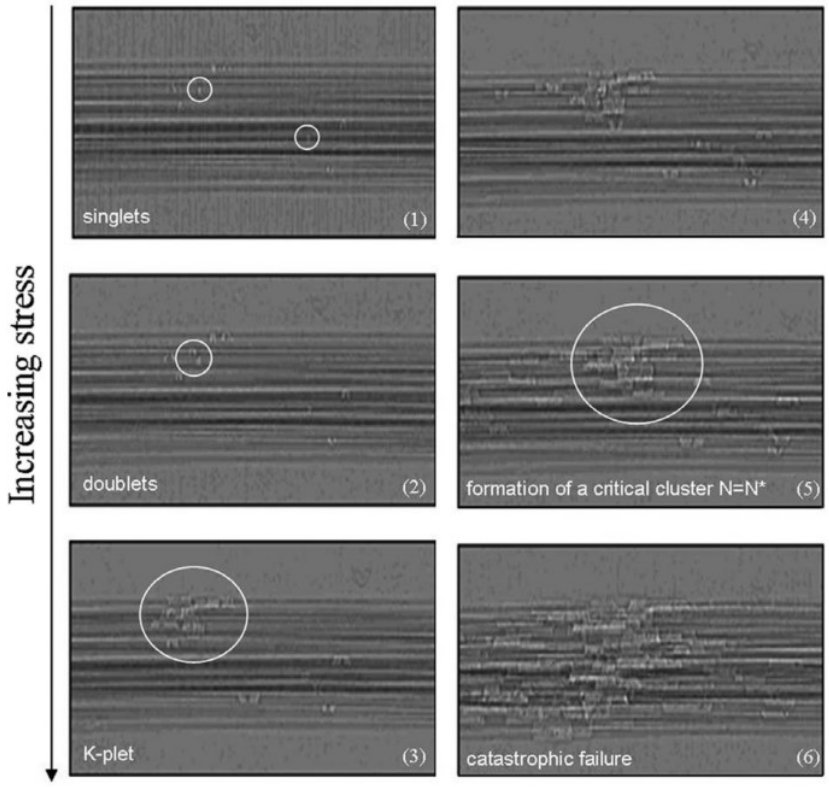

Figure 3.2 Characteristics of UD longitudinally tensile failure (Figure reprinted from [62])

Realizing the urgent need for clarifying "critical fracture plane" formation mechanism, in the present section, a FE analysis was carried out to investigate the

possible mechanism for “critical fracture plane” formation. The carbon fiber/epoxy UD composite with 60% of fiber volume fraction is selected and fibers are assumed to be hexagonally packed with uniform inter-fiber spacing. Two different scenarios are studied and presented. One is for fiber breaks due to manufacturing process, in that case, only fiber breakage is present and matrix cracking near fiber break is expected to be the subsequent failure event. The other case is for fiber breaks at its weakest location during loading application, in that case, due to high shear stress concentration near fiber break, fiber/matrix debonding is usually expected following fiber breakage.

Fractography study by Purslow [54] suggests that the fracture zone in UD composite under tensile loading originates from a single fiber fracture source. As a result, In the composite a pre-existing broken fiber resulting from manufacturing process or loading application is placed as a nucleation site for critical fracture plane formation. The critical facture plane is considered to be formed once the 6 nearest intact neighboring fibers are broken due to the resulting stress enhancement. For composites with high fiber volume fraction, the distance between fibers is very small and thus the effects of fibers on the stress field near broken fiber become dominant. As a result, the 6 nearest neighboring fibers could be simplified using an axisymmetric ring of fiber with cross section area equals to the total sum of cross section areas of those 6 fibers as shown in Figure 3.3. Another ring of matrix is placed around neighboring fiber ring in order to ensure the fiber volume fraction equals to 0.6. Rest of the composite is then modelled as another ring with homogenized composite properties, resulting in an axisymmetric model containing 5- cylinder rings (Figure.3.3). Such model has been

successfully used to calculate the strain energy release rate of a single fiber-matrix debond in author's previous research [98].

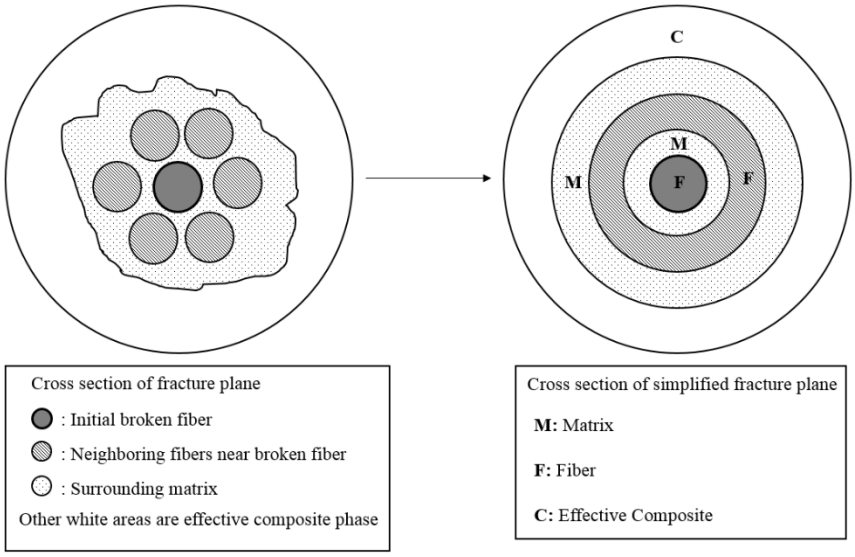

Figure 3.3 Illustration of simplified composite model

3.2 Case I: Fiber breaks due to manufacturing process

3.2.1 Finite element model descriptions

Manufacturing induced defects such as voids, fiber misalignments and fiber breakages are commonly found in composites. The effects of former two types of defects have been well investigated in the past[99-104]. However, few studies have been done to clarify the effects of fiber breaks due to manufacturing process. Discrete broken fiber could be present even for a carefully manufactured composite structures. Such fiber breakage usually would not cause any fiber/matrix debonding from it. Upon loading, it's expected that such fiber break would cause local stress concentration resulting in further

local damages. Given the preferred condition, the accumulation of local damages might lead to the final failure of UD composite. In order to investigate that failure mechanism, a FE study is conducted using the axisymmetric model discussed in the previous section.

Details of the FE model are in Figure 3.4a and the FE mesh near the debond tip region, indicated by a rectangle in the figure, is displayed in Figure 3.4b. In Figure 3.4a, z axis is the fiber axis and r axis is the radius axis in a cylindrical coordinate system In the present paper, based on a convergence study conducted in [98], the model length L = 800μm is taken. At this length, the stress results are found to be independent of the model length. The fiber break is sketched as a solid horizontal line in Fig. 2 (a) and is placed at the distance d = 200 μm from the bottom plane. Initial computations showed that the crack path was affected by the symmetry boundary conditions applied at the plane of the broken fiber end, likely as an artifact of numerical implementation of the boundary conditions. Instead, by shifting the bottom plane of the model by this distance, the effect was nearly eliminated. In the FE model, fiber radius r_f = 4μm. Inter-fiber distance ID = 2μm, which is close to the normal inter-fiber distance of a hexagonally packed fiber composite with 60% fiber volume fraction. The radius of the neighboring fiber ring RMI is chosen such that the cross-sectional area of the neighboring fiber ring equals to the total cross section areas of the six neighboring fibers. The radius of last matrix ring, RMO, was selected to ensure that the fiber volume fraction in the fiber/matrix unit represented by the four-cylinder rings equals to 60%. The composite radius RC=5×RMO so that beyond which obtained results become independent on the

composite radius. To be consistent, the same material properties adopted from previous section are shown in Table 3.1.

As shown in Figure 3.4a, at z=0 plane, displacement along z axis is constrained. The whole model is subjected to a uniform displacement along fiber direction z on the top plane. The thermal residual stresses are accounted for by imposing a uniform temperature change of -100°C, which corresponds approximately to the cooldown temperature for epoxies during curing. The residual stresses due to curing induced shrinkage are not included, as these have been found to be small in comparison to the thermal stresses [94]. First order axisymmetric FE elements CAX4 were adopted in the current study using FE software ABAQUS [105].

The stress analysis is conducted outside a local region or core region near fiber break within which material behaves significantly different from elastic theory due to high stress concentration. Depending on the theories and experimental methods [106-110], the shape and size of the core region may vary. However, it will later be shown that the effect of exact shape and the size of the core region will not be significant in the present study. As a result, to simplify the problem, the core region is assumed to be a circle with a radius of r_0 = 0.2 μm. Series of ring elements are placed in the matrix part of core region with an angular resolution of 2.25° (Figure 3.4b).

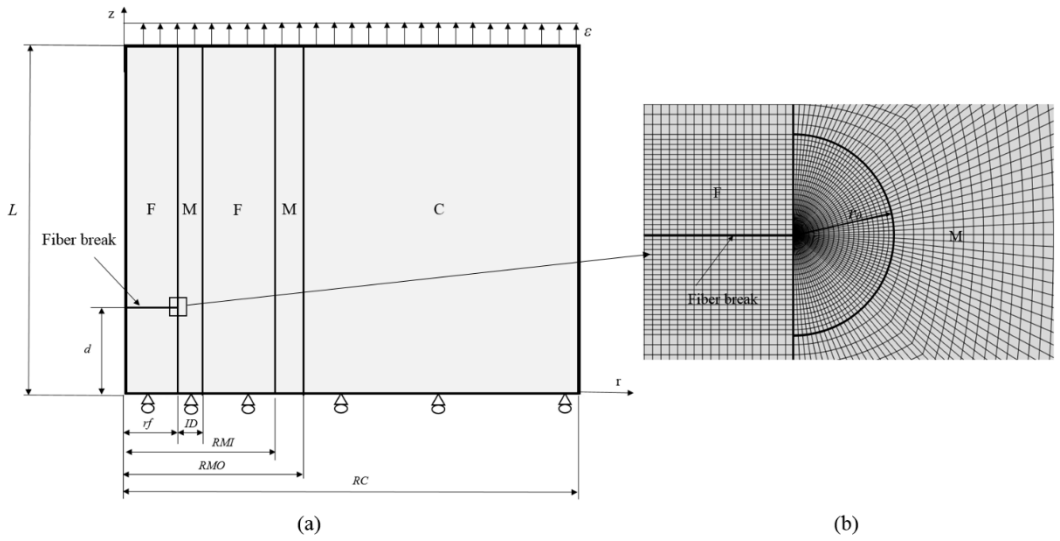

Figure 3.4 a) Illustration of numerical model for case I. F: fiber, M: matrix, C: composite; b) Detail of near debond tip region mesh

Table 3.1 Thermo-elastic properties of constituents

Material	E_1 (GPa)	E_2 (GPa)	υ_{12}	G_{12} (GPa)	υ_{23}	α_1 (1/°c)	α_2 (1/°c)
CF	500	30	0.2	20	0.45	$-1\cdot10^{-6}$	$7.8\cdot10^{-6}$
Epoxy	3.5	3.5	0.4	1.25	0.4	$60\cdot10^{-6}$	$60\cdot10^{-6}$
CF/EP (V_f=0.6)	301.4	11.04	0.27	4.06	0.54	$0.66\cdot10^{-6}$	$35.85\cdot10^{-6}$

3.2.2 Matrix cracking

Under axial tension of the model, the first event of failure is expected to be in the matrix close to the existing fiber break. As we discussed in the previous section, due to the constraint of stiffer fibers, stress field near fiber/matrix interface is triaxial. Depending on the level of triaxiality, brittle typed matrix cracking or ductile matrix cracking would occur. Asp el al.[24] argued that under triaxial stress state, matrix cavitation is the main cause for brittle typed cracking which depends on the local

dilatational energy density. On the other hand, ductile matrix cracking depends on distortional energy density. In order to characterize the stress field near fiber break outside the core region, distortional energy density (denoted U_d) and dilatational energy density (denoted U_v) distributions are calculated. The expressions for the two energy densities are given in Eqn.3.1 and Eqn.3.2, from which it is apparent that their expressions are similar to Von mises stress and hydrostatic stress, respectively. However, contradicted to their stress counterparts, energy densities are independent of temperature.

$$U_d = \frac{[(\sigma_1 - \sigma_2)^2 + (\sigma_1 - \sigma_3)^2 + (\sigma_2 - \sigma_3)^2]}{12G} \tag{3.1}$$

$$U_v = \frac{(1-2\upsilon)(\sigma_1+\sigma_2+\sigma_3)^2}{6E} \tag{3.2}$$

Where σ_1, σ_2 and σ_3 are the principal stresses, υ, G and E are the Poisson's ratio, shear modulus and Young's modulus of matrix, respectively.

In the present study, a temperature change of $\Delta T = -100°C$ is applied first to the model to simulate the thermal cooldown process, followed by the mechanical loading. Figure 3.5a and Figure 3.5b show the energy density distribution in matrix material around fiber break at very small apply strain of 0.00575%. To better demonstrate the result, core region is not shown in the figure. Although the exact energy density value

would change with increasing applied load, the characteristic of energy density distribution remains the same: the maximum distortional energy density develops near fiber/matrix interface (Figure 3.5a) while the maximum dilatational energy density develops along fiber break plane, which is also the plane of symmetry (Figure 3.5b). Both maximum energy density component occurs at the outside boundary of the core region.

Based on the above observations, we could now re-visit the effects regarding the shape and size of core region. As shown in Figure 3.5b, maximum dilatational energy density occurs at fiber break plane, which is the plane of symmetry. As a result, regardless of whether it is a circular shape as most of the researchers proposed or the mises elastic-plastic boundary proposed by Theocaris and Andrianopoulos [109], the most critical location will always be along that fiber break plane. Meanwhile, the size of core region would only affect the damage initiation strain, it will not alter the mechanism found in the current section. As a result, it is reasonable to assume that the following statement made in the present study is independent of the choice of the core region.

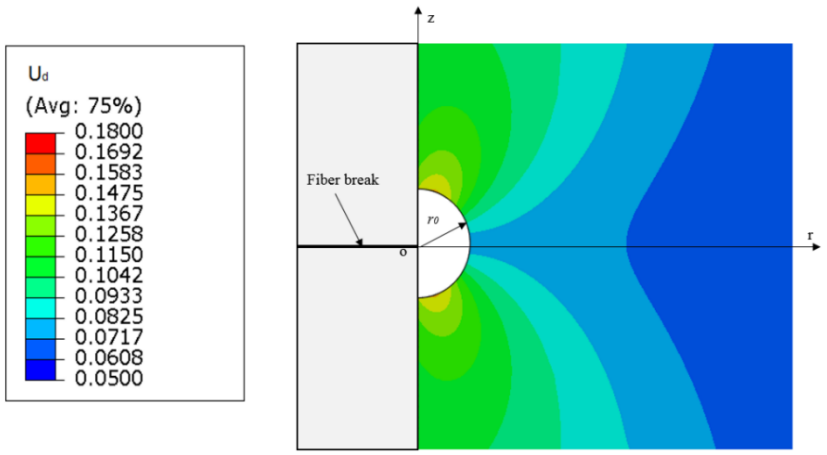

a)

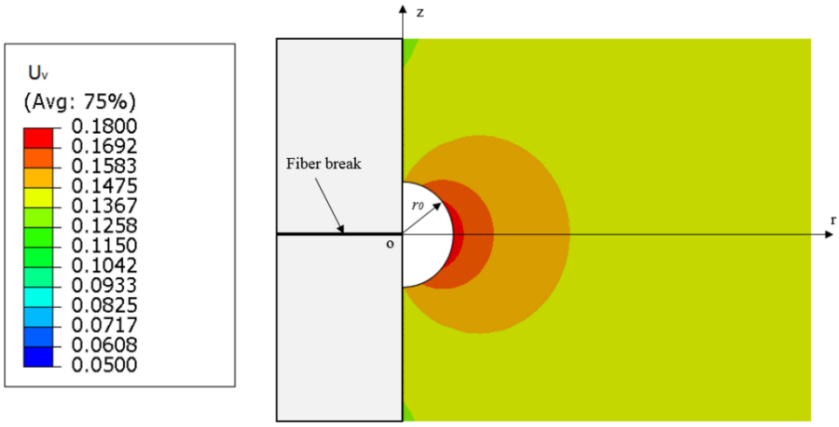

b)

Figure 3.5 a) Distortional energy density distribution and b) Dilatational energy density distribution

In the FE model, due to the constraint of close packed neighboring stiff fibers, tri-axial stress state develops within matrix material near fiber/matrix interface. Meanwhile, along fiber break plane where maximum dilatational energy density occurs, the stress state is found to be very close to equal tri-axiality, as shown in Figure 3.6

where the maximum energy density attained just out the core region w.r.t applied loading is displayed. In the figure, the energy densities at 0% applied strain corresponds to the thermal residual stresses contribution. For typical epoxy resin, Asp et al. [24] conducted poker chip experiment and found the critical dilatational energy density to be 0.13~0.2MPa for formation of a matrix crack from unstable cavitation growth. As shown in Figure 3.6, within that range, the Von mises stress corresponding to the maximum distortional energy density is around 26.7 to 34.1 MPa, which is well below that required for matrix yielding. Moreover, at the location of maximum dilatational energy density, distortional energy density is much smaller (dash dot line). As a result, it could be concluded that in the present study, for relatively high fiber volume fraction UD composite, under tensile loading, the presence of tri-axial stress state develops within matrix material and inhibits matrix plastic deformation around fiber break. This agrees well with the experimental findings by Lorenzo and Hahn [111] as they conducted static and fatigue tensile loading of a composite layer consisting of multiple fiber bundles and found no plastic deformation in the matrix.

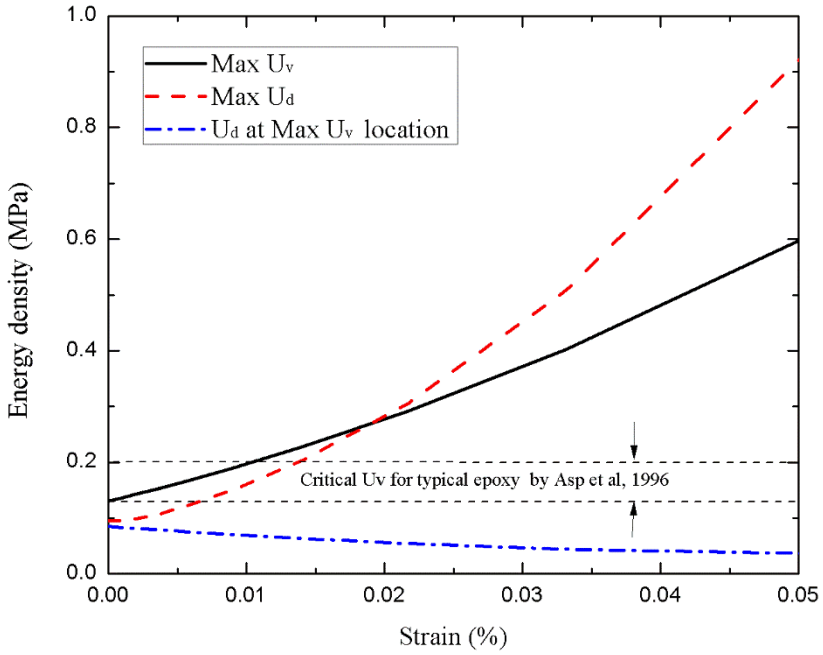

Figure 3.6 Variations of the maximum energy densities with the applied load

In order to predict failure initiation in the matrix near fiber break, critical dilatational energy density criterion is adopted. This criterion was proposed by Asp et at [24] and states that under tri-axial stress state, if the distortional energy density is lower than that required for yielding, matrix cracking initiates through micro-cavitation when dilatation energy density (right hand side of Eqn 3.2) reaches a critical value U_{vc} (0.2MPa in the present study). For the extreme case where each principal stress component is the same, i.e. under hydrostatic tension, micro-cavity would expand in a spherical shape and once criticality is reached, crack would form in a star-shape with no preferred propagation direction. However, if bias among three principal stresses exists, as is the case in the current study (Figure 3.7), it would be expected that cavity to expand

in an ellipsoid shape and crack will likely to initiate normal to the maximum principal stress direction.

From Figure 3.6 it is found that thermal stresses significantly increase the dilatational energy density in matrix (see energy density value at 0% of strain) and thus a cavitation-induced matrix crack initiates at a very low applied strain around 0.015%. Similar thermal residual stress effect has been report by Maligno et al [112] and Asp et al. [25] as they found the presence of thermal residual stress facilitates the matrix failure of UD composite under longitudinal and transverse loading, respectively. At around 0.015% of applied strain, the direction of maximum principal stress at the location of maximum U_v is found to be the same as fiber axial direction, as a result, cavitation-induced matrix crack is most likely to form perpendicular to the fiber direction and propagates towards neighboring fibers. It should be noted that since cavitation-induced matrix crack initiates at a very low applied strain, further loading is still required for matrix crack propagation.

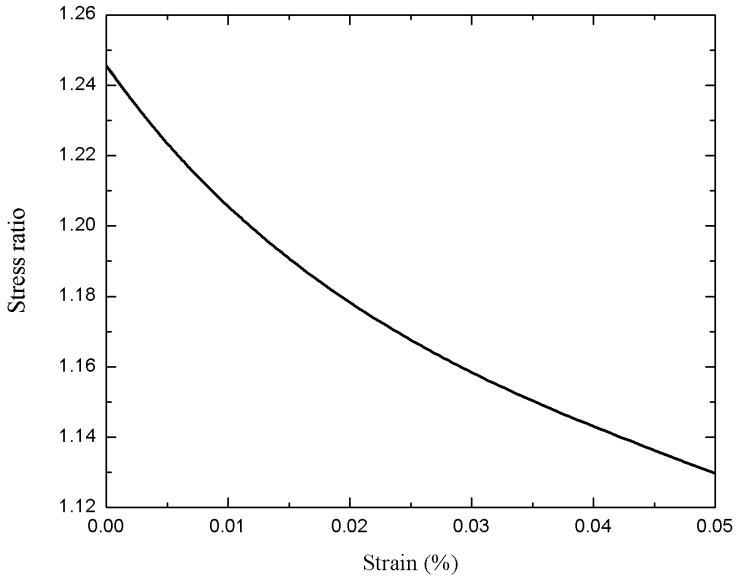

Figure 3.7 Stress ratio between maximum principal stress and mean principal stress

To study the matrix crack propagation, fracture mechanics based method is adopted and crack propagation is simulated by using the Extended Finite Element method (XFEM) implemented in ABAQUS. The concept of XFEM is first introduced in [73], it could predict crack path accurately without remeshing. In the present study, an initial matrix cavitation-induced crack (marked by white line) with length of 0.2μm is placed perpendicular to the fiber axis (Figure 3.8). Once initial matrix crack is formed, thermal stresses becomes negligible compared to the stress concentration near crack tip. As a result, only mechanical loading is applied when simulating crack propagation. A linear mixed mode crack propagation criterion is used (Eqn 3.3). G_I and G_{II} are calculated Mode I and Mode II energy release rate (ERR) for the matrix crack based on virtual crack closure technique (VCCT), critical Mode I ERR G_{IC} and Mode II ERR G_{IIC}

is chosen as 200 J/m^2 and 1000 J/m^2, respectively. The matrix cracking process simulated by XFEM is an element-by-element crack propagation: for a certain crack length, once the crack propagation criterion is met, the matrix crack propagates through the whole length of an element in a direction perpendicular to the local maximum tangential stress and the same process is repeated until crack propagate to neighboring fiber.

$$\frac{G_I}{G_{Ic}} + \frac{G_{II}}{G_{IIc}} = 1 \tag{3.3}$$

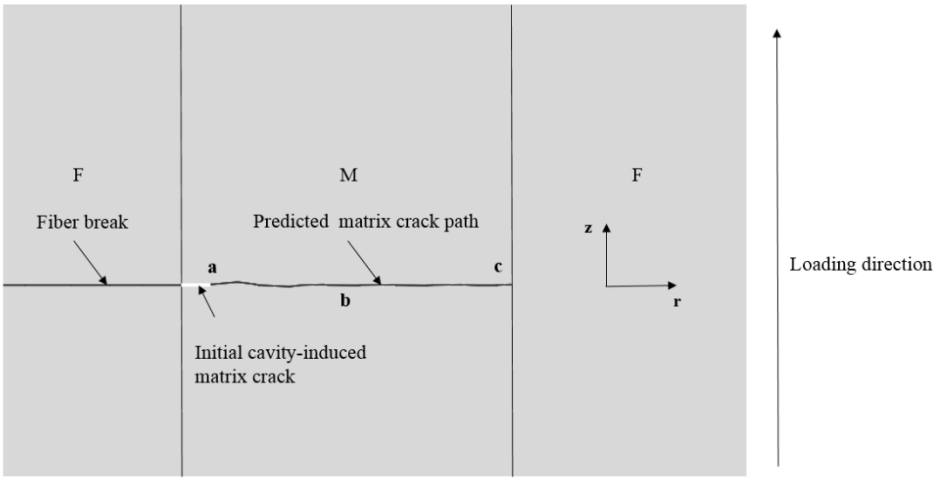

Figure 3.8 Predicted matrix crack trajectory based on XFEM. The complete axisymmetric model is shown in Figure 3.4

The predicted matrix crack path is displayed in Figure 3.8 It is found that matrix crack propagates perpendicular to the fiber axis towards neighboring fiber. The little deviation in the beginning stage of matrix cracking is due to fact that in the FE

calculation, even though fiber break plane is a symmetric plane along, there will be very small shear stress along that plane, and that shear stress is higher closer to broken fiber, which slightly perturbs the symmetric plane condition and thus cause the small deviation of horizontal matrix crack at the beginning.

3.2.3 Neighboring fiber breakage

Evans et al. [113] found that for aligned stiff fiber composites, when a matrix crack propagates to the fiber, it is not likely that the matrix crack will cut through fiber and propagate, instead, it would tend to deflect along fiber axis causing fiber/matrix debonding. For composites with good fiber/matrix interfacial bonding, it would also be expected that matrix crack being constrained between fibers. Both scenarios have been found in the experiment work conducted by Lorenzo and Hahn [111]. As a result, to form the critical fracture plane, neighboring intact fibers are most likely to fail as a result of stress enhancement caused by surrounding fiber breakage and subsequent matrix cracking.

Previous studies, e.g. [114-119], dealing with stress enhancement in the fibers neighboring a broken fiber have not considered the effect of a matrix crack emanating from the broken fiber end. We do that here using the FE model described above. The mean value of the stress concentration factor (SCF), as shown in Eqn. (3.4), defined as the ratio of the local tensile mean stress (averaged over the fiber-ring cross-section) to the remote stress in the fiber, is calculated for the initial condition when only fiber break is present, i.e., with no matrix crack, and when the matrix crack has grown to different

lengths indicated by labels a, b and c in Figure 3.8. Figure 3.9 shows the variation of the mean SCF along the axial distance of the fiber ring measured from the fiber-break plane. Due to symmetry, only results above fiber break plane is plot. Four cases are studied which corresponds to initiation of matrix crack, i.e. no crack and different matrix crack tip position marked in Figure 3.9. As shown in Figure 3.9, maximum SCF increases with matrix propagation and reaches the maximum when crack propagates to neighboring fiber. This result is expected as more load has to be shared by neighboring fibers with the growth of matrix crack. The drop of the tensile stress below the remote level seen in Figure 3.9 is to maintain the overall strain compatibility, as explained in [119].

$$SCF = \frac{\sigma_{t\_ave}}{\sigma_{t\_n}} \tag{3.4}$$

Where σ_{t_ave} is the local tensile mean stress (averaged over the fiber-ring cross-section) and σ_{t_n} is the remote tensile stress.

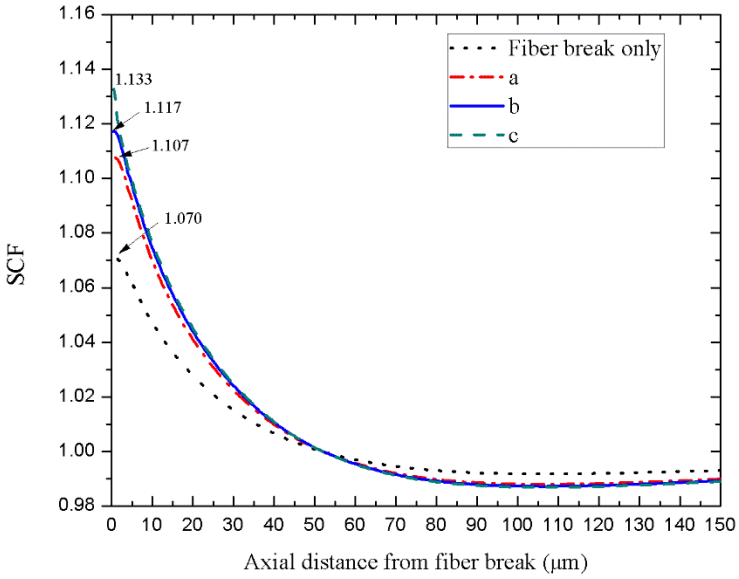

Figure 3.9 Mean stress concentration factor in fibers neighboring a broken fiber at different stages of matrix crack growth. For crack-tip locations a, b and c, see Figure 3.8

Fiber breakage process is considered to be a statistical process since strength along fiber axis is not constant. As a result, SCF itself is not sufficient to evaluate the neighboring fiber breakage process, a more accurate way is to incorporate obtained stress enhancement information into a statistical model, which has been done by some of the pioneered work [46-48, 51, 52, 120, 121], however, in those research, the effect of matrix cracking is neglected. As discussed and shown (Figure 3.9) in the current study, matrix cracking has quite a significant effect on the obtained maximum SCF, so a more complete model has to take that into account.

The stress enhancement information when matrix crack propagates to neighboring fibers is adopted since it's more critical. Assuming no further damage

developed (i.e. no further fiber/matrix debonding) and no matrix plasticity, the probability of failure of neighboring fibers is then calculated by assuming the strength of fiber follows a Weibull distribution such that the probability of survival of a fiber of a certain length is given by

$$P(\sigma)=\exp[-(l/l_0)^{\alpha}(\sigma/\sigma_0)^{m}] \quad (3.5)$$

Where $P(\sigma)$ is the probability of survival, l the fiber length and σ the local mean stress. The statistical data σ_0 the characteristic strength of 3270 MPa, l_0 the standard length of 62mm and m the shape parameter of 5.3 adopted from [115]. Correlation factor α =0.6 adopted from [121] are used in the calculation.

For each small size of element along fiber axis z, tensile mean stress is taken to be constant when the probability of survival is calculated. Based on the weakest link theory, the probability of survival of a certain length of fiber is then given by the product of $P(\sigma)$ of each element. The probability of failure $F(\sigma)$ is then obtained by one minus the probability of survival. In the present study, the probability of failures over three regions of different fiber length are calculated: region I is the whole fiber length of 800μm in the model; region II is the stress enhancement region of 96μm where local mean tensile stress at neighboring fiber is larger than the nominal tensile stress, region III is the region up to 2 fiber diameters (8μm from above and below, respectively) distance away from fiber break, where stress enhancement at the neighboring fiber is the most significant. Then followed a similar approach by Nedele and Wisnom in [115,

119], the factor for the enhanced probability of failure (the ratio of probability of failure of neighboring fibers to the probability of failure of the same length subjected to the nominal tensile stress) is calculated at a medium overall applied strain 0f 0.6% and results are listed in Table 3.2.

Table 3.2 The enhanced probability of failure factor calculated over different fiber regions at a reference applied strain of 0.6%.

	Enhanced probability of failure factor		
	Region I	Region II	Region III
Only fiber break	1.000	1.141	1.380
Fiber break with matrix crack	1.002	1.244	1.670

Based on the results from Table 3.2, it's shown that although the stress enhancement cause by the local damage events (i.e. fiber breakage and matrix cracking) seems to have much smaller effect on the overall failure of neighboring fibers, as also reported by Nedele and Wisnom [115, 119], it significantly increases of probability of fiber failure at a local region closed to the location of matrix crack tip where that stress enhancement is the largest. As a result, it would be expected that the critical fracture plane formed by this mechanism is to be a small localized region close to the initial fiber break plane. This supports the experimental finding in the X-ray tomography study [63], which showed most broken fibers to be in the range 0 – 2.5 μm axial distance.

3.3 Case II: Fiber breaks during loading

3.3.1 FE model description

In the previous section, the mechanisms of the critical fracture plane nucleating from a manufacturing induced broken fiber has been discussed. On the other hand, when a UD composite is under a tensile applied load that is large than the lowest scatter bound of fiber strength, discrete fiber break would also occur at its weakest location during loading. At this section, we'll try to investigate the possible mechanisms if this type of fiber breakage initiates the formation of critical fracture plane. Unlike previous case, if a fiber breaks during loading, because of high shear stress concentration near fiber break, fiber/matrix debonding from fiber break is expected, usually an order of a few fiber diameter depending on the material properties[122]. The following discussion will be based on pure mechanical loading first and effects of thermal stresses will be addressed in Section 2.4.

To investigate Case II, the same FE model as the one used in case I is adopted except for the addition of initial debond crack emanating from fiber break, as displayed in Figure 3.10. In this study, instead of placing debond crack along fiber/matrix interface, the debond crack is modelled at a very small distance (t =0.1μm) away from interface. By doing so we take into account a common experimental observation: the so-called interface debond may actually be a longitudinal matrix crack, as a thin layer of matrix is often found to be attaching to the pulled-out fibers especially for composites with good fiber/matrix interfacial bonding (Figure 3.11a). Meanwhile, although stress field is symmetric with respect to fiber break in the numerical model, in reality, due to

the unstable nature of initial debonding as well as statistical distribution of material properties, it's quite common that the debond crack only grows along one direction away from fiber break (shown in Figure 3.11b). Readers can refer to the experimental work conducted by Gamstedt and his colleagues [123, 124] for more details of such damage features. As a result, in our model, initial debond crack (or longitudinal matrix crack) is assumed to grow along positive fiber axis and initial debond length from d_l from 1μm to 10μm when the energy release rate (ERR) for the debond crack is become constant is studied.

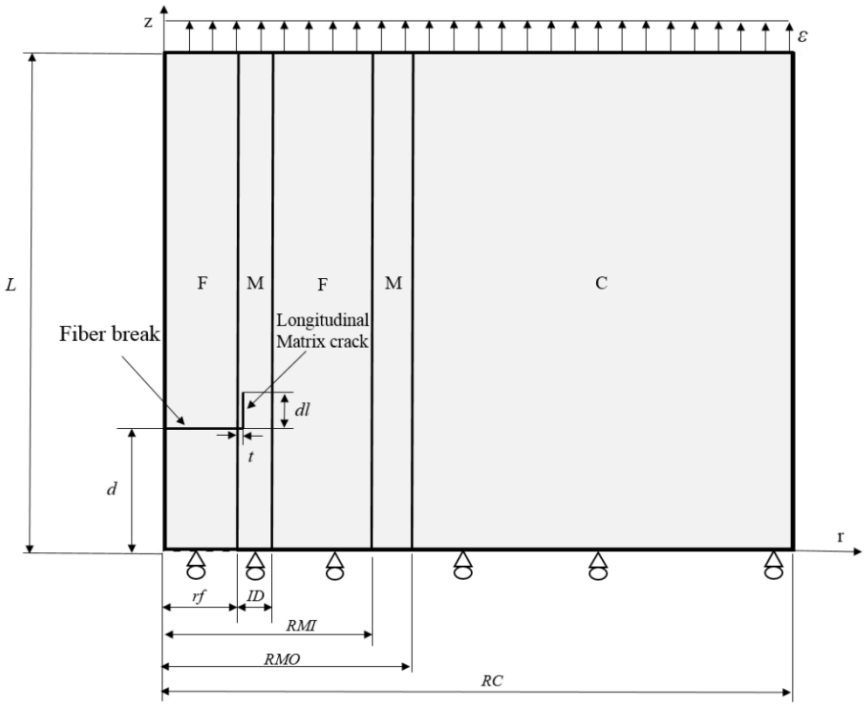

Figure 3.10 Illustration of the numerical model for Scenario II

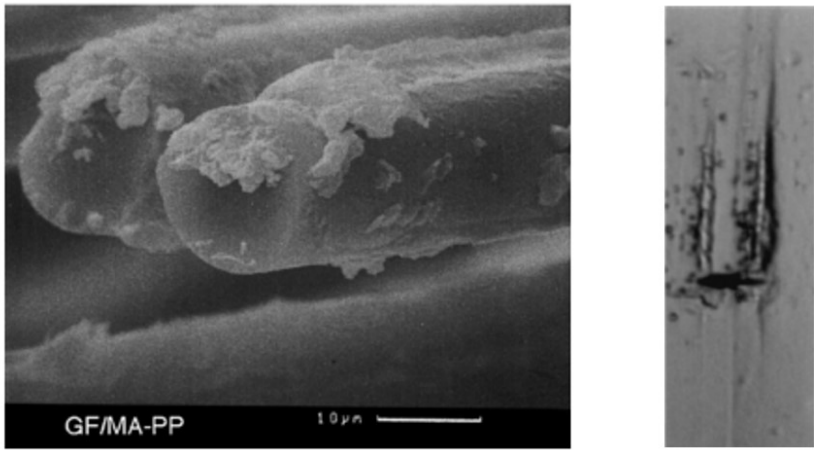

a) b)

Figure 3.11 a) Matrix attached to pull-out fibers and b) Debond growth in one direction from fiber break (Figure 3.11a reprinted from [124], Figure 3.11b reprinted from [123])

Under longitudinal tension, the debond crack is found to grow in pure Mode II under tensile loading [98] and thus surface interpenetration is expected if no contact constraint is imposed between both debond surfaces, resulting in an artificial Mode I ERR value G_I. However, as proven by Whitcomb [89], for a Mode II dominated crack growth, non-contact analysis would not significantly affect the obtained ERR, and total value of obtained G_{II} and artificial G_I could well approximate the G_{II} result in a contact case. That is also supported by current authors when conducting the research work on the interfacial debond growth [98] (not reported), it is found that for non-contact analysis, the sum of G_{II} and artificial G_I as well as the total ERR obtained through J integral method agree well with the obtained G_{II} results in the contact analysis (less than 1.5% of difference). As a result, in our model, no contact constraint is imposed in order to achieve numerical efficiency.

3.3.2 Matrix cracking

Unlike previous case when matrix-cavitation becomes dominant mechanism due to the close to equal-triaxial stress state around the fiber break. It's found that once the initial debond crack is formed, the tri-axial stress field around debond tip becomes dominated by the deviatoric part of stress, indicating that shape changing of materials would be more dominant than the volume change under such stress state. However, due to the constraint of neighboring close-packed fibers, potential matrix plasticity should be localized and restricted to a very small region near debond tip. As a result, brittle matrix cracking is still expected. Based on the characteristic of the stress state, it is not difficult to image that if there existing a crack liked matrix flaw near debond tip, it would tend to change its shape to form a initial kinked matrix crack with very small length in a direction that is the most favorable for further crack propagation. As a result, A matrix crack is assumed to form as a kinked-out debond crack at a kink angle θ, as illustrated in Figure 3.12. The most favorable value of this angle will maximize the total ERR. This angle was found by numerically calculating the total ERR for all kink angles, including $\theta = 0$ (no kinking), $\theta > 0$ (kinking inwards toward the fiber) and $\theta < 0$ (kinking outwards toward the matrix), and the results are listed in Table 3.3 for six different debond lengths. It is noted that the thermal stresses were not considered in the calculation of the kinking angles listed in Table 3.3. However, separate computations indicated that the kink angles were affected by the thermal stresses only until approximately 0.2% mechanical strain, beyond which the kink angles were governed by mechanical loading. This result will be discussed in Section 2.4.

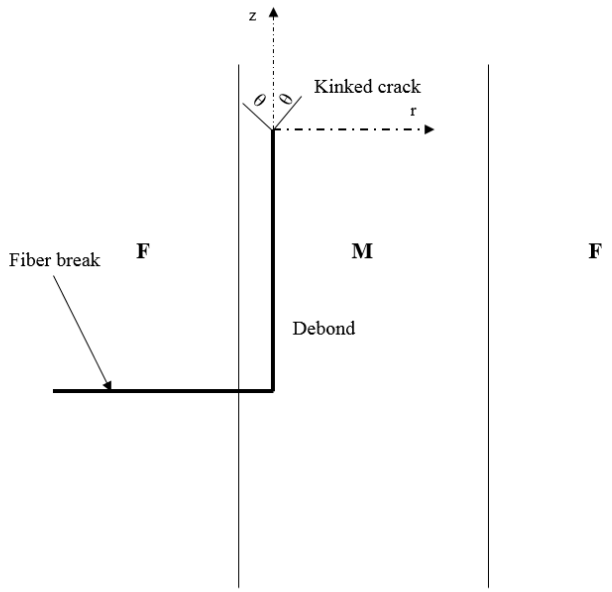

Figure 3.12 Description of potential kinked crack. F: Fiber, M: Matrix

Table 3.3 Kink angles corresponding to maximum ERR for different debond lengths.

	Debond length (μm)						
	1.0	2.0	3.0	4.0	6.0	8.0	Average
Kink angle θ (°)	-78.26	-78.08	-78.48	-78.88	-79.24	-78.98	-78.65

Note: negative θ indicates clock-wise kinking w.r.t positive fiber axis z (Fig. 8)

Based on the results listed in Table 3.3, it is clear that the potential kinking angle is almost the same for each debond length, the small variation might due to the perturbation from fiber break as well as debond surface interpenetration. The obtained kinking angles lay within the range predicted by He and Hutchinson [88] based on maximum ERR for crack kinking cases from the same materials interface and dissimilar

materials interface that is similar as the fiber/matrix interface in our model characterized by Dundurs parameters [125], as indicated in Figure 3.13, which further validates the obtained results given that fact that debond crack is modelled as a longitudinal matrix crack close to the interface. In order to evaluate the competition between debond crack growth and kinked crack propagation, we compared the ERR of debond crack and potential kinked crack. For kinked crack, the kinking angle is set as -78.654° by averaging of kinking angle for each debond length. ERR at a reference applied strain (0.1%) for debond crack at a certain length and potential kink crack emanating from it with very small length of 0.204μm is then calculated by VCCT method and plotted in Figure 3.14. It should be noted that all ERR results are obtained after convergence check is performed. As shown in Figure 3.14, ERR for both debond crack and kinked crack is decreasing with increasing debond length, which similar to the findings for interface debond crack [98]. For each debond length, ERR of kinked crack is larger than that of debond crack, more importantly, although the kinking angle is predicted based on the maximum ERR criterion, the ERR of that kinked crack is found to be almost pure Mode I, indicating that the kinking angle where ERR is the maximum is the same angle that make crack grow in pure Mode I locally. Similar experimental and numerical findings are also reported by Xie et al [90]. For epoxy materials, Mode I critical facture toughness is usually smaller than the corresponding Mode II component, and thus it could be concluded that for debond crack lying within matrix, once the kinked crack is formed, it would deviate immediately from original debond crack plane and propagate towards neighboring fiber and matrix crack is more likely to kink out at shorter debond length.

Finally, it should be noted that although not reported in the present paper, present conclusion holds for the interface debond crack case except that the predicted kinking angle as well as ERRs would be different. For interface debond crack, criterion proposed by He and Huchinson [88] could be used to evaluate the competition between its growth and kinked crack growth. However, one major challenge one has to face is to determine the related interface properties.

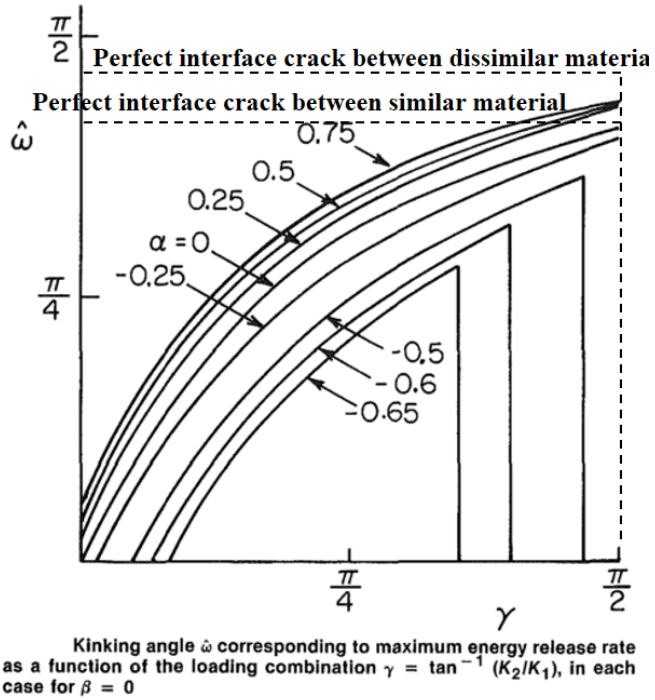

Figure 3.13 Predicted kinking angle based on reference (Figure adapted from [88])

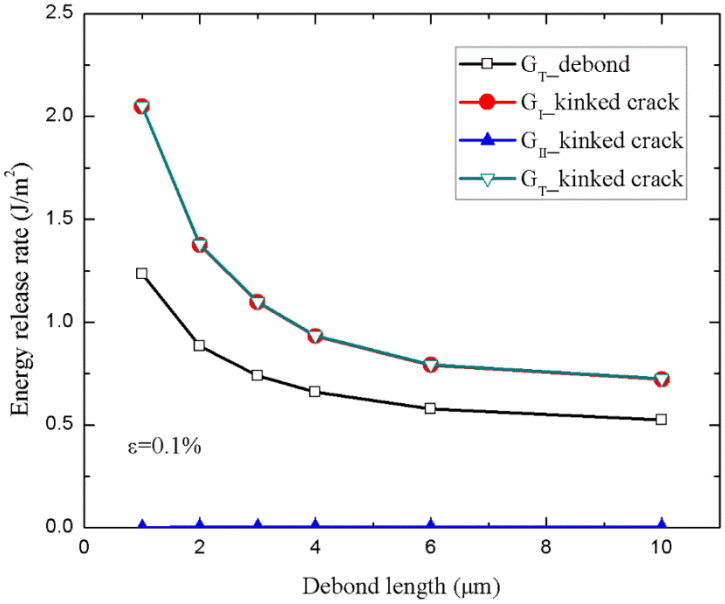

Figure 3.14 ERR of debond crack and kinked crack for at each debond crack length. 0.1% applied strain

Once kinked crack is formed, similar approach as described in section 3.2.2 is adopted to predict crack propagation path using XFEM method implemented in ABAQUS. For each debond length, a kinked crack with length of 0.204μm is placed at debond tip in an angle θ = -78.654° (Figure 3.12). Matrix crack propagation criterion is the same as the one used in section 3.2.2. It's found that matrix crack propagates to neighboring fiber at lower applied strain when initial debond crack is shorter as ERR is larger for the kinked crack. The predicted kinked crack path at each debond length is put together and displayed in Figure 3.15. As shown in Figure 3.15, for shorter debond crack (i.e. d_l =1μm and d_l =2μm), kinked crack is close to propagate perpendicular to the loading direction, which is similar to the no debond case studied in section 3.2.2. For longer debond, however, it is found that matrix crack propagates along initial kinking

angle until it comes closer to the neighboring fiber when it diverts and tend to propagate along fiber/matrix interface, which is the reflection of change of local stress state when the crack grows closer to the neighboring fiber as matrix crack tends to grows in a direction that could retain Mode I fracture locally.

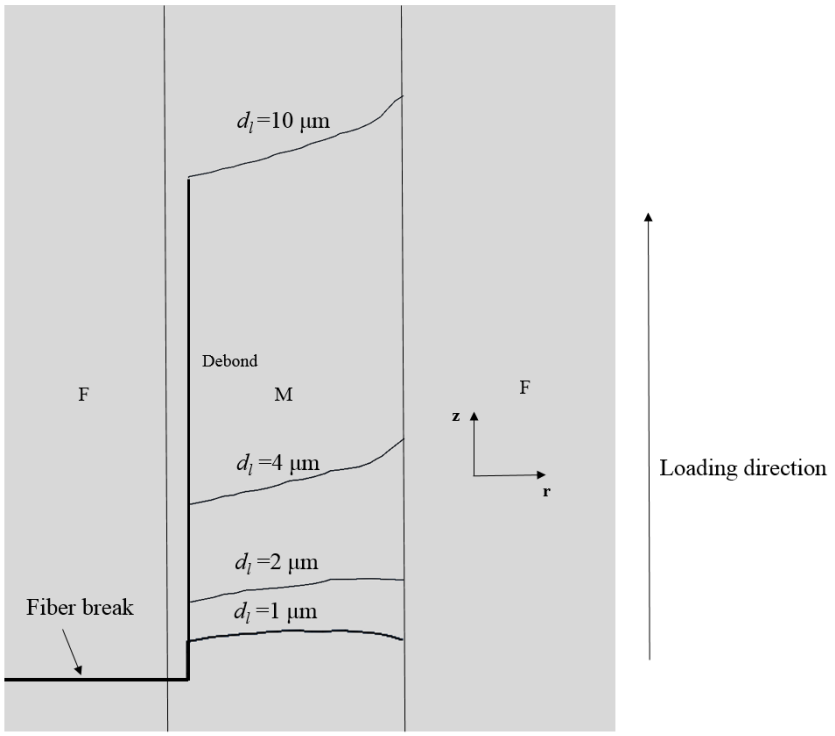

Figure 3.15 Superposition of predicted matrix crack path for different initial debond length. F: Fiber, M: Matrix.

3.3.3 Neighboring fiber breakage

For each initial debond length, when the kinked crack propagates to neighboring fiber, mean tensile SCF along neighboring fiber is calculated and stress enhancement region is selected and plotted in Figure 3.16 to show the SCF distribution. As displayed

in Figure 3.16, the presence of debond causes stress redistribution along neighboring fiber and thus varies the location of maximum SCF. Meanwhile, the maximum SCF is decreasing with increasing initial debond length. However, it's found that neighboring fibers at longer debond case has larger region experiencing relatively high tensile stress concentration compare to the shorter debond case where peak stress concentration only occur at a very narrow region. Combining with the fact that fiber strength is not constant along fiber axis, SCF itself again is not sufficient to evaluate the fiber breakage process, a statistical analysis has to be carried out.

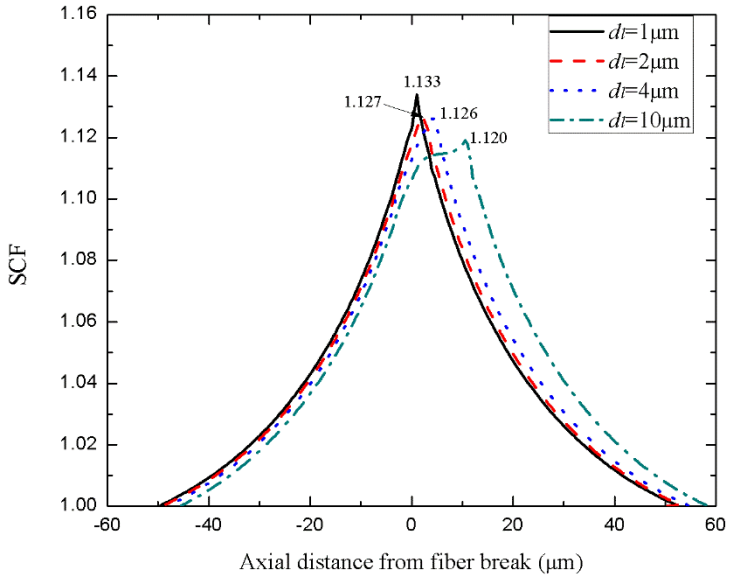

Figure 3.16 Mean tensile SCF within stress enhancement region in neighboring fiber when matrix crack propagates to neighboring fiber

The statistical model adopted here is the same as the one discussed in section 3.2.3. Based on the findings from section 3.2.3, it's known that the effect of stress

enhancement is very local, as a result, the enhanced probability of failure factor at medium applied strain of 0.6% is studied here for two local regions with different fiber length where region I corresponds to the stress enhancement region as shown in Figure 3.16, and region II is the region up to ±10μm from matrix crack tip, all results are listed in Table 3.4. Meanwhile, for initial debond length d_l =10μm, comparison of enhanced probability of failure factor is made for regions up to ±5μm from fiber break and matrix crack tip, respectively in order better evaluate which region of neighboring fiber is more prone to break. Those results are shown in Table 3.5.

Table 3.4 The enhanced probability of failure factor F(σ) over two different fiber regions for different initial debond lengths at the applied strain of 0.6%.

	d_l=1.0 μm		d_l=2.0 μm		d_l=4.0 μm		d_l=10.0 μm	
	Region I	Region II	Region I	Region II	Region I	Region II	Region I	Region II
F(σ)	1.245	1.696	1.245	1.695	1.253	1.711	1.271	1.699

Table 3.5 The enhanced probability of failure factor F(σ) over different fiber regions for dl =10.0μm and applied strain of 0.6%.

	d_l=10μm	
	±4μm from fiber break	±4μm from matrix crack tip
F(σ)	1.692	1.750

From Table 3.4 it is shown that larger higher stress concentration region for longer debond compensates its lower Maximum SCF, as a result, the probability of failure over stress enhancement region is close to the same for each debond case. Meanwhile, it once again suggests that the stress enhancement will only significantly

increase the probability of failure of neighboring fiber over a very local region close to crack tip. Results from Table 3.5 further demonstrate that local region is most likely to be the region close to crack tip instead of fiber break. Based on the above finding, it could be concluded that for the case critical fracture plane nucleates from fiber breaks during loading application, the critical fracture plane would most likely to show a stagger pattern, which has been commonly found during experiment. It would also be expected that for composite with good fiber/matrix bonding (i.e. shorter debond length), the critical fracture plane would be more coordinated, otherwise it would show a more random pattern involving longer length of pulled-out fibers. That may help explain the commonly found "brittle typed" UD composites fracture and "brush like" UD composite fracture during experiments [123, 124].

3.4 Effects of thermal stresses

Similar to Section 2, we chose to present the study based on mechanical loading first in order to maintain the generality of the results as curing temperature varied and depends on the applications and material systems specifically. Once the general trends under mechanical loading has been understood, we then proceed to discuss the effects of thermal stresses. In the present section, to include the thermal stress, two steps of the analysis were carried out. In the first step, thermal cool down process was simulated by applied $\Delta T = -100°$ of temperature change. At the second step, mechanical loading is applied by applying uniform displacement to the model.

For Case I discussed in Section 3.2, it's found that instead of fiber/matrix interface debonds from fiber break, cavitation induced matrix cracking tends to be the first failure event upon loading and matrix crack propagates perpendicular to the fiber axis. As a result, it's interesting to study the effects of thermal stresses on matrix crack propagation process in Case I.

In order to study matrix crack propagation, energy release rate (ERR) was calculated for initial cavitation induced matrix crack with length =0.2μm as demonstrated in Figure 3.8. Results on ERR is shown in Figure 3.17. It's found that that the presence of thermal stresses increases ERR of matrix crack. This is due to the overall tensile stress developed within matrix material as a result of thermal cooldown. Due to the longitudinal thermal coefficient mismatch between matrix and fiber material (see Table 3.1), after thermal cooldown, matrix materials tend to shrink while fibers want to expand. As a result of strain compatibility, tensile stress developed within matrix and fibers are subjected to compression after thermal cooldown. However, despite the increase on ERR, the thermal stress contribution is still small compared to the contribution of mechanical loading, especially at applied load level when the matrix crack starts propagation (at around 0.17% of mechanical applied strain). More importantly, the predicted crack path is not influenced by the thermal stress. As a result, it is concluded that the trend discussed on matrix cracking based on mechanical loading does not change with the inclusion of thermal stresses. Regarding fiber breakages process, due to the compressive stress developed during cooldown as discussed above, it's expected that higher applied load is needed to break the neighboring fiber as

compared to mechanical loading case, however, the whole statistically analysis should hardly be affected.

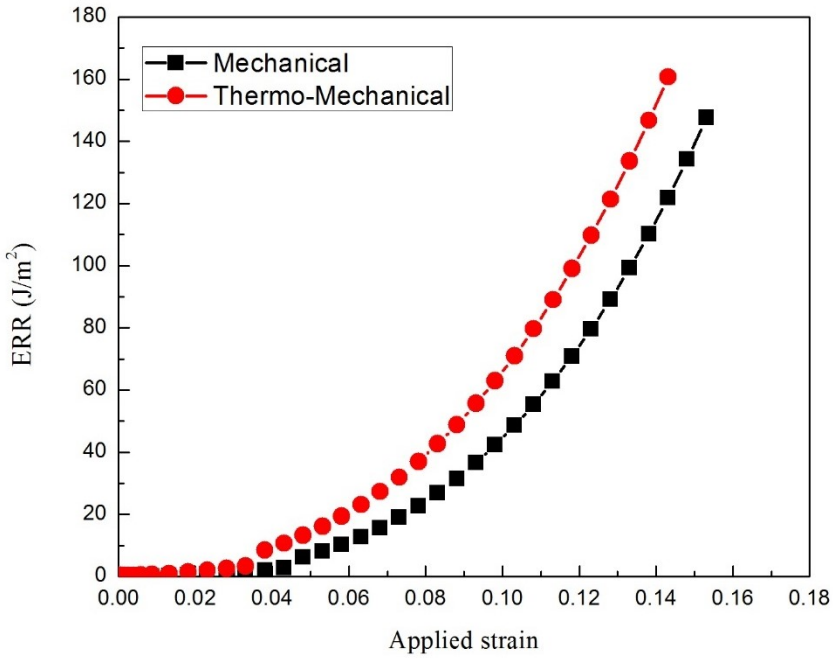

Figure 3.17 Effect of thermal stresses on matrix crack ERR for Case I

We now consider Case II where fiber breaks due to applied load. In that case, Fiber/matrix debonding is expected, and the main focus is weather the presence of thermal stress would affect the debond crack kinking process significantly such as altering the predicted kinking angle and change the conclusion that predicted kinking angle is independent of initial debond length.

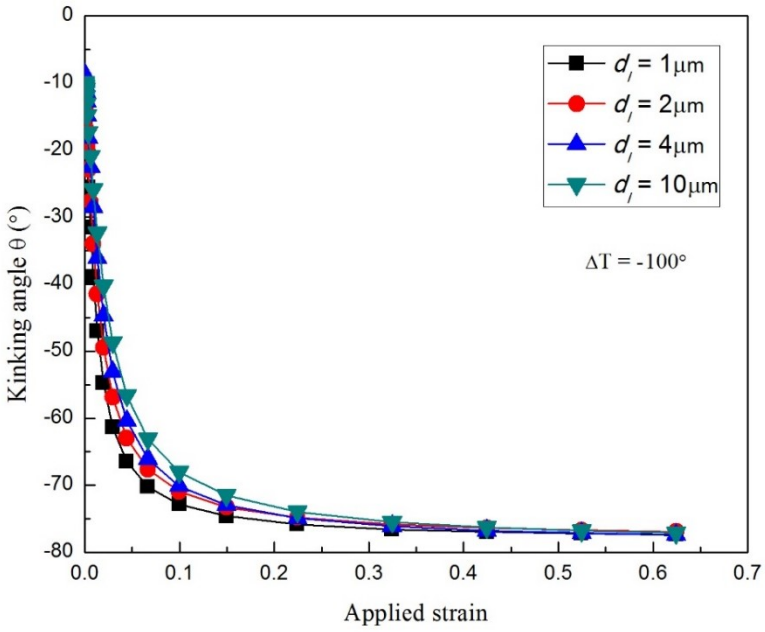

Figure 3.18 Effect of thermal stress on predicted kinking angle for Case II

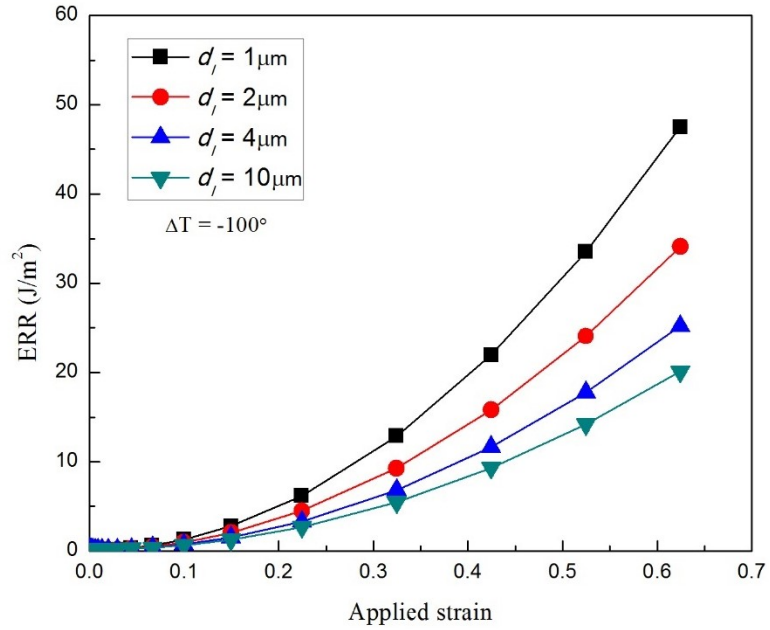

Figure 3.19 Variation of ERR of kinked crack for different initial debond cases under thermo-mechanical loading for Case II

Figure 3.18 shows the results of predicted kinking angle against applied mechanical strain based on maximum energy release rate criterion. It's shown that within small applied strain range (less than 0.2%), the predicted angle varied significantly with increasing applied strain for each initial debond length. That was due to the significant contribution of thermal stresses for small applied load. With the increase of mechanical loading, the predicted angle is found to converge to the 76.8° predicted in the present paper. Figure 3.19 shows the ERR of potential kinked crack of the same length (0.204 μm) for four initial debond cases. It's very clear from Figure 3.19 that the ERR of kinked crack is too small for kinking to occur at applied strain less than 0.2% and kinking is most likely to occur at higher applied load when predicted kinking angle is almost the same for each initial debond cases at -76.8°, as indicated in Figure 3.18. As a result, it's concluded that presence of thermal stresses has insignificant effects on crack kinking in Case II. For matrix crack propagation and subsequent neighboring fiber breakage, same conclusions are expected as for Case I.

3.5 Summary

In this section, possible mechanisms for the formation of a "critical fracture plane" in UD composites with high fiber volume fraction under tensile loading has been investigated numerically. It has been found that the critical fracture plane is most likely to nucleate from individual broken fiber (we assumed one here). Depending on how the broken fiber is introduced, two different cases are studied. If the critical fracture plane nucleates from a broken fiber induced by the manufacturing process, then due to the

constraint of the closely spaced neighboring stiff fibers, nearly equal-triaxial stress state developed in the matrix between fiber inhibits matrix plasticity. As a result, cavitation-induced matrix crack initiates close to the broken fiber end upon loading and propagates perpendicular towards the neighboring fiber upon further loading. The presence of thermal stress is found to help facilitate the initiation of cavitation-induced matrix crack. The fiber break and the subsequent matrix crack increase the probability of failure of the fibers in the local region lying close to the initial broken fiber end. As a result, the critical fracture plane would be expected to be relatively flat.

For the case of fiber breaks during loading at the weak positions along the fiber length, fiber/matrix debonding is expected to result due to high shear stress concentration at the broken fiber end. The length of the debond crack depends on the fiber/matrix interface properties. In the present section, we considered the debond cracks as longitudinal matrix cracks, which are often seen in experiments, especially for composites with good fiber/matrix interfacial bonding. The debond crack is found to kink out in a direction that retains Mode I fracture locally, and the kinking angle is found to be almost constant regardless of the initial debond length even with the inclusion of thermal stresses. As a result, once a kinked crack is formed, brittle matrix cracking would quickly develop and propagate towards neighboring fibers. Depending on the initial debond length, matrix cracking path varies. The matrix crack not only enhances the stress concentration in the neighboring fibers, the crack tip also relocates the highest stress concentration points along neighboring fibers as it approaches the fibers. This significantly increases the probability of failure of fibers in the vicinity of the crack tip.

As a result, a staggered pattern of critical fracture plane is expected to form. The critical fracture plane will be more coordinated among fibers for good fiber/matrix bonding, while it would display more random features with longer length of pulled-out fibers for composites with relatively weak fiber/matrix bonding.

4. CONCLUDING REMARKS AND RECOMMENDED FUTURE WORK

4.1 Concluding remarks

In the past few decades, fiber reinforced polymer composites have seen themselves in virtually every aspect of industrial applications, from larger structures like aircrafts and wind turbine blades to smaller personal items such as laptops. However, the full potential of composite materials remains to be harnessed. Various reasons contribute to this situation, among which the lack of understanding of their failure mechanisms stands out the most. Due to the architecture of a composite, its properties could be tailored to meet different design requirements by simply varying the layups or constituents of a composite. However, such advantage also poses great challenges, as various failure mechanisms occur simultaneously or sequentially at various length scales when subjected to loading.

In this dissertation, we first highlighted the importance of proper understanding on failure mechanisms in a composite in Section 1. I was demonstrated that lack of understanding of composite failure mechanisms is one of the major causes contributing to the overly conservative design of structural components. Meanwhile, although investigations on failure mechanisms do not always provide accurate prediction of the composite failure directly, they are vital for the development of failure models as they clarify the most important parameters that govern the failure process. Without proper consideration of those governing parameters, the accuracy of failure models is doubtful even though they may match selected experimental data well.

In Section 2, we investigated the plausible failure mechanisms for UD composites subjected to transverse tension. When the tensile load is applied to a UD composite transversely, the composite often fails by forming transverse cracks. Based on available experimental observations, it is generally recognized that the macro-size transverse crack is formed by coalescence of individual fiber/matrix interfacial debond through matrix cracking. At this moment, it is extremely difficult to clarify the exact mechanism of fiber/matrix debonding due to the limitation of experimental techniques. However, in the case of pure transverse tension, as stress state in the close vicinity of fiber/matrix interface becomes equi-triaxial or nearly equi-triaxial, it is likely that cavitation induced matrix cracking occurs and induces interface debonding.

In the present study, we only discussed the subsequent failure process after debonding initiates, i.e. debond growth, debond crack kinking and link-up of debonds. Two most plausible scenarios were investigated: 1. transverse crack forms from single fiber/matrix interfacial debond and 2. transverse crack forms by link-up of multiple debonds. For single debond scenario, its growth along interface has been investigated thoroughly in author's previous research and it is found that debond growth is mixed mode for small debond angles and is Mode I dominated, and with increase of debond angle, its growth becomes Mode II dominated and up to a certain angle (60° ~70° of half debond angle for single debond) when debond surfaces come into contact and Mode I component of ERR vanishes causing debond growth to stop. The debond crack kinking has been studied and it has been found that kinking would most likely occur before debond surfaces come into contact and the debond angle at kinking increases with

increasing inter-fiber distance. This angle is smaller than the angle observed in single fiber composite case. This result was supported by a most recent published microscopic observation conducted by a Spanish research group [91]. Once kinking occurs, the kinked crack is found to propagate towards nearby fibers in a direction that would retain pure Mode I growth of the kinked crack. As kinked crack propagates closer to the nearby intact fiber, it causes high radial tensile stress concentration in that fiber, likely leading to the initiation of a debond in that fiber. The same process of debond growth, debond cracking and kinking crack propagation leading to the initiation of a new debond in a neighboring fiber repeats and results in the final formation of macro-size transverse crack. Based on the results obtained from two different inter-fiber distances, it has been found that Scenario I is more favorable for larger inter-fiber distances. For Scenario II, we first simplified the problem by studying the link-up of two nearby debonds. It was found that the presence of two debonds facilitates the growth of debond, debond crack kinking as well as kinked crack propagation. Meanwhile, it was shown that the mutual enhancement intensified as debonded fiber got closer to each other. As a result, transverse crack formed by Scenario II requires a much lower applied load level compared to that in Scenario I.

Based on the discussion in Section 2, it is clear that fiber/matrix interface properties, matrix fracture toughness as well as fiber volume fraction (in terms of inter-fiber distance) are three material characteristics that govern the failure process of a UD composite under transverse tension. Among all three parameters, the first two are quite expected, however the fiber volume fraction is somewhat surprising. For UD

composites, there is often a misunderstanding that a higher fiber volume fraction gives better performance. While the stiffness increases with the fiber volume fraction, the results obtained from present study suggests that the improvement in transverse failure does not follow. A recent study [126] by the author's colleagues further validates the argument as they found cavitation induced matrix cracking to occur at a much lower strain in higher fiber volume fraction case. Again, present results prove the need to better understand the corresponding failure mechanisms.

The transverse failure of UD composites in Section 2 is often considered as the first failure event in a composite with general layups due to its relative low strain to failure. For final failure of composites, it is usually controlled by the strength of UD plies along loading direction. In Section 3, the failure mechanisms of UD composites under longitudinal tension was discussed. Unlike transverse failure, the exact longitudinal failure process of UD composites is difficult to observe experimentally as it involves the breakage of individual fiber within the composites, which is impossible to track directly other than for a small region. Recently, with the applications of X-ray tomography, more direct experimental observations are made and it is generally recognized that the final failure of a UD composite occurs when a so-call "critical fracture plane" is formed and propagates unstably, leading to the separation of composites. Based on the analytical and experimental results, it is clear that the "critical fracture plane" only contains a small number of fibers, although the exact number of fibers is still uncertain. For many years, research on longitudinal failure of composites was heavily focused on the accumulation of broken fibers without properly accounting

for linkage of broken fibers. As a result, although various models have been proposed and claim to be in good agreement with experimental strain to failure, they do not match the failure characteristics observed, which makes their validity doubtful. Moreover, broken fiber accumulation models do not provide all the information regarding materials parameters that govern the longitudinal failure of a UD composite as fiber breakage, by itself, does not form the "critical fracture plane".

Realizing the discrepancy discussed above, we investigate the plausible mechanisms responsible for "critical fracture plane" formation and try to identify the most important material parameters that govern this formation process using an axisymmetric FE model. Two different cases are studied: I. Fiber breaks during manufacturing process and II. Fiber breaks during loading. For Case I, it was found that upon loading, cavitation induced matrix cracking would most likely occur near a fiber break. The propagation of matrix crack was then simulated based on XFEM, and it was found that matrix crack propagates towards neighboring intact fibers in a direction perpendicular to the tensile loading direction. The neighboring fiber breakage was analyzed based on a statistical approach and it was found that the initial fiber break, along with subsequent matrix crack significantly increase the probability of failure of a local region near initial fiber break plane in neighboring fibers. As a result, it is expected that the critical fracture plane resulting from initial manufacturing induced fiber break to be planar. For Case II, due to the shear stress concentration, fiber/matrix interfacial debond is expected as soon as fiber breaks. The exact length of initial debond depends on the interface properties of composites. In Section 3, we investigated four different

initial debond cases and it was found that the angle at which the debond crack kinks out is not sensitive to the length of debond. However, the subsequent matrix crack propagation path depends highly on the debond length. The larger the initial debond, the more tilted subsequent matrix cracking path is. When matrix crack propagates to neighboring fibers, based on the statistical analysis, it is found that the presence of debond results in larger positive influence region in neighboring fibers where local mean tensile stress is higher than the nominal stresses and region closer to matrix crack tip in neighboring fibers has higher probability of failure. As a result, for larger initial debond case, the nearby fiber would most likely break far away from the initial fiber break plane, resulting in a more staggered shape of "critical fracture plane". Since the length of initial debond is a representative of fiber/matrix interface quality, we could also conclude that for composites with relatively poor fiber/matrix interface properties, the "critical fracture plane" would be less planar and more fiber pull-outs are expected, resulting in a "brush" like failure characteristics. Finally, based on the discussions on Section 3, it is clear that the material parameters that govern the formation of "critical fracture plane" are fiber strength and flaw distributions, matrix toughness as well as fiber/matrix interfacial properties.

4.2 Recommended future work

The research on composite materials is a lifelong adventure, it does not stop with the end of a PhD study. Despite the results we have at this moment, there is still much

more work needed to be done towards a better understanding of composite materials and we will discuss some of the future research plans in this section.

The work presented in this dissertation intends to clarify the failure mechanisms of UD composites under transverse and longitudinal tension and identify the most important governing material parameters, which is vital for the future development of failure models that could accurately capture the underlining failure characteristics and predict the occurrence of failures with accuracy. For transverse failure, the debond growth, debond crack kinking as well as link-up of individual debond have been properly addressed in the present dissertation. For future research, there are two potential areas of interests. The first one is the initiation of fiber/matrix interfacial debonding. As discussed in Section 2, one of the most obvious causes for fiber/matrix interfacial debonding is manufacturing induced poor fiber/matrix interfacial bonding. However, for composites with proper fiber/matrix interfacial bonding, the exact mechanism for debond initiation is still under debate. In order to properly investigate it, we might need to look into smaller scales, i.e. the scale of polymer chains, which is difficult from experimental and numerical modeling, though. The other area of interest that is more suitable for current author to work on is to investigate if there is a critical state such as numbers of link-up debonds beyond which transverse crack grows unstably. This is a similar concept as the “critical fracture plane” under longitudinal tension and the results obtained from this study would be very helpful for the future development of failure mode that could predict the strain to failure (often based on the observation of macro-size transverse crack) under transverse tension precisely.

For failure of UD composite under longitudinal tension, it is of great importance to identify the numbers of broken fiber in a "critical fracture plane" correctly. One should expect the number to be varied with different loading and material systems. At this moment, majority of failure models proposed are based on the idea of accumulations of broken fibers while ignoring the roles of fiber/matrix interfacial debonding and matrix cracking. As a result, proposed models could not capture the exact failure characteristics. There is no denial of the importance of fiber breakage itself, however, as shown in Section 3, presence of fiber/matrix interfacial debonding as well as matrix cracking determines the location where neighboring intact fibers have the highest probability of failure. As a result, regarding future work, one of the possibility is to work on the failure model to predict failure strain of UD composite under longitudinal tension. As major improvement to the existing failure models, the interfacial debonding and matrix cracking should be accounted in future models and the new statistical analysis on fiber breakage should be able to address the influence of interface debonding and matrix cracking on calculated probability of failure of intact fibers.

REFERENCES

1. Bennett, S., D. Johnson, and W. Johnson, *Strength-structure relationships in PAN-based carbon fibres.* Journal of Materials Science, 1983. 18(11): p. 3337-3347.

2. Shindo, A., *Polyacrylonitrile (PAN)-based carbon fibers*, in *Comprehensive Composite Materials*, Anthony Kelly and C. Zweben, Editors. 2000, Elsevier. p. 1-33.

3. Csanádi, T., et al., *Nanoindentation derived elastic constants of carbon fibres and their nanostructural based predictions.* Carbon, 2017. 119(Supplement C): p. 314-325.

4. Miyagawa, H., et al., *Transverse elastic modulus of carbon fibers measured by Raman spectroscopy.* Materials Science and Engineering: A, 2005. 412(1): p. 88-92.

5. Maurin, R., et al., *Transverse properties of carbon fibres by nano-indentation and micro-mechanics.* Applied Composite Materials, 2008. 15(2): p. 61.

6. Hull, D. and T. Clyne, *An introduction to composite materials*. 1996: Cambridge University Press.

7. Dwight, D.W., *1.08 - Glass Fiber Reinforcements A2 - Kelly, Anthony*, in *Comprehensive Composite Materials*, C. Zweben, Editor. 2000, Pergamon: Oxford. p. 231-261.

8. Kim, J.K. and Y.W. Mai, *Interfaces in composites*. 1993: Wiley Online Library.

9. Narkis, M., E. Chen, and R. Pipes, *Review of methods for characterization of interfacial fiber‐matrix interactions.* Polymer Composites, 1988. 9(4): p. 245-251.

10. Subramanian, S., et al., *Characterization of the fiber-matrix interphase and its influence on mechanical properties of unidirectional composites.* Journal of Composite Materials, 1996. 30(3): p. 309-332.

11. Barlow, C., J. Peacock, and A. Windle, *Relationships between microstructures and fracture energies in carbon fibre/PEEK composites.* Composites, 1990. 21(5): p. 383-388.

12. Aveston, J. and A. Kelly, *Theory of multiple fracture of fibrous composites.* Journal of Materials Science, 1973. 8(3): p. 352-362.

13. Garrett, K. and J. Bailey, *Multiple transverse fracture in 90 cross-ply laminates of a glass fibre-reinforced polyester.* Journal of Materials Science, 1977. 12(1): p. 157-168.

14. Parvizi, A. and J. Bailey, *On multiple transverse cracking in glass fibre epoxy cross-ply laminates.* Journal of Materials Science, 1978. 13(10): p. 2131-2136.

15. Laws, N., G.J. Dvorak, and M. Hejazi, *Stiffness changes in unidirectional composites caused by crack systems.* Mechanics of Materials, 1983. 2(2): p. 123-37.

16. Hashin, Z., *Analysis of cracked laminates: a variational approach.* Mechanics of Materials, 1985. 4(2): p. 121-136.

17. Talreja, R., *Transverse cracking and stiffness reduction in composite laminates.* Journal of Composite Materials, 1985. 19(4): p. 355.

18. Nairn, J.A., *The strain energy release rate of composite microcracking: a variational approach.* Journal of Composite Materials, 1989. 23(11): p. 1106-1129.

19. Varna, J. and L. Berglund, *Multiple transverse cracking and stiffness reduction in cross-ply laminates.* Journal of Composites Technology and Research, 1991. 13(2): p. 97-106.

20. Varna, J. and L.A. Berglund, *Thermo-elastic properties of composite laminates with transverse cracks.* Journal of Composites Technology and Research, 1994. 16(1): p. 77-87.

21. Talreja, R. and C.V. Singh, *Damage and failure of composite materials*. 2012: Cambridge University Press.

22. Tarpani, J.R., et al., *Mechanical performance of carbon-epoxy laminates. Part II: quasi-static and fatigue tensile properties.* Materials Research, 2006. 9: p. 121-130.

23. Asp, L.E., L.A. Berglund, and P. Gudmundson, *Effects of a composite-like stress state on the fracture of epoxies.* Composites Science and Technology, 1995. 53(1): p. 27-37.

24. Asp, L., L.A. Berglund, and R. Talreja, *A criterion for crack initiation in glassy polymers subjected to a composite-like stress state.* Composites Science and Technology, 1996. 56(11): p. 1291-1301.

25. Asp, L., L.A. Berglund, and R. Talreja, *Prediction of matrix-initiated transverse failure in polymer composites.* Composites Science and Technology, 1996. 56(9): p. 1089-1097.

26. Carraro, P.A. and M. Quaresimin, *Modelling fibre–matrix debonding under biaxial loading.* Composites Part A: Applied Science and Manufacturing, 2014. 61(0): p. 33-42.

27. Koyanagi, J., S. KIMURA, and H. KAWADA, *Mixed-mode interfacial debonding simulation in single-fiber composite under a transverse load.* Journal of Solid Mechanics and Materials Engineering, 2009. 3(5): p. 796-806.

28. Ghosh, S., et al., *Interfacial debonding analysis in multiple fiber reinforced composites.* Mechanics of Materials, 2000. 32(10): p. 561-591.

29. Zhandarov, S. and E. Mäder, *Characterization of fiber/matrix interface strength: applicability of different tests, approaches and parameters.* Composites Science and Technology, 2005. 65(1): p. 149-160.

30. Gamstedt, E. and B. Sjögren, *Micromechanisms in tension-compression fatigue of composite laminates containing transverse plies.* Composites Science and Technology, 1999. 59(2): p. 167-178.

31. Romanov, V.S., et al., *Modelling evidence of stress concentration mitigation at the micro-scale in polymer composites by the addition of carbon nanotubes.* Carbon, 2015. 82: p. 184-194.

32. Toya, M., *A crack along the interface of a circular inclusion embedded in an infinite solid.* Journal of the Mechanics and Physics of Solids, 1974. 22(5): p. 325-348.

33. París, F., J. Cano, and J. Varna, *The fiber-matrix interface crack—a numerical analysis using boundary elements.* International Journal of Fracture, 1990. 82(1): p. 11-29.

34. Varna, J., L. Berglund, and M. Ericson, *Transverse single-fibre test for interfacial debonding in composites: 2. Modelling.* Composites Part A: Applied Science and Manufacturing, 1997. 28(4): p. 317-326.

35. Varna, J., F. Paris, and J.C. del Cano, *The effect of crack-face contact on fiber/matrix debonding in transverse tensile loading.* Composites Science and Technology, 1997. 57(5): p. 523-532.

36. García, I.G., V. Mantič, and E. Graciani, *Debonding at the fibre–matrix interface under remote transverse tension. One debond or two symmetric debonds?* European Journal of Mechanics - A/Solids, 2015. 53: p. 75-88.

37. Mantič, V., et al., *A linear elastic-brittle interface model: application for the onset and propagation of a fibre-matrix interface crack under biaxial transverse loads.* International Journal of Fracture, 2015. 195(1-2): p. 15-38.

38. Muñoz-Reja, M., et al., *Crack onset and propagation at fibre–matrix elastic interfaces under biaxial loading using finite fracture mechanics.* Composites Part A: Applied Science and Manufacturing, 2015.

39. París, F., E. Correa, and V. Mantič, *Kinking of transversal interface cracks between fiber and matrix.* Journal of Applied Mechanics, 2007. 74(4): p. 703-716.

40. Sandino, C., E. Correa, and F. París, *Numerical analysis of the influence of a nearby fibre on the interface crack growth in composites under transverse tensile load.* Engineering Fracture Mechanics, 2016. 168, Part B: p. 58-75.

41. Tanaka, M., et al., *Influence of non-uniform fiber arrangement on tensile fracture behavior of unidirectional fiber/epoxy model composites.* Composite Interfaces, 2005. 12(3-4): p. 365-378.

42. Vaughan, T.J. and C.T. McCarthy, *Micromechanical modelling of the transverse damage behaviour in fibre reinforced composites.* Composites Science and Technology, 2011. 71(3): p. 388-396.

43. Yang, L., et al., *Microscopic failure mechanisms of fiber-reinforced polymer composites under transverse tension and compression.* Composites Science and Technology, 2012. 72(15): p. 1818-1825.

44. Zhang, T. and Y. Yan, *Micromechanical analysis of transverse damage of fibre-reinforced composites.* Composite Interfaces, 2016. 23(1): p. 75-88.

45. Zhang, H., et al., *Transverse single-fibre test for interfacial debonding in composites: 1. Experimental observations.* Composites Part A: Applied Science and Manufacturing, 1997. 28(4): p. 309-315.

46. Rosen, B.W., *Tensile failure of fibrous composites.* AIAA journal, 1964. 2(11): p. 1985-1991.

47. Zweben, C., *Tensile failure of fiber composites.* AIAA journal, 1968. 6(12): p. 2325-2331.

48. Zweben, C. and B.W. Rosen, *A statistical theory of material strength with application to composite materials.* Journal of the Mechanics and Physics of Solids, 1970. 18(3): p. 189-206.

49. Harlow, D.G. and S.L. Phoenix, *The chain-of-bundles probability model for the strength of fibrous materials I: analysis and conjectures.* Journal of Composite Materials, 1978. 12(2): p. 195-214.

50. Harlow, D.G. and S.L. Phoenix, *The chain-of-bundles probability model for the strength of fibrous materials II: a numerical study of convergence.* Journal of Composite Materials, 1978. 12(3): p. 314-334.

51. Batdorf, S., *Tensile strength of unidirectionally reinforced composites—I.* Journal of reinforced plastics and composites, 1982. 1(2): p. 153-164.

52. Batdorf, S. and R. Ghaffarian, *Tensile strength of unidirectionally reinforced composites—II.* Journal of Reinforced Plastics and Composites, 1982. 1(2): p. 165-176.

53. Wisnom, M.R. and D. Green, *Tensile failure due to interaction between fibre breaks.* Composites, 1995. 26(7): p. 499-508.

54. Purslow, D., *Some fundamental aspects of composites fractography.* Composites, 1981. 12(4): p. 241-247.

55. Blassiau, S., A. Thionnet, and A.R. Bunsell, *Micromechanisms of load transfer in a unidirectional carbon fibre–reinforced epoxy composite due to fibre failures. Part 1: Micromechanisms and 3D analysis of load transfer: The elastic case.* Composite Structures, 2006. 74(3): p. 303-318.

56. Blassiau, S., A. Thionnet, and A.R. Bunsell, *Micromechanisms of load transfer in a unidirectional carbon fibre–reinforced epoxy composite due to fibre failures. Part 2: Influence of viscoelastic and plastic matrices on the mechanisms of load transfer.* Composite Structures, 2006. 74(3): p. 319-331.

57. Thionnet, A., H.Y. Chou, and A. Bunsell, *Fibre break processes in unidirectional composites.* Composites Part A: Applied Science and Manufacturing, 2014. 65: p. 148-160.

58. Thionnet, A., H.-Y. Chou, and A. Bunsell, *Fibre Break Failure Processes in Unidirectional Composites. Part 1: Failure and Critical Damage State Induced by Increasing Tensile Loading.* Applied Composite Materials, 2014. 22(2): p. 119-140.

59. Swolfs, Y., I. Verpoest, and L. Gorbatikh, *Issues in strength models for unidirectional fibre-reinforced composites related to Weibull distributions, fibre packings and boundary effects.* Composites Science and Technology, 2015. 114: p. 42-49.

60. Swolfs, Y., I. Verpoest, and L. Gorbatikh, *A review of input data and modelling assumptions in longitudinal strength models for unidirectional fibre-reinforced composites.* Composite Structures, 2016. 150: p. 153-172.

61. Vanegas-Jaramillo, J.D., et al., *Analytical model for predicting the tensile strength of unidirectional composites based on the density of fiber breaks.* Composites Part B: Engineering, 2018. 141: p. 84-91.

62. Aroush, D.R.-B., et al., *A study of fracture of unidirectional composites using in situ high-resolution synchrotron X-ray microtomography.* Composites Science and Technology, 2006. 66(10): p. 1348-1353.

63. Scott, A., et al., *In situ fibre fracture measurement in carbon–epoxy laminates using high resolution computed tomography.* Composites Science and Technology, 2011. 71(12): p. 1471-1477.

64. Scott, A., et al., *Damage accumulation in a carbon/epoxy composite: Comparison between a multiscale model and computed tomography experimental results.* Composites Part A: Applied Science and Manufacturing, 2012. 43(9): p. 1514-1522.

65. Garcea, S.C., et al., *Fatigue micromechanism characterisation in carbon fibre reinforced polymers using synchrotron radiation computed tomography.* Composites Science and Technology, 2014. 99: p. 23-30.

66. Swolfs, Y., et al., *Synchrotron radiation computed tomography for experimental validation of a tensile strength model for unidirectional fibre-reinforced composites.* Composites Part A: Applied Science and Manufacturing, 2015. 77: p. 106-113.

67. Garcea, S.C., I. Sinclair, and S.M. Spearing, *Fibre failure assessment in carbon fibre reinforced polymers under fatigue loading by synchrotron X-ray computed tomography.* Composites Science and Technology, 2016. 133: p. 157-164.

68. Na, W., D. Kwon, and W.-R. Yu, *X-ray computed tomography observation of multiple fiber fracture in unidirectional CFRP under tensile loading.* Composite Structures, 2018. 188: p. 39-47.

69. *http://www.fibremodproject.eu/news-and-blogs/item/let-us-stop-the-hypocrisy-of--nicely-matching-experimental-validations*

70. Rybicki, E.F. and M. Kanninen, *A finite element calculation of stress intensity factors by a modified crack closure integral.* Engineering Fracture Mechanics, 1977. 9(4): p. 931-938.

71. Krueger, R., *Virtual crack closure technique: History, approach, and applications.* Applied Mechanics Reviews, 2004. 57: p. 109.

72. Krueger, R. and D. Goetze, *Influence of finite element software on energy release rates computed using the virtual crack closure technique*. 2006: National Aeronautics and Space Administration, Langley Research Center.

73. Moës, N., J. Dolbow, and T. Belytschko, *A finite element method for crack growth without remeshing.* International Journal for Numerical Methods in Engineering, 1999. 46(1): p. 131-150.

74. Zhuang, L., R. Talreja, and J. Varna, *Transverse crack formation in unidirectional composites by linking of fibre/matrix debond cracks.* Composites Part A: Applied Science and Manufacturing, 2018. 107: p. 294-303.

75. Zhuang, L., R. Talreja, and J. Varna, *Tensile failure of unidirectional composites from a local fracture plane.* Composites Science and Technology, 2016. 133: p. 119-127.

76. Hobbiebrunken, T., et al., *Evaluation of interfacial strength in CF/epoxies using FEM and in-situ experiments.* Composites Part A: Applied Science and Manufacturing, 2006. 37(12): p. 2248-2256.

77. Mantič, V., *Interface crack onset at a circular cylindrical inclusion under a remote transverse tension. Application of a coupled stress and energy criterion.* International journal of Solids and Structures, 2009. 46(6): p. 1287-1304.

78. Kushch, V.I., et al., *Numerical simulation of progressive debonding in fiber reinforced composite under transverse loading.* International Journal of Engineering Science, 2011. 49(1): p. 17-29.

79. Bouhala, L., et al., *Modelling of failure in long fibres reinforced composites by X-FEM and cohesive zone model.* Composites Part B: Engineering, 2013. 55: p. 352-361.

80. Neogi, A., N. Mitra, and R. Talreja, *Cavitation in epoxies under composite-like stress states.* Composites Part A: Applied Science and Manufacturing, 2017.

81. Pupurs, A. and J. Varna, *Steady-state energy release rate for fiber/matrix interface debond growth in unidirectional composites.* International Journal of Damage Mechanics, 2015: p. 1056789515624000.

82. *ANSYS Academic Research, Release 16.0*. 2016: Canonsburg, Pennsylvania.

83. Sun, C.T. and C.J. Jih, *On strain energy release rates for interfacial cracks in bi-material media.* Engineering Fracture Mechanics, 1987. 28(1): p. 13-20.

84. Raju, I.S., J.H. Crews, and M.A. Aminpour, *Convergence of strain energy release rate components for Edge-Delaminated composite laminates.* Engineering Fracture Mechanics, 1988. 30(3): p. 383-396.

85. Sun, C. and M. Manoharan, *Strain energy release rates of an interfacial crack between two orthotropic solids.* Journal of Composite Materials, 1989. 23(5): p. 460-478.

86. Zhuang, L., et al., *Effects of Inter-Fiber Spacing on Fiber-matrix Debond Crack Growth in Unidirectional Composites under Transverse Loading* Composites: Part A, 2017. Submitted.

87. Martyniuk, K., et al., *3D in situ observations of glass fibre/matrix interfacial debonding.* Composites Part A: Applied Science and Manufacturing, 2013. 55: p. 63-73.

88. He, M.-Y. and J.W. Hutchinson, *Kinking of a crack out of an interface.* Journal of Applied Mechanics, 1989. 56(2): p. 270-278.

89. Whitcomb, J.D. *Strain-energy release rate analysis of cyclic delamination growth in compressively loaded laminates*. 1984. ASTM International.

90. Xie, D., et al., *Fracture criterion for kinking cracks in a tri-material adhesively bonded joint under mixed mode loading.* Engineering Fracture Mechanics, 2005. 72(16): p. 2487-2504.

91. Correa, E., et al., *Microscopical observations of inter-fibre failure under tension.* Composites Science and Technology, 2018. 155: p. 213-220.

92. Zhuang, L., R. Talreja, and J. Varna, *Effect of cooldown induced fiber/matrix interfacial disbond on transverse failure in composites*, in *32nd ASC Technical Conference, 2017,* West Lafayette, Indiana.

93. Wood, C. and W. Bradley, *Determination of the effect of seawater on the interfacial strength of an interlayer E-glass/graphite/epoxy composite by in situ*

observation of transverse cracking in an environmental SEM. Composites science and technology, 1997. 57(8): p. 1033-1043.

94. Wisnom, M., et al., *Mechanisms generating residual stresses and distortion during manufacture of polymer–matrix composite structures.* Composites Part A: Applied Science and Manufacturing, 2006. 37(4): p. 522-529.

95. Pupurs, A., et al., *Interface debond crack growth in tension–tension cyclic loading of single fiber polymer composites.* Composites Part A: Applied Science and Manufacturing, 2013. 44: p. 86-94.

96. Sjögren, B. and L.A. Berglund, *The effects of matrix and interface on damage in GRP cross-ply laminates.* Composites Science and Technology, 2000. 60(1): p. 9-21.

97. Awerbuch, J. and H. Hahn, *Fatigue and proof-testing of unidirectional graphite/epoxy composite*, in *Fatigue of Filamentary Composite Materials*. 1977, ASTM International.

98. Zhuang, L. and A. Pupurs. *Effect of neighboring fibers on energy release rate during fiber/matrix debond growth*. in *16th European Conference on Composite Materials, ECCM 2014*. 2014.

99. Judd, N. and W. Wright, *Voids and their effects on the mechanical properties of composites- an appraisal.* Sampe Journal, 1978. 14: p. 10-14.

100. Bowles, K.J. and S. Frimpong, *Void effects on the interlaminar shear strength of unidirectional graphite-fiber-reinforced composites.* Journal of Composite Materials, 1992. 26(10): p. 1487.

101. Varna, J., et al., *Effect of voids on failure mechanisms in RTM laminates.* Composites Science and Technology, 1995. 53(2): p. 241-249.

102. Huang, H. and R. Talreja, *Effects of void geometry on elastic properties of unidirectional fiber reinforced composites.* Composites Science and Technology, 2005. 65(13): p. 1964-1981.

103. Talreja, R., *Defect damage mechanics: broader strategy for performance evaluation of composites.* Plastics, Rubber and Composites, 38, 2009. 2(4): p. 49-54.

104. Zhuang, L. and R. Talreja, *Effects of voids on postbuckling delamination growth in unidirectional composites.* International Journal of Solids and Structures, 2014. 51(5): p. 936-944.

105. *ABAQUS/Standard User's Manual.* Version 6.12.

106. Sih, G.C., *Strain-energy-density factor applied to mixed mode crack problems.* International Journal of fracture, 1974. 10(3): p. 305-321.

107. Theocaris, P., *The caustic as a means to define the core region in brittle fracture.* Engineering Fracture Mechanics, 1981. 14(2): p. 353-362.

108. Theocaris, P., *Experimental determination of the core region in mixed-mode fracture*, in *Mixed Mode Crack Propagation*. 1981, Sijthoff and Noordhoff. p. 21-36.

109. Theocaris, P.S. and N.P. Andrianopoulos, *The mises elastic-plastic boundary as the core region in fracture criteria.* Engineering Fracture Mechanics, 1982. 16(3): p. 425-432.

110. Sih, G., *A special theory of crack propagation*, in *Mechanics of Fracture Initiation and Propagation*. 1991, Springer. p. 1-22.

111. Lorenzo, L. and H.T. Hahn, *Fatigue failure mechanisms in unidirectional composites.* Composite Materials: Fatigue and Fracture, 1986: p. 210-232.

112. Maligno, A.R., N.A. Warrior, and A.C. Long, *Effects of inter-fibre spacing on damage evolution in unidirectional (UD) fibre-reinforced composites.* European Journal of Mechanics - A/Solids, 2009. 28(4): p. 768-776.

113. Evans, A.G., M.Y. He, and J.W. Hutchinson, *Interface debonding and fiber cracking in brittle matrix composites.* Journal of the American Ceramic Society, 1989. 72(12): p. 2300-2303.

114. Hedgepeth, J.M. and P. Van Dyke, *Local stress concentrations in imperfect filamentary composite materials.* Journal of composite materials, 1967. 1(3): p. 294-309.

115. Nedele, M.R. and M.R. Wisnom, *Three-dimensional finite element analysis of the stress concentration at a single fibre break.* Composites Science and Technology, 1994. 51(4): p. 517-524.

116. Beyerlein, I.J. and S.L. Phoenix, *Stress concentrations around multiple fiber breaks in an elastic matrix with local yielding or debonding using quadratic influence superposition.* Journal of the Mechanics and Physics of Solids, 1996. 44(12): p. 1997-2039.

117. Ohno, N., S. Okabe, and T. Okabe, *Stress concentrations near a fiber break in unidirectional composites with interfacial slip and matrix yielding.* International Journal of Solids and Structures, 2004. 41(16): p. 4263-4277.

118. Hedgepeth, J.M., *Stress concentrations in filamentary structures.* NASA TND-882, 1961.

119. Nedele, M. and M. Wisnom, *Stress concentration factors around a broken fibre in a unidirectional carbon fibre-reinforced epoxy.* Composites, 1994. 25(7): p. 549-557.

120. Scop, P.M. and A.S. Argon, *Statistical theory of strength of laminated composites II.* Journal of composite materials, 1969. 3(1): p. 30-47.

121. Beyerlein, I.J. and S.L. Phoenix, *Statistics for the strength and size effects of microcomposites with four carbon fibers in epoxy resin.* Composites Science and Technology, 1996. 56(1): p. 75-92.

122. Talreja, R., *Fatigue of composite materials: damage mechanisms and fatigue-life diagrams.* Proceedings of the Royal Society of London. A. Mathematical and Physical Sciences, 1981. 378(1775): p. 461-475.

123. Gamstedt, E. and R. Talreja, *Fatigue damage mechanisms in unidirectional carbon-fibre-reinforced plastics.* Journal of Materials Science, 1999. 34(11): p. 2535-2546.

124. Gamstedt, E.K., L.A. Berglund, and T. Peijs, *Fatigue mechanisms in unidirectional glass-fibre-reinforced polypropylene.* Composites Science and Technology, 1999. 59(5): p. 759-768.

125. Dundurs, J., *Discussion: "Edge-Bonded Dissimilar Orthogonal Elastic Wedges Under Normal and Shear Loading" (Bogy, D. B., 1968, ASME J. Appl. Mech., 35, pp. 460–466).* Journal of Applied Mechanics, 1969. 36(3): p. 650-652.

126. Elnekhaily, S.A. and R. Talreja, *Damage initiation in unidirectional fiber composites with different degrees of nonuniform fiber distribution.* Composites Science and Technology, 2018. 155: p. 22-32.